SCIENCE • TECHNOLOGY • RESEARCH HIGHLIGHTS • VISIONS

Dissertation
31

Cellulose, starch and their derivatives for industrial applications

Structure-property studies

Lauri Kuutti

VTT SCIENCE 31

Cellulose, starch and their derivatives for industrial applications

Structure-property studies

Lauri Kuutti

To be presented with the permission of the Faculty of Science of the University of Helsinki for public criticism in Auditorium E204 at the Physicum, Gustaf Hällströmin katu 2 A, Helsinki, on May 24th, 2013 at 12 o'clock noon.

ISBN 978-951-38-7997-6 (Soft back ed.)
ISBN 978-951-38-7998-3 (URL: http://www.vtt.fi/publications/index.jsp)

VTT Science 31

ISSN-L 2242-119X
ISSN 2242-119X (Print)
ISSN 2242-1203 (Online)

JULKAISIJA – UTGIVARE – PUBLISHER

VTT
PL 1000 (Tekniikantie 4 A, Espoo)
02044 VTT
Puh. 020 722 111, faksi 020 722 7001

VTT
PB 1000 (Teknikvägen 4 A, Esbo)
FI-02044 VTT
Tfn +358 20 722 111, telefax +358 20 722 7001

VTT Technical Research Centre of Finland
P.O. Box 1000 (Tekniikantie 4 A, Espoo)
FI-02044 VTT, Finland
Tel. +358 20 722 111, fax + 358 20 722 7001

Kopijyvä Oy, Kuopio 2013

Cellulose, starch and their derivatives for industrial applications
Structure-property studies

Selluloosan, tärkkelyksen ja niiden johdosten teollisia sovelluksia. Rakenteen ja ominaisuuksien tutkimuksia. **Lauri Kuutti.** Espoo 2013. VTT Science 31. 72 p. + app. 55 p.

Abstract

Despite the similarity of their structural basic units, cellulose- and starch-based materials behave differently in many industrial applications. In this thesis, the structure and properties of these polysaccharides and their selected derivatives were studied by means of five comprehensive examples.

In the first investigation, highly crystalline cellulose was identified from *Valonia macrophysa* vesicles by atomic force microscopy. The role of water as a possible modifier on the surface of cellulose was found to be very important. The monoclinic phases were found on the cellulose surfaces with a lateral resolution of about 4 Å, indicating that water molecules cannot penetrate and thus disturb the surface structure of monoclinic cellulose. On the other hand, the absence of triclinic phases was explained by the used measuring geometry without liquid cell.

The ageing of metastable oat and barley thermoplastic starch films was followed by frictional imaging. As a consequence of the ageing, the films lose some of their mechanical properties. In the oat films, glycerol used as a plasticiser diffused from the starch-glycerol-water matrix to the surface of thermoplastic starch, resulting in areas with low friction. In the case of barley starch films, the ageing first resulted in short range reorientation of polymers and finally slow crystallization of amylopectin branches.

Solution precipitation techniques were applied to produce ideally spherical starch ester particles (with a diameter about half the wavelength of visible light), suitable for fillers in paper coatings in the third study. Particles assume their shape and size spontaneously when solvated starch polymer is mixed with non-solvent, due to the free mobility of the modified starch chains. Starch pigment has improved affinity to paper surface and it can be used as such or mixed with other pigments to enhance the optical or printing properties of paper.

Starch-based pigmenting materials with improved optical performance were prepared in the laboratory by the complexation approach. Analytical results indicated that the complexation of carboxymethyl starch and inorganics strongly depends on the carboxymethyl group in the starch-based hybrid pigmented materials. The formed insoluble hybrids were mostly amorphous and the crystalline contribution of the inorganic component was not evident. The resulting precipitates exhibited composite structures.

Finally, three starch-based and two cellulose-based polymers were selected for flocculation and filtration tests. In shearless dewatering conditions, the retention and dewatering properties of the starch-based polymers were similar to those of commercial polyacrylamide-based polymers. The flow studies in higher shear

conditions showed that with the studied dosages the starch-based polymers could not reach the flocculation levels needed to maintain sufficient retention properties. The performance of the cellulose-based polymers as flocculating agents was less efficient. The reasons for the more limited performance of the polysaccharide-based flocculants were too low molecular weight and the charge density distribution. Better understanding of how to improve the hydrodynamic properties of bio-based polymers will be essential when planning new bio-based flocculants.

The deeper understanding of the relationships between the desired structures and properties of polysaccharides helps to utilize them more effectively. In this way it is possible to obtain better bio-based and environmentally sustainable products in the competition with the current products based on conventional petrochemistry.

Keywords cellulose, starch, derivative, industrial, application, structure, property

Selluloosan, tärkkelyksen ja niiden johdosten teollisia sovelluksia
Rakenteen ja ominaisuuksien tutkimuksia

Cellulose, starch and their derivatives for industrial applications. Structure-property studies.
Lauri Kuutti. Espoo 2013. VTT Science 31. 72 s. + liitt. 55 s.

Tiivistelmä

Selluloosa- ja tärkkelyspohjaisten materiaalien ominaisuudet eroavat toisistaan huomattavasti monissa teollisissa sovelluksissa perusyksiköiden rakenteellisista yhtäläisyyksistä huolimatta. Tässä työssä tutkittiin näiden polysakkaridien ja niiden valikoitujen johdosten rakenteen vaikutusta ominaisuuksiin viiden kattavan esimerkin avulla.

Ensimmäisessä työssä tutkittiin atomivoimamikroskoopilla hyvin kiteisen selluloosanäytteen Valonia macrophysa -rakkuloiden pintaa. Vesi todettiin merkittäväksi selluloosapinnan mahdollisena muokkaajana. Selluloosan pinnasta löydettiin monokliinisiä kidepintoja. Löytö tarkoittaa, että vesimolekyylit eivät pääse tunkeutumaan monokliinisiin selluloosapintoihin ja siten häiritsemään niitä. Toisaalta trikliinisten kidepintojen puuttuminen selitettiin johtuvan ilman nestekennoa toteutetusta mittausgeometriasta.

Kitkakuvaamisella seurattiin puolipysyvien kaura- ja ohralämpömuovautuvien tärkkelyskalvojen vanhenemista. Kalvot menettivät vanhenemisen seurauksena osan mekaanisista ominaisuuksistaan. Kaurakalvoissa pehmittimenä käytetty glyseroli tunkeutui tärkkelys-glyseroli-vesi-matriisista lämpömuovattavan tärkkelyksen pinnalle aiheuttaen alhaisen kitkan alueita. Ohratärkkelyskalvojen tapauksessa ikääntyminen aiheutti ensiksi polymeerien uudelleensuuntautumista ja lopulta amylopektiinihaarojen hitaan kiteytymisen.

Kolmannessa työssä liuoksista tuotettiin saostustekniikalla ideaalisen pyöreitä tärkkelysesteri-pigmenttejä (halkaisija on noin puolet näkyvän valon aallonpituudesta) mahdollisiksi täyteaineiksi paperin päällystyksiin. Partikkeleiden oletetaan saavuttavan muotonsa ja kokonsa spontaanisti muunnettujen tärkkelysketjujen vapaan liikkuvuuden takia, kun tärkkelysliuos sekoitetaan ei-liuottimeen. Tärkkelyspigmentillä on parantunut affiniteetti paperin pintaan, ja sitä voidaan käyttää joko sellaisenaan tai sekoitettuna muun pigmentin kanssa parantamaan paperin optisia tai painatusominaisuuksia.

Optisilta ominaisuuksiltaan parannettuja tärkkelyspohjaisia pigmenttimateriaaleja valmistettiin laboratoriossa kompleksoimalla. Analyyttiset tulokset osoittivat, että karboksimetyylitärkkelyksen ja epäorgaanisten komponenttien kompleksointi riippuu voimakkaasti tärkkelyspohjaisten hybridipigmenttimateriaalien karboksimetyyliryhmästä. Liukenemattomat hybridit olivat useimmiten amorfisia.

Viimeiseksi kolme tärkkelys- ja kaksi selluloosapohjaista polymeeriä valittiin flokkulaatio- ja suodatuskokeisiin. Leikkautumattomissa vedenpoisto-olosuhteissa tärkkelyspohjaisten polymeerien retentio- ja vedenpoisto-ominaisuudet ovat sa-

manlaiset kuin kaupallisilla polyakryyliamidipohjaisilla polymeereillä, joita käytettiin vertailuaineina. Virtaustutkimus suuremmissa leikkausvoimissa osoitti, että tutkituilla annostuksilla tärkkelyspohjaiset polymeerit eivät kykene saavuttamaan tarvittavia flokkulaatioita ylläpitämään riittäviä retentio-ominaisuuksia. Selluloosapohjaisten polymeerien teho flokkulantteina oli tärkkelyspohjaisia heikompi. Syy polysakkaridipohjaisten flokkulanttien rajoittuneeseen tehokkuuteen oli liian pieni molekyylipaino ja varaustiheysjakauma. Parempi tietämys siitä, kuinka biopohjaisten polymeerien hydrodynaamisia ominaisuuksia voidaan parantaa, on oleellista suunniteltaessa uusia biopohjaisia flokkulantteja.

Molekyylirakenteiden ja ominaisuuksien välisen yhteyden syvällisempi ymmärrys helpottaa polysakkaridien tehokkaampaa hyödyntämistä. Tällä tavalla on mahdollista saavuttaa parempia biopohjaisia ja ympäristöä säästäviä tuotteita kilpailtaessa nykyisten konventionaalisten petrokemian tuotteiden kanssa.

Avainsanat selluloosa, tärkkelys, johdos, teollinen, sovellus, rakenne, ominaisuus

Preface

The work was carried out in several projects during the years 1993–2011 at the VTT Technical Research Centre of Finland. The purposes or goals of the projects varied according to the prevailing scientific or business interests. Financial support from the VTT Research Programme on Biodegradable Plastics, VTT Nanopap project (Improvement of Optical Properties of Paper by Increasing Refractive Indices of Materials), VTT Fiber-based Innovation Chain, Finnish Funding Agency for Technology and Innovation (TEKES), Omya Oyj, J.M. Huber Finland Oy, UPM-Kymmene Oyj and M-real Oyj is gratefully acknowledged.

I am very grateful to Professor Jouko Peltonen from Åbo Akademi Universtity for sharing his knowledge in surface science and especially for the jointly spent hundreds of hours in a dark Faraday cage. My deepest gratitude is addressed to Soili Peltonen, who introduced me to the world of bio-based materials. I also thank the late Hannu Mikkonen for many fruitful and inspiring discussions about chemistry and life itself. I am very grateful to Jaakko Pere for inspiring discussions, active co-operation in many successful projects and for his contribution to the never-ending debate over whether biochemistry is more powerful than chemistry. Thesis plus antithesis means synthesis.

Professor Raimo Alen and Professor Matti Elomaa are thanked for their excellent review of the thesis and Michael Bailey for the language revision. Special thanks go to Dr. Klaus Niemelä for his unofficial, but invaluable advice during the process.

I warmly thank Dr. Leif Laaksonen for helpful advice and discussions, professor Jarl Rosenholm for providing use of the microscope, Professor Junji Sugiyama and Professor Henri Chanzy for providing their structural data before publication, and Dr. Andrepeter Heiner for valuable critical discussion. The late Professor Olle Teleman is also warmly acknowledged and remembered.

I thank my co-authors at VTT, Dr. Pirkko Forsell, Sanna Haavisto, Sari Hyvärinen, Kirsi Kataja, Riikka Koski, Dr. Hanna Kyllönen, Dr. Kaisa Putkisto, Pia Qvintus, Dr. Tapani Suortti; at Valio Dr. Päivi Myllärinen; at Aalto University Dr. Kimmo Koivunen, Prof. Hannu Paulapuro; at the University of Helsinki Prof. Markku Leskelä, Prof. Sirkka Liisa Maunu, Jere Tupala and Tommi Virtanen.

I also thank my colleagues Teija Jokila, Dr. Harri Setälä, Teuvo Kanerva and the other people in the Regiment of Rajamäki, in the laboratory and in the pilot facility. My humblest thanks go to them for friendship, criticism, coffee breaks and innumerable discussions.

Finally, my thoughts go to Pirkko, Pekka, Tuomas and Elina for making life worth living.

Academic dissertation

Supervisor — Professor Heikki Tenhu
Laboratory of Polymer Chemistry
Department of Chemistry
University of Helsinki
Finland

Reviewers — Professor Raimo Alen
Laboratory of Applied Chemistry
Department of Chemistry
University of Jyväskylä
Finland

Professor Matti Elomaa
Centre for Materials Research
Faculty of Chemical and Materials Technology
Tallinn University of Technology
Estonia

Opponent — Professor Tapani Vuorinen
Department of Forest Products Technology
School of Chemical Technology
Aalto University
Finland

List of publications

This thesis is based on the following five publications, which are referred to in the text by their Roman numerals I–V:

I Kuutti, L., Peltonen, J., Pere, J., Teleman, O. Identification and surface structure of crystalline cellulose studied by atomic force microscopy. Journal of Microscopy, 1995, 178, pp. 1–6.

II Kuutti, L., Peltonen, P., Myllärinen, P., Teleman, O., Forssell, P. AFM in studies of thermoplastic starches during ageing. Carbohydrate Polymers, 1998, 37, pp. 7–12.

III Mikkonen, H., Kuutti, L., Kataja, K., Qvintus-Leino, P., Peltonen, S. Novel method for preparation of spherical starch ester pigment with excellent optical properties in paper coatings. In: Ritschkoff, A.-C., Koskinen, J., Paajanen, M. (Eds.). Applied Material Research at VTT. Symposium on Applied Materials, Espoo, Finland, 2006. VTT Symposium 244. VTT Technical Research Centre of Finland. Pp. 235–243.

IV Kuutti, L., Putkisto, K., Hyvärinen, S., Peltonen, S., Koivunen, K., Paulapuro, H., Tupala, J., Leskelä, M., Virtanen, T., Maunu, S.L. Starch-hybrid fillers for paper. Nordic Pulp and Paper Research Journal, 2010, 25(1), pp. 114–123.

V Kuutti, L., Haavisto, S., Hyvärinen, S., Mikkonen, H., Koski, R., Peltonen, S., Suortti, T., Kyllönen, H. Properties and flocculation efficiency of cationized biopolymers and their applicability in papermaking and in conditioning of pulp and paper sludge. BioResources, 2011, 6(3), pp. 2836–2850.

Author's contributions to the publications

Publication I: Lauri Kuutti was in close cooperation with Dr. Peltonen, Mr. Pere and Prof. Teleman in drawing up the research plan. Lauri Kuutti performed all the molecular modeling activities, took part in the experimental Atomic Force Microscopy (AFM) measurements, converted the artificial AFM images from the calculated Connolly surfaces and analysed the results and wrote the manuscript with Dr. Peltonen and prof. Teleman.

Publication II: Lauri Kuutti was in close cooperation with Dr. Peltonen and Dr. Forsell in drawing up the research plan. Lauri Kuutti took part in the experimental AFM measurements and analysed the results of AFM images and wrote the manuscript with Dr. Peltonen.

Publication III: Lauri Kuutti took part in the experimental work by optimising the particle size distribution and producing the spherical starch ester pigments in close cooperation with Phil. Lic. Mikkonen and Phil. Lic. Peltonen and wrote the manuscript with them.

Publication IV: Lauri Kuutti was in close cooperation with Dr. Putkisto in drawing up the research plan and wrote the manuscript with her. Lauri Kuutti prepared the water insoluble starch-hybrid fillers for the optical tests, performed the air jet milling with Mr. Minkkinen and analysed the results with the other authors.

Publication V: Lauri Kuutti was in close cooperation with Dr. Kyllönen in drawing up the research plan and wrote the manuscript with Dr. Kyllönen and Ms. Haavisto, M.Sci. (Eng.). All chemically cross-linked cationised flocculants and the simple jar tests were performed by Lauri Kuutti.

Contents

Abbreviations

adSPHOS	Acetylated distarch phosphate
AFM	Atomic force microscopy
A-PCC	Aragonitic precipitated calcium carbonate
CCD	Charge-coupled device
^{13}C CP/MAS	Carbon 13 solid state cross-polarization magic angle spinning
CMC	Carboxymethyl cellulose
CMS	Carboxymethyl starch
C-PAM	Commercial polyacrylamide
DC	Direct current
DP	Degree of polymerisation
DMSO	Dimethylsulfoxide
DS	Degree of substitution
DSC	Differential scanning calorimetry
dSPHOS	Di-starch phosphate
Eh-type	an amylose single helix crystal type
ESCA	Electron spectroscopy for chemical analysis
EU	European Union
FAO	Food and Agriculture Organization of the United Nations
FFM	Friction force microscopy
FFT	Fast Fourier transform
FTIR	Fourier transform infrared
GPC	Gel permeation chromatography

HEC	Hydroxyethylcellulose
HES	Hydroxyethylstarch
HPS	Hydroxypropylstarch
IEA	International Energy Agency
IPCC	Intergovernmental Panel on Climate Change
ISO	International Organization for Standardization
LED	Light emitting diode
MFC	Microfibrillated cellulose
MS	Molecular substitution
na	not available
nd	not detected
NFC	Nanofibrillated cellulose
NMR	Nuclear magnetic resonance
NTU	Nephelometric turbidity units
PCC	Precipitated calcium carbonate
PDI	Polydispersity index
RH	Relative humidity
RI	Refraction index
SCIT	Starch citrate
SEM	Scanning electron microscopy
SPHOS	Starch phosphate
TGA	Thermogravimetry
TMP	Thermomechanical pulp
ToF-SIMS	Time-of-flight secondary ion mass spectrometry
TPS	Thermoplastic starch
TS	Total solids
Va-type	an amylose single helix crystal type
Vh-type	an amylose single helix crystal type
WAS	Waste activated sludge
WEA	World Economics Association

WEC	World Energy Council
XRD	X-ray diffractogram
XRF	X-ray fluorescence

Symbols

k	Spring constant
M_n	Number average molecular weight
M_w	Weight average molecular weight
T_g	Glass transition temperature

1. Introduction

1.1 Background

The efficient utilisation of polymers from renewable resources has attracted much attention in many fields as biodegradable alternatives to products derived from the petrochemical industry. It is estimated that the world is currently consuming petroleum at a rate 100 000 times faster than nature can replace it [1]. Widespread concern over greenhouse gas emissions creates both political and social pressure to find new innovative solutions to the production of energy, fuels and bio-based products.

The total live dry biomass on earth is about 560 billion tonnes organic bond carbon [2] and the total annual primary production of biomass is just over 100 billion organic bond carbon (56 billoin C/a for terrestrial primary production, and 48 billion tonnes C/a for oceanic primary production) [3]. Primary production is the production of organic compounds from atmospheric or aquatic carbon dioxide, principally through the process of photosynthesis.

The biomass consists of annual and perennial plants. The world's total aboveground forest biomass amounts to 420 billion tonnes, of which more than 40 % is located in South America [4–6]. The total sustainable world-wide biomass energy potential is about 100 EJ/a, from which the amount of woody biomass is 41.6 EJ/a, energy crops 37.4 EJ/a, straw 17.2 EJ/a and others 7.6 EJ/a. The amount of woody biomass energy potential is about 30 % of the total global energy consumption [7–8]. Only 6 billion tons of the annually produced 170–200 billion tons of biomass is currently utilised, and less than 3 % of this amount is used in applications, mostly for nutrition [9–10]. The total global agricultural area (4889 million hectares) was greater than world's forest area (4039 million hectares) in 2009 [11].

Bioenergy could in principle provide all the world's energy requirements, but its realistic technical and economic potential is much lower [12]. The World Energy Council (WEC) Survey of Energy Resources in 2001 estimated that bioenergy could theoretically provide 2900 EJ/a, but that technical and economic factors limit its current practical potential to just 270 EJ/a [13]. Annual oil extraction was about 160 EJ/a and the world oil reserves were 6263 EJ [12]. Table 1 summarises the world energy statistics for the year 2009.

Table 1. World energy statics in EJ/a by International Energy Agency (IEA) in 2009 [14].

Energy supply	**496.8**
Oil	164.5
Coal	134.1
Natural gas	104.5
Renewables & waste	49.6
Nuclear	29.6
Hydro	11.0
Other (geothermal, solar, wind, etc.)	3.5

Projections of WEC, World Economics Association (WEA) and Intergovernmental Panel on Climate Change (IPCC) estimate that by 2050 bioenergy could supply a maximum of 250–450 EJ/a, representing around one quarter of the global final energy demand.

The main components of biomass are cellulose, lignin, hemicelluloses and extractives and, as non-wood structural component, starch. Cellulose is the most abundant natural polymer. It exhibits biocompatibility and is insoluble in water and most organic solvents. It is also nontoxic, biodegradable, and inexpensive. Lignin is an amorphous, thermoplastic, three-dimensional polymer network consisting of phenolpropanoid units. Lignin binds the cellulose fibres together, providing wood with mechanical strength and rigidity to resist external forces. Hemicelluloses are heteropolysaccharides based on a variety of monosaccharides (xylose, arabinose, glucose, mannose and galactose) and are present along with cellulose in almost all plant cell walls. Cellulose is partly crystalline, strong and resistant to hydrolysis, while hemicelluloses have random and amorphous structures with little strength. They are easily hydrolysed by dilute acids, as well as by a group of enzymes. Hemicelluloses are partly water-soluble polysaccharides, but can be usually dissolved by alkalis [15].

Starch is the most abundant storage carbohydrate and is generated in many plants by photosynthesis. The starch molecules are stored in tubers, roots, seeds and fruits. Starch is composed of small granules which are insoluble in cold water [16].

Although a tremendous variety of biomass resources is available, only four basic chemical structures present in biomass are of importance for the production of fuels and products: monosaccharides and polysaccharides (sugars, starches, cellulose and hemicelluloses), lignins (polyphenols), triacylglycerides or lipids (vegetable oils and animal fats and proteins (vegetable and animal polymers made up amino acids) [16–17]. Table 2 presents chemical compositions of wood and non-wood feedstock. The DP of non-wood hemicelluloses is typically lower than that in wood [18].

Table 2. Chemical composition of wood and non-wood feedstock (% of the dry matter) [18].

Component	Wood feedstock	Non-wood feedstock
Carbohydrates	65–80	50–80
Cellulose	40–45	30–45
Hemicellulose	25–35	20–35
Lignin	20–30	10–25
Extractives	2–5	5–15
Proteins	< 0.5	5–10
Inorganics	0.1–1	0.5–10
SiO2	< 0.1	0.5–7

1.2 Structure-property relationships of glucans

1.2.1 Cellulose

1.2.1.1 General aspects

Cellulose is a linear polymer produced by plants. It is a structural polysaccharide and the most abundant natural polymer. It is a hydrophilic, highly crystalline polymer with high molecular mass. The degree of polymerisation (DP) may be as high as 15 000 and the molecular mass may be up to 2.4 x 10^6 g/mol. It is soluble in only the most aggressive solvents such as ionic liquids [19] and cannot be thermally processed because it degrades before it melts.

Cellulose is a linear homopolymer composed of the (1→4)-linked β-glucopyranose units (Figure 1). In 1838, Anselme Payen, a French chemist, reported that the cell walls of almost any plant are constructed of the same substance called les cellules (cellule = cell). Sponsler and Dore in 1926 were the first to put forward the idea that cellulose is built up of long parallel chains comprising glycopyranose units, thus reconciling the idea of long molecules with the relatively short spacing indicated by X-ray diagrams [16].

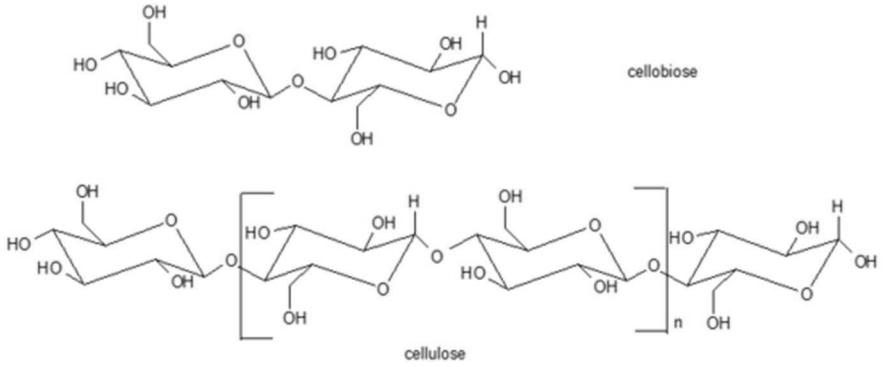

Figure 1. A molecular representation of the cellulose molecule and its basic unit, cellobiose.

The three-dimensional structure of crystalline cellulose has been the focus of several investigations (Figure 2) [20–23]. Atalla and VanderHart in1984 [24] showed by high resolution solid-state ^{13}C CP/MAS NMR spectroscopy that two phases, cellulose Iα (triclinic) and cellulose Iβ (monoclinic), coexist in several native celluloses [24]. The ratio Iα / Iβ varies greatly depending on the cellulose substrate. Whereas Iα-rich specimens have been found in the cell wall of some algae and in bacterial cellulose, Iβ-rich specimens have been found in cotton, wood and ramie fibres [25–26]. ^{13}C CP/MAS NMR spectroscopy was also used to show that the Iα phase is metastable and can be converted into the thermodynamically more stable Iβ phase by hydrothermal annealing [27–28]. Pure Iβ cellulose has been isolated from animal cellulose [29]. The unit cell parameters of both crystalline phases were published in 1991 [30] and the crystallographic structure of cellulose Iα was first reported by Nishiyama [31]. Iα and Iβ celluloses can be found not only within the same cellulose sample, but also along a given microfibril [30]. This dimorphism caused difficulties in interpreting X-ray fibre and electron diffraction patterns from algae samples [30]. The reason for these allomorphs of cellulose I in nature is still open for scientific discussion.

1.2.1.2 Supermolecular structure

Cellulose occurs in various crystalline forms, which vary slightly in the dimensions and angles of the unit cell [32]. The polymorphy of cellulose and its derivatives has been well documented during recent decades. Six polymorphs of cellulose (I, II, III_I, III_{II}, IV_I and IV_{II}) can be interconverted [22, 33–34]. Two polymorphs of cellulose I have now been found to be a mixture of two polymorphs Iα and Iβ. Cellulose II, which is thermodynamically the most stable crystalline form, can be found after re-crystallisation or mercerisation with aqueous sodium hydroxide [35–36]. Celluloses III_I and III_{II} [37–38] are formed from celluloses I and II, respectively, typically by treatment with liquid ammonia and the subsequent evaporation of excess am-

monia [39–40]. Polymorphs IV_I and IV_{II} are obtained by heating celluloses III_I and III_{II} respectively in hot glycerol [41]. In addition, cellulose is found abundantly in amorphous form, usually incorporated with cellulose I.

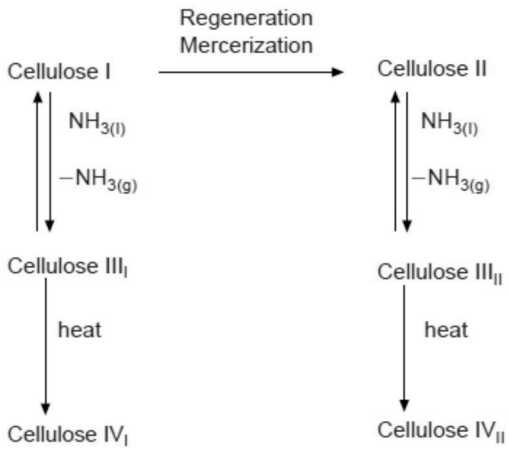

Figure 2. Interconversion of the polymorphs of cellulose according to O'Sullivan [32].

In many cellulose polymorphs there are two intermolecular hydrogen bonds between adjacent glucopyranose units and one intramolecular bond, which has been presented in many papers during recent decades [20–22, 24, 42]. The better molecular identification of the solid materials by new chemical or physical analytical equipment reveals more and more of the true structural details of the crystalline celluloses. The interpretations of inter- and intramolecular hydrogen bond systems in crystalline cellulose have improved. The dominant intramolecular hydrogen bond is O3-H---O5, which exists in both of the polymorphs. The difference appears in the intermolecular bonding: the dominant hydrogen bond for cellulose I is O6-H---O3, whereas cellulose II has its dominant bond at O6-H---O2. Cellulose II has an antiparallel packing, whereas the chains in cellulose I run in parallel directions [42–44].

The capability to form hydrogen bonds is essential for the supermolecular structures of cellulose. The strong hydrogen bonds are responsible for the rigid, linear shape of the cellulose chains. The supermolecular structures from wood fibres to smaller sub-units, in many cases user-defined terminological units such as micro- or elementary fibrils, reveal new fibre structures with characteristic crystalline surfaces [45]. The microfibrils form lamellas or bundles, sometimes also called macrofibrils, which are the primary components of wood fibre walls. Wood fibres are disintegrated first to macrofibrils, then to well-defined, homogeneous micro- or elementary fibrils and finally to fibrils. The degraded material is called microfibrillar cellulose or microfibrillated cellulose (MFC) [46–47]. The terms nanofibrillar cellulose (NFC) or nanocellulose are also used for these fibrils of nanoscale thickness [48–49]. Strong acid hydrolysis (e.g. the mineral acids HCl or H_2SO_4) combined with mechanical shearing produces a medium or high aspect ratio (20–200) and highly

crystalline nanowhiskers. They are also called colloidal cellulose, cellulose micelles, cellulose nanorods, cellulose nanocrystals, or nanocrystalline cellulose [50–51].

In higher plants the smallest cellulose structure is an elementary fibril, consisting of 36 parallel aligned and hydrogen bonded cellulose molecules in amorphous and crystalline regions (Figure 3) [45, 52]. The lateral dimension is 2–4 nm [53–54] and when a cellulose elementary fibril is joined or coated with other wood constituents, a microfibril is formed [52, 55]. A molecular structural model of a microfibril estimates the width of a microfibril to be 3–20 nm [47, 50, 54].

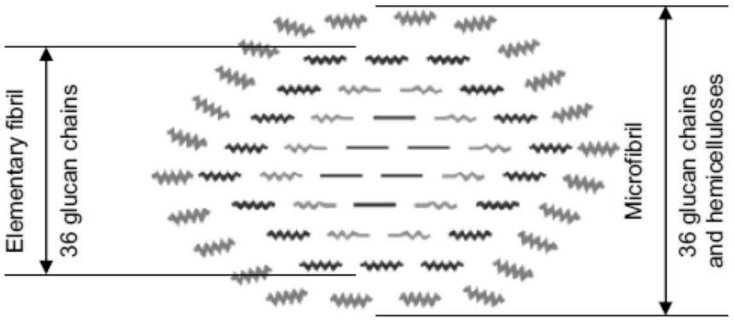

Figure 3. Molecular structural model (cross-section) of a microfibril containing a 36-chain elementary fibril [45]. Layers from inside out: 6 true crystalline glucan chains, 12 sub-crystalline glucan chains, 18 sub-crystalline or non-crystalline glucan chains, and an outer coating with 24 hemicellulose chains.

The characteristic crystal surfaces change depending on the relative amounts of cellulose Iα and Iβ (Figure 4). In Iβ there are two conformationally distinct chains in a monoclinic unit cell, whereas in Iα there is one chain in a triclinic unit cell [31]. The most common crystal surfaces of crystalline celluloses are for the monoclinic (110 and 1–10) and the triclinic (010 and 100) crystal faces [56]. The multiple possibilities for hydrogen bonding of O2 and O6 atoms are probably the reason why O2 and O6 are also the most reactive of the hydroxyl groups on the crystalline surface, whereas O3 is practically unreactive due to the strength of the intrachain O3-H---O5 bond [57].

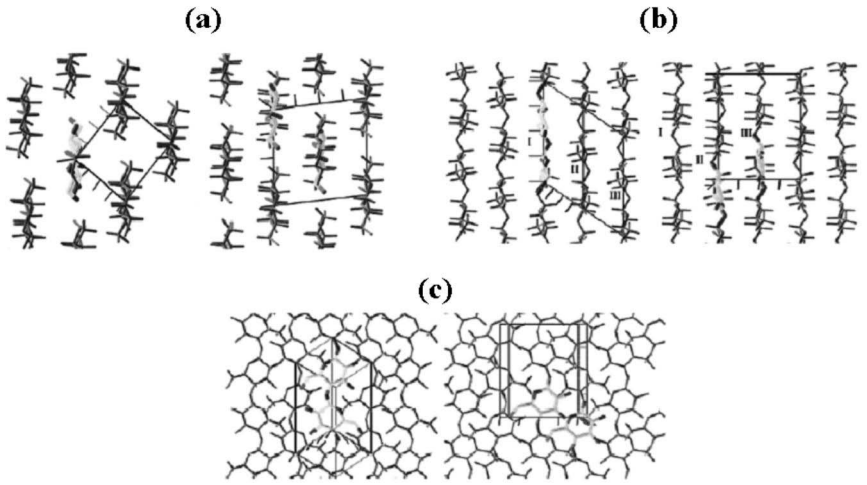

Figure 4. The unit structures of cellulose Iα (triclinic, left) and Iβ (monoclinic, right) in different projections: (a) down the chain axes, (b) perpendicular to the chain axis, and (c) perpendicular to the hydrogen-bonded sheets [39]. Adapted from Kontturi [57].

High degree of crystallinity in cellulose samples means stronger mechanical properties. The degree of crystallinity varies from 40 % to 90 % depending on the origin of the samples. In hardwood the crystallinity is between 32 % and 35 % and in softwood between 37 % and 42 %. The crystallinity of cellulose in wood pulps is between 60 % and 70 % [18]. *Valonia* celluloses have a degree of crystallinity in excess of 90 % [41]. The ultimate example is highly crystalline nanowhiskers, which have very good mechanical properties for advanced applications. The stiffness of crystalline cellulose has been shown to be of the order of 140–220 GPa, which is similar to that of Kevlar and even higher than that of glass fibres; both these fibres are used commercially to reinforce plastics. Films made from nanocellulose have been shown to have high strength (over 200 MPa), high stiffness (around 20 GPa) and high strain (12 %) [58].

1.2.2 Starch

Starch is a polysaccharide that is present in plants with the function of storing energy. It is produced in the form of spherical granules in roots, seeds, tubers, stems, leaves and fruits of plants [59]. The size of granules varies based on the origin of the starch from 1 to more than 100 µm. It is commercially produced worldwide from maize (80.9 %), wheat 8.6 %, potato (5.3 %), rice and tapioca (5.1 %). These plants produce a large amount of starch, 60–90 % of the plant's dry mass. Starch occurs as semi-crystalline small particles, which are insoluble in water at room temperature. Starch is a homopolymer of glucose consisting of the

α-(1→4)-linked amylose and the α-(1→4)- and the α-(1→6)-linked amylopectin (Figure 5). Amylose is essentially a linear polymer (M_w 10^5–10^6 g/mol), whereas amylopectin is highly branched (M_w 10^7–10^9 g/mol) [59]. The chains of amylose form single or double helices [60]. The linear outer chains of the amylopectin form left-handed double helical structures with strong hydrogen bonding of the hydroxyl groups. Several types of crystallinity are observed in the granules, denoted as A-, B- or C-type [61–64]. The crystalline regions are arranged as thin lamellar domains [65–66]. In nature, the crystallinity of starch granules varies from 15 % to 45 % depending on the source. Native starch is biodegradable in water and is relatively stiff and brittle. By increasing the amylose content the material becomes more flexible and stronger [67].

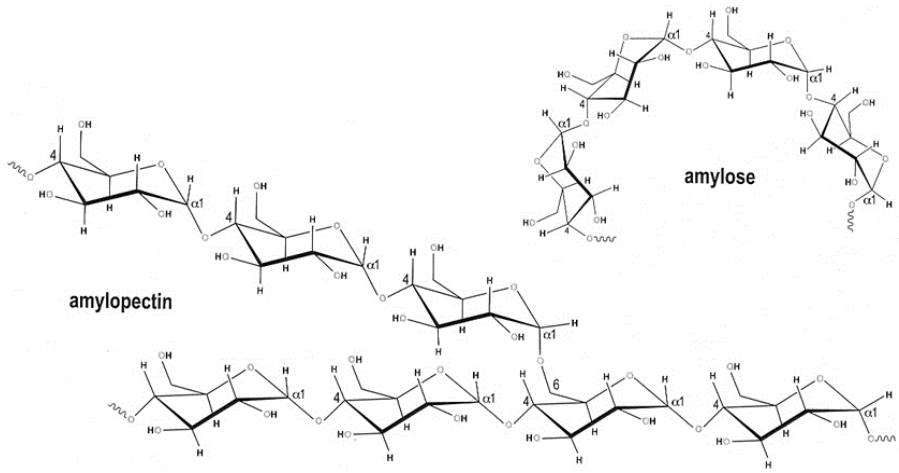

Figure 5. A molecular representation of the two components of the starch molecule.

Most starch used commercially is modified; the modification can be effected either chemically or mechanically [16]. Chemically this is done by modifying the three hydroxyl groups present on the glucose repeating unit. Starch can, for example, be modified by reaction with acetic acid, succinic acid, ethylene oxide, propylene oxide, sodium tripolyphosphate and cationisation agents. Ionic groups may be introduced into the starch backbone by etherification. Anionic starches are used in construction, sizing and textile printing. Cationic starch ethers are mainly used in the paper industry and as flocculants and as retention chemicals. Cross-linking of starch is also an important reaction and the main target of cross-linking is to increase shear stability and to impart better thickening properties (Figure 6).

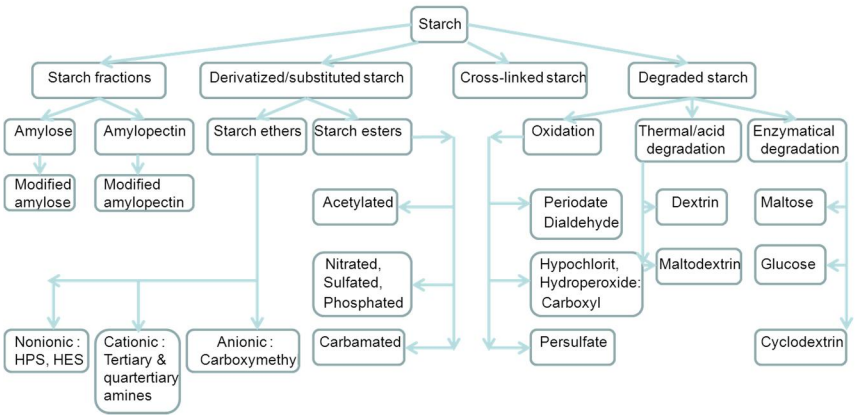

Figure 6. Types of starch modification [16]. HPS=hydroxypropylstarch and HES= hydroxyethylstarch.

Starch can be processed to mouldable thermoplastic material at high temperature under shear [68–69]. During processing the semi-crystalline structure is lost and the molecules are partially depolymerized into a homogeneous, amorphous polymeric material. If water is used as plasticiser the product is brittle, but in the presence of other plasticisers, such as glycerol, materials with varying mechanical properties can be prepared. Even if stored at constant humidity and temperature the mechanical properties of thermoplastic starch (TPS) films change with time [70]. As a new innovation, the German company Biotec produces TPS resins and owns a large number of patents for extrusion technologies, blending and modifying of thermoplastic processable starch [10]. Biotec has pilot scale facilities for blown film extrusion. It produces a range of plasticiser-free thermoplastics under the brand-name Bioplast®, and a pure thermoplastic starch, Bioplast® TPS.

The properties of processed starch (thermoplastic starch) will depend on a number of factors, such as amylose content, molecular mass, crystallinity, humidity, process method and time [67]. The crystallinity of amylose takes many forms. Single-helical amylose crystals are denoted in literature as Va, Vh and Eh by comparison of the diffraction data of the TPS materials with literature and diffraction data of the prepared reference compounds [71]. The humidity will have a great impact on the properties of TPS due to the fact that water acts as a plasticiser. High humidity starch films are therefore soft and flexible, whereas low humidity starch films are brittle and weak. Starch has low permeability to oxygen and can therefore be used for food packaging. Sensitivity to humidity and rapid ageing due to water evaporation from the matrix make TPS unsuitable for many applications. Foamed starch has also been formed into plates, cups and packaging cushions.

1.3 Modification technologies

1.3.1 Cellulose

Cellulose is the major constituent of paper, paperboard and card stock and of textiles made from cotton, linen and other plant fibres. The technical and industrial utilisation of lignocellulose-containing materials has focused on paper and pulp production, soluble cellulose derivatives such as viscose and other cellulose-based synthetic fibres, wood-based sugar production, wood liquefaction and nitration of cellulose. The main modification technologies are chemical reactions in heterogeneous and in homogeneous conditions [72–73].

Cellulose can be converted to other useful products by reorientation of its fibre structure. The most important chemical pulping processes are sulphate and sulphite pulping, which produce the fibres for paper and board production. In mercerisation, cotton is treated in a 10–25 % caustic soda solution under stress. The process increases the diameter of the fibres, shortens them and gives a high lustre. The cellulose crystal form changes from cellulose I to cellulose II [72]. Hydrocelluloses are produced by the hydrolytic degradation of celluloses. These microcrystalline celluloses are used in the foodstuff industry as non-digestible thickeners and stabilisers [74].

In the regeneration of celluloses, the cellulose molecules are dissolved and then regenerated in the form of fibres [10]. The viscose fibre industry is the oldest man-made fibre business in the world and the commercial production began in 1905 [72]. During the dissolving process the DP is drastically reduced. Disadvantages are the treatment of the enormous quantities of water used and the generally poor fibre properties. Cellulose can be converted into cellophane, a thin transparent film, and into rayon, an important fibre that has been used for textiles. These fibres are called “regenerated cellulose fibres”. An environmentally friendly method to produce rayon is the Lyocell process [75].

Cellulose is used to make water-soluble adhesives and binders such as carboxymethyl cellulose (CMC). Cellulose fibres are also used in liquid filtration, sometimes in combination with diatomaceous earth or other filtration media, to create a filter bed of inert material. Cellulose is further used to make hydrophilic and highly absorbent sponges [10, 76].

1.3.2 Starch

Starch production technologies depend on the type of raw material, because there are some basic differences between cereals, roots and tubers [10, 16]. Native starch has a granular structure and it is used in this form in only a few specific applications. Natural starch can be modified chemically, physically and enzymatically or by a combination of these methods. For normal applications starch is converted into a hydrated or gelatinized form. One important factor which must be taken into account in starch processing is depolymerisation. Above 160–180 °C

depolymerisation of starch occurs, resulting in a rapid drop in intrinsic viscosity. The physical or chemical factors involved are temperature, shear stress, shear rate, residence time, water content and plasticiser/chemical content. The four main modification technologies are slurry processes, dry reactions, paste reactions and extrusion cooking [10, 16, 67].

In slurry processes (heterogeneous condition), the grain structure of starch remains substantially unchanged. Starches are usually suspended in aqueous solution with continuous circulation and are treated chemically, physically or enzymatically. The maximum slurry concentration, from

20 % to 50 %, depends on the extent of swelling. The modified starches are usually washed free from chemicals and salts, drained and dried in dryers [10, 16, 77]. In dry process, the starches are dried under vacuum and then subjected to thermal treatments at high temperatures up to 180 °C with or without the addition of chemicals. The granular structure is changed slightly during dry reactions [10, 16, 77].

Paste reactions are performed under homogeneous reaction conditions to obtain a high degree of substitution (DS). In these processes starches are converted into an amorphous structure by steam or alkali gelatinization and subsequently subjected to high temperatures over a relatively short period of time. The technology is applied to concentrations of up to 40 % dry mass, but because of the high viscosity the reactions need vigorous mixing [10, 16, 77].

Extrusion has become an increasingly important method of processing starch-based products. Extrusion is a thermo-mechanical process in which softened or plasticised materials are forced by pressure through a die or an opening to create a specific form [16, 77].

Derivatisation of native starch can be achieved by extrusion, slurry/paste or dry/semi-dry processes. In these processes, starch molecules are degraded, chemically modified by functional groups or changed by hydrothermal properties [10, 77]. The aim of derivatisation is to change the natural properties of starch (for example by adding hydrophobic or hydrophilic ionic substituents or altering the molecular mass) and to introduce new properties in order to allow application of the starch in different areas without losing too many of the original structural properties. The most widespread use of starch and starch derivatives in the European Union (EU) is the paper, board and corrugating industry (approximately 70 % [10]). Other important fields are binding materials in textile finishing, adhesives, cosmetics, pharmaceuticals, construction, paints, crude oil extraction, agrochemicals and starch plastics such as starch blends and starch composites [10].

1.4 Comparison between cellulose and starch

Cellulose does not dissolve in water and the reason is the high crystallinity and as a consequence of crystallinity, a high melt enthalpy [72]. The higher the degree of crystallinity in cellulose samples, the stronger are the mechanical properties. It is also tasteless and odourless. Although some forms of cellulose can be safely eaten by humans, e.g. the outer shells of corn, the animals that really can digest

cellulose are few. Termites and cud-chewing cows, deer, or buffalo, can utilise enzymes that break cellulose down into glucose [78]. In contrast, starch is edible and can be safely eaten by humans due to the presence of enzymes that can break it down into glucose [16].

Untreated starch becomes soluble in water when heated due the starch gelatinization process. The granules swell and burst, the semi-crystalline structure is lost and the smaller amylose molecules start leaching out of the granule, forming a network that holds water and increasing the mixture's viscosity [79]. Unlike amylopectin, amylose is insoluble in water. It also reduces the crystallinity of amylopectin and hinders infiltration of water into starch. The higher the amylose content, the less expansion potential and the lower the gel strength for the same starch concentration [80]. The two fractions of starch have different specific properties. Amylopectin is responsible for the partial crystallinity of starch, with the crystalline properties resulting from clusters of layers of the amylopectin molecules. The crystalline units are separated by amorphous layers of amylose molecules [16].

1.5 Specific applications of glucans

1.5.1 Pigments and fillers

Inorganic pigment and filler materials are used to improve optical and printability properties as well as the cost performance of paper [81–82]. Plastic coating pigments typically consisting of petroleum-derived, modified polystyrene have been used only for special printing applications to replace mineral pigments. The reasons for utilisation of mineral materials are cost-effectiveness, availability, high brightness and opacity.

The opacity goal of starch-based non-mineral paper pigments and fillers has been approached from three different directions. The first approach has been to process rigid, water-insoluble pigment particles of modified starch with particle sizes optimised for maximum light scattering [83–85]. In the second approach, relatively rigid and porous pigment particles have been formed. The assumption has been that appropriate pore structure in rigid pigment may increase its light scattering properties [86]. The third approach abandoned completely the solid and rigid pigment structures and has been based on creation of light-scattering interfaces using foam or microcapsules. A stabilised rigid foam structure coated on paper and containing suitably sized microcapsule structures may also contribute to improved light scattering [87].

The contribution of inorganic fillers to the light-scattering properties of paper is partly based on their preventive effect on bonding between fibres. This is, however, also observed as decreased strength, limiting the possibilities to increase the filler content of paper above the current level. Furthermore, at high filler content, the paper bulk is usually reduced, due to the relatively high specific gravity of inorganic fillers. The bulk is further reduced in calendaring [81]. Fillers also contribute to the light scattering effect by increasing the number of solid-air interfaces

in the paper structure. However, the refractive indices (RI) of current fillers are usually close to that of cellulose, restricting the light scattering effect on the filler-fibre interfaces [86–87].

1.5.2 Flocculants

Due to legislation and increased taxes, landfills are rapidly being eliminated as a final destination for wastes in Europe [88] and other disposal methods are becoming more important. Waste activated sludge (WAS) is a difficult type of sludge to dewater and its dry solids content after traditional dewatering processes can still be less than 15 %. Cationic flocculants, but also anionic and non-ionic flocculants, are needed for mechanical dewatering depending on the sludge to be handled. Synthetic flocculants are highly efficient, but they have poor biodegradability infertilizer use, and the environmental aspects of these compounds are more and more in the focus of a critical discussion. In Germany sludges treated with polyacrylamides will be excluded from disposal in areas under cultivation by the end of 2013 [89].

The cationising agent most commonly used today is 2,3-epoxypropyltrimethylammonium chloride or, alternatively, a corresponding cationising agent with a chlorohydrin functional nature [90]. The cationised starch compounds are stable over a very wide pH range. This characteristic is advantageous during long term storage, since high pH range gives an increased resistance to microbiological attack. The flocculation efficiency of the various cationic starches depends on (a) the amino group type and follows the order: quaternary > tertiary > secondary > primary and (b) the chemical structure of the flocculants, i.e. the flocculants prepared by grafting have higher flocculation efficiency than those prepared via etherification.

Bio-based flocculants can be produced from starch (amylose- and amylopectin-based) [91], cellulose [92], chitosan [93–94], phosphate-modified glucomannan [95], or by grafting acrylamide onto natural polysaccharides such as guar gum [96] and carboxymethyl cellulose [97]. Starch derivatives have the potential to replace petroleum-based flocculants and chelating agents [98–99] in applications in which their use is limited by environmental regulations.

1.6 Aims of the present study

Despite the similarity of their structural basic units, cellulose- and starch-based materials behave differently in many applications. The capability to form hydrogen bonds is an essential characteristic of all polysaccharides, including these glucans. The more complex the polymeric structure and the chemical interaction system, the greater is the diversity of the physical structures that are found. The polysaccharides can be converted into useful products by opening and reorientation of their native structure. For this reason, to obtain relevant data on the structure and properties of complex polysaccharide-based materials, the aims of this study were:

- to understand the influence of water on the surface structure of highly crystalline cellulose. Only a few agents can disrupt the hydrogen bonding system of crystalline cellulose and thus influence on the surface structure of cellulose.
- to elucidate the ageing phenomena of metastable TPS films. The material properties changed during ageing phenomena and conventional analytical methods could not give any clear indication of the reasons for the material changes. Are the reasons for the behaviour of TPS films based on the differences of the linear or branched starches?
- to produce and identify spherical starch ester pigments with improved optical properties.
- to produce insoluble hybrid materials for filler application by the complexation approach using soluble starch derivatives and inorganics.
- to produce biodegradable bio-based flocculants and to evaluate their potential as papermaking retention and dewatering aids.

2. Experimental

This section summarises the used materials, the synthetic methods and the characterisation of the studied materials. Due to the large number of different materials, the description of the materials has been simplified as much as possible. Details of the methods used are given in the original publications I–V.

2.1 Materials

2.1.1 Cellulose and starch samples

Highly crystalline *Valonia* celluloses contain 60 % to 70 % of the Iα crystalline phase. *Valonia macrophysa* vesicles were pretreated with dilute alkali and an excess of distilled water to remove residual hemicelluloses. Small vesicle pieces (2 mm x 2 mm) were placed on sample stubs (Paper I).

Thermoplastic barley and oat starch films were prepared by plasticisation of a starch/glycerol/water mixture in a twin screw extruder and processing the plasticised mixture to films in a single screw extruder. The processing was repeated three times to ensure homogeneity. Water content of the feed was about 12 % by mass and glycerol content 30 % by mass (dry basis). The fresh films were near-transparent. The ageing occurred under controlled conditions by storing for one to five weeks at constant, relative humidity (RH) and temperature (RH 50 %, 20 °C) (Paper II).

Chemically cleaved starch acetate (M_w 50 000–250 000 g/mol with DS value of 2 to 3, glass transition temperature 158–160 °C and ISO brightness value 88) was used as starting material for preparation of highly porous precipitated starch acetate. In the method, 60 g starch derivative was dissolved in a mixture of 200 ml alcohol, 300 ml acetone and 50 ml water at 40 °C and after complete dissolution, 300 ml alcohol was added to the solution. Water (2000 ml, 60 °C) was added rapidly to the starch acetate solution with continuous stirring at 150 rpm. The water contained 5 g surface-active agent to prevent agglomeration of the primary particle. During the dilution step a milky particle dispersion was formed. The formed dispersion was evaporated from the organic solvents at 60 °C for several hours to remove especially acetone, which was a good plasticiser of starch acetate derivatives.

After evaporation of the acetone and ethyl alcohol, 3 wt% $NaNO_3$ was added to the dispersion in order to salt out the formed particles to the bottom of the bottle. The precipitation was washed twice with an excess of water to remove the small particles and impurity agents. The product was collected by centrifugation and the dry content was between 20 % and 30 % (Paper III).

The precipitation experiments were performed by mixing aqueous solutions of the anionic starch derivative and the inorganic component. The polymer components were carboxymethyl starch (CMS), starch citrate (SCIT), starch phosphate (SPHOS) and commercial distarch phosphates (dSPHOS) and acetylated distarch phosphates (adSPHOS). The prepared aqueous solutions typically contained 1 g polymer in 20 ml distilled water (Paper IV).

Starch was phosphorylated by a reaction with mono- and disodium hydrogen phosphate under dry conditions at elevated temperature. Native potato starch was slurried in the solution and the mixture was stirred and conditioned overnight at room temperature. The mixture was placed in an oven in an open dish to dehydrate at 50 °C for 24 h and the dry mixture was ground in a mortar mill. The oven temperature was adjusted to 130 °C and the dried and ground mixture was allowed to react further for 3 h. The reaction product was washed with an excess of water, the precipitate was dried and the water-soluble part was ultrafiltrated and freeze-dried. The soluble fraction was used in the further experiments (Paper IV).

Citric acid was dissolved in water under constant stirring and adjusted to pH 3.5 with aqueous sodium hydroxide. Starch was added into the solution and the mixture was conditioned overnight at room temperature. The mixture was placed in an oven in an open dish to dehydrate at 50 °C for 24 h. Reaction products were washed with an excess of water. The precipitate was dried and the water-soluble part was ultrafiltrated and freeze-dried. The soluble fraction was used in the trials (Paper IV).

The synthesis of CMS was carried out in two steps. In the first step, alkalisation was performed by mixing hydrolysed starch, ethanol and aqueous sodium hydroxide at room temperature. The reaction mixture was stirred for 20 minutes, then monochloroacetic acid was added and the reaction mixture was heated up to about 58 °C and stirred at this temperature for 4 h. The sample was purified by dissolving in water, neutralised and precipitated with ethanol. Precipitated sample was filtered and dried under vacuum at 40 °C (Paper IV).

Two hybrid materials were selected to be prepared using a larger batch size for filler studies. The polymer component was CMS (DS 1.06), 100 g dissolved in 2000 ml water. Similar masses and concentrations of aqueous solutions using $BaCl_2$ and $ZrO(NO_3)_2 \times H_2O$ were also prepared. The pH of the barium-containing mixture was kept at 9.1 and the pH of the zirkonium-containing mixture was adjusted from the original 1.8 to 6.0. The formed precipitates were recovered by filtration, washed with ethanol and oven-dried at 50 °C (Paper IV).

For the jar test, various starch-based materials, such as enzymatically hydrolysed potato starch (N %: 0.4–2.8 %), hydroxypropylated starches or acetylated potato starch (DS 0.9–2.5), maize starch (amylose rich, N %: 1.3–1.6 %), or enzymatically hydrolysed barley starch (N %: 0.66 %) were chemically or enzymati-

cally modified before the cationisation. The starting material for the cationised modification of CMC, lignin and chitosan were commercial samples. The flocculants had not been optimised for further studies with respect to molecular mass, molecular mass distribution, chemical structure of the polymers, or the nature or ratio of functional groups on the polymeric backbone (Paper V).

2.1.2 Inorganic salts

The criteria for selection of the inorganic salts were solubility in water and, if available, the refractive index values obtained from the literature. Table 3 summarises the solubility of the used inorganic salts. These salts were calcium chloride ($CaCl_2$), barium chloride ($BaCl_2$), zinc acetate [$Zn(O_2CCH_3)$], zinc acetyl acetonate [$Zn(OCCH_3CHCOCH_3)_2$ x H_2O], zirconium nitrate [$Zr(NO_3)_4$ x H_2O], zirconyl nitrate hydrate [$ZrO(NO_3)_2$ x H_2O], zirconium oxochloride ($ZrOCl_2$ x H_2O) and titanium potassium oxalate [$TiO(OCOCOOK)_2$]. All the chemicals were commercial ones used as received without further purification and the chemicals were of technical grade (Paper IV).

Table 3. Solubility values and appearance of aqueous solutions of the inorganic salts used.

Inorganic salt	Solubility in grams per 100 ml cold water	Solubility, 1 gram in 20 ml cold water
calcium chloride	74.5	soluble, clear
barium chloride	37.5	soluble, clear
zinc acetate	30	soluble, clear
zinc acetylacetonate	very soluble	soluble, milky
zirconium nitrate	very soluble	soluble, milky
zirconyl nitrate hydrate	na	soluble, milky
zirconium oxychloride	na	soluble, clear
titanium potassium oxalate	na	soluble, clear

2.1.3 Flocculants

Cellulose- and starch-based polymers with different charge densities and molecular masses were screened in pre-tests and the best ones were chosen for flocculation and filtration tests (Table 4, A–E). The pre-tested flocculants were further modified and compared to commercial polyacrylamide-based flocculants (C-PAM) used in industry (Table 4, F–I). The starting material was hydroxypropyl starch (M_w 2 300 000 g/mol) made in a pilot plant [100]. As a hydroxyethyl cellulose sample, Aqualon's Natrosal 250 MBR (M_w 220 000 g/mol) was used. To increase the molar mass of selected samples, epichlorohydrin was used as a cross-linking agent. The cross-linking and cationisation of the hydroxypropyl starch sample was carried out as follows: an aqueous suspension of 70 g hydroxypropyl starch and 0.5 ml

epichlorohydrin in 1000 ml water (pH > 11) was stirred at low speed at room temperature and then stirred for 1 hour at 60 °C. On the next day, 35 g 50 % NaOH (catalyst for the cationic reaction) and 85 g Raisacat 151 (2,3-epoxypropyltrimethylammonium chloride) were added to the solution at room temperature and stirred for 10 hours at 80 °C. The pH of the suspension was adjusted to 7.0 and the product was purified by ultrafiltration and freeze dried.

The aim was to examine the applicability of new organic flocculants in conditioning of WAS from a paper mill. The sludge was coagulated with ferric sulphate and/or flocculated using flocculants with different charge densities and molecular masses (Table 4) (Paper V).

Table 4. Flocculants used in flocculation and filtration tests and the information of modified polymers. HPS = hydroxypropyl starch, HEC = hydroxyethyl cellulose and C-PAM= commercial cationic polyacrylamide and PDI = polydispersity index.

Polymer	Charge density [meqv/g]	M_w (g/mol)	M_n (g/mol)	PDI	Material	Special information
A	+0.78	2 300 000	330 000	7	HPS	
B	+0.95	220 000	67 000	3.3	HEC	
C	+1.1	2 220 000	300 000	7.5	HPS	Cross-linking product of A
D	+3.74	2 080 000	430 000	4.9	HPS	Cross-linking product of A
E	+0.33	170 000	32 000	5.2	HEC	
F	~+1	~5–7 000 000	-	-	C-PAM	Comm. flocculant
G	~+1	~1 500 000	-	-	C-PAM	Comm. flocculant
H	~+1.2	~9 500 000	-	-	C-PAM	Comm. flocculant
I	~+1.2	~4 500 000	-	-	C-PAM	Comm. flocculant

2.2 Characterisation

2.2.1 Crystalline cellulose surfaces by AFM (Paper I)

A combination of molecular modeling and atomic force microscopy (AFM) techniques was used to study the surface structure of crystalline cellulose. A Nanoscope II AFM with a 100 µm cantilever tip with a spring constant of k = 0.38 N/m was used to image the samples [101]. All images (400 x 400 pixels) were measured in air. Both height (constant deflection) and force (tip deflection is recorded according to the topographical changes on the sample surface) modes were used. The measuring unit was placed on a vibration-isolating table to eliminate external noise. In addition, high-pass filtering via both the electronics and software was used to cut off low-frequency noise.

2.2.2 AFM studies of thermoplastic starch surfaces (Paper II)

Small pieces of TPS films (4 mm x 4 mm) were cut and placed on sample stubs. All images were measured in air in the constant force mode (constant deflection). The roughness values were measured for images of the same size, 5 µm x 5 µm. When the tip is scanned sideways, the friction force causes a torsion in the tip cantilever. A micrograph showing this torsion is termed friction force microscopy (FFM) [102–104] and can be used e.g. to resolve different phases in phase-separated thin films [105]. The friction images were measured during retrace scanning, meaning that dark colour indicates high friction and light colour low friction. The microscope was placed on a vibration damping table to eliminate external noise.

2.2.3 Connolly surfaces and artificial AFM images (Paper I)

A Connolly surface is a solvent-excluded surface (also known as the molecular surface), which is imagined as a cavity in bulk solvent. It is calculated in practice via a rolling-ball algorithm, first implemented three-dimensionally by Connolly [106]. The Connolly algorithm was used to generate the solvent accessible surfaces for crystalline cellulose faces, starting from the atomic coordinates [107]. The Connolly surface is the surface described by the centre of a probe sphere rolling over the actual surface and was calculated with the Discover program [108].

The artificial AFM images were generated from the generated Connolly surfaces of the crystal faces, i.e. one layer of cellulose chains containing 7–9 chains each with 9–12 glucose units depending on the crystal face. Each crystal face was rotated into the xy-plane with the cellulose chains parallel to the y-axis. The generated crystal face was rectangular (dimensions of the order of 20–40 Å) and typically limited by four glycosidic oxygen atoms. The z-coordinate as a function of x- and y-coordinates was extracted from the Connolly surface and copied until the desired image size (13–14 nm) and resolution (200 x 200) were reached. Finally the height information was scaled to the vertical scale used in the AFM image (from 0 nm to 1.36 nm).

2.2.4 Filler particles (Paper III)

The produced filler particles were analysed by scanning electron microscopy (SEM) in order to provide information concerning the morphology of the primary particles and by Coulter® N4 Plus Particle Size Analyzer to determine the particle size distributions.

2.2.5 Components and formed hybrids (Paper IV)

The DS of CMS was determined by potentiometric titration. The degree of phosphorylation was determined by total phosphorus content. The thermal characteristics of the derivatives were determined by differential scanning calorimetry (DSC) and thermogravimetry (TGA). The chemical structures of modified polymers and formed insoluble hybrids were evaluated using Fourier transform infrared (FTIR) spectroscopy.

RI of solid particles was evaluated according to the Becke line test in immersion liquids. An optical transmission microscope and a set of immersion liquids in the RI range of 1.40–1.70 were used. The fine-ground sample, immersed in a drop of a test liquid, was placed on the glass slide and covered with a cover glass. When the RI of the sample and the liquid level were the same, the crystals appear transparent and their edges fade [109].

X-ray diffractograms (XRDs) were measured with a PANalytical X'Pert Pro MPD diffractometer using CuK(α) radiation detected with a PIXcel detector. All solid state NMR spectra were measured with a Varian Unity INOVA 300 spectrometer.

The grinding of formed hybrid precipitates was performed using a Hosokawa Micron Multi-processing System equipped with Alpine Fluidised Bed Opposed Jet Mill 100 AFG, a classifier and a feed cooling system. Cooling of the sample container and the feeding screw was with liquid nitrogen and the classifier speed was 7000 rpm.

A combustion analysis was made using a standard method to obtain the dry contents and mass fraction of inorganic components. The samples were first dried at 105 °C overnight to assess the dry content. After drying the samples were annealed at 550 °C to determine the ash content.

The element composition of the ground samples was determined using a Philips PW2404 X-ray fluorescence spectrometer (XRF) and semi-qualitative SemiQ-software. Fluorine and heavier elements were analysed.

The particle size distributions of the ground products were measured in water using a laser light scattering analyser. SEM analysis was used for particle morphology examination after a thin gold coating.

2.2.6 Flocculants (Paper V)

Quantitative determination of nitrogen in chemical substances was performed by the Kjeldahl method. Gel permeation chromatography (GPC) was used to analyse molar mass distributions and mass average molar masses. The molar masses of the cross-linked samples were also evaluated by the viscosity measurement with a Brookfield DV-II+Pro viscometer at 25 °C. A simple jar test was conducted as a pre-test for examination of the applicability of new organic flocculants. 4 beakers of a suspension of 0.05 % kaolin or 0.1 % thermomechanical pulp (TMP) fines were used for flocculation studies at pH 4 and pH 7. Immediately after the addition

of flocculants, all the suspensions were stirred at a constant speed of 100 rpm for 10 min, followed by slow agitation at 40 rpm for 10 min. The suspensions were then allowed to settle for 15 min. The turbidities of the suspensions were measured with a Hach Model 2100P Portable Turbidimeter. The dose of flocculants was varied within the range of 0 ppm to 4 ppm.

2.2.7 Sludge treatments (Paper V)

Two different types of laboratory-scale dewatering methods were tested for WAS: batch type gravity filtration and continuous belt filter pressing. Gravity filtration tests were carried out using a filter cloth in a funnel, when the sludge was coagulated and/or flocculated in a separate mug and decanted to the funnel in an identical manner. Success of the filtration was determined by measuring the amount of filtrate, the dry solid content of the gathered cake and the filtrate, and the turbidity of the filtrate.

Drainage and retention efficiency of each polymer were studied with a laboratory-scale drainage device. The experiments were carried out with a typical news furnish containing 30 % of filler with initial total consistency of 8 g/l. After the measurement, the filtrate in the flask was collected and analysed for turbidity. The efficiency of the polymers was evaluated as the change in the dewatering rate and the change in turbidity of the filtrate.

The state of flocculation in the furnish after addition of the polymers was studied in a laboratory flow loop system with a contraction channel simulating the conditions in the headbox of a paper machine. The average size of flocs was determined downstream after the abrupt contraction in the slit channel using a pulsed light emitting diode (LED) light source and a fast charge-coupled device (CCD) camera. After correcting the images for uneven illumination, the floc size was determined in the flow direction and the transverse direction as a run-length average of the median thresholded image [110–112]. The retention efficiency was evaluated by calculating the mean intensity and deviation of the intensity of the light transmitted through the channel. The light scattering efficiency of pulp decreases as the filler particles attach onto fibres. As a result, the mean intensity and deviation of intensity increase when more light is able to pass the pulp layer flowing in the channel.

3. Results and discussion

3.1 Characterisation of the chemical systems by image analyses

3.1.1 Surface structure of crystalline cellulose by AFM measurements (Paper I)

Hundreds AFM images were taken in order to obtain high quality images of highly crystalline cellulose on a molecular scale for the image processing. High resolution images of the cellulose substrate were obtained repeatedly by using the height mode. Figure 7 shows the membrane surface of a *Valonia macrophysa* vesicle (11 nm x 11 nm) with a surface roughness less than 1.7 nm. The height difference between light and dark spots in the middle of the image was between 0.25 nm and 0.4 nm. The two-dimensional fast Fourier transform (FFT) of the raw data (Figure 8) gave crystal parameters. The FFT spectra contained several bright spots revealing the periodicities and regularities of the surface, i.e. an indication of the crystallinity.

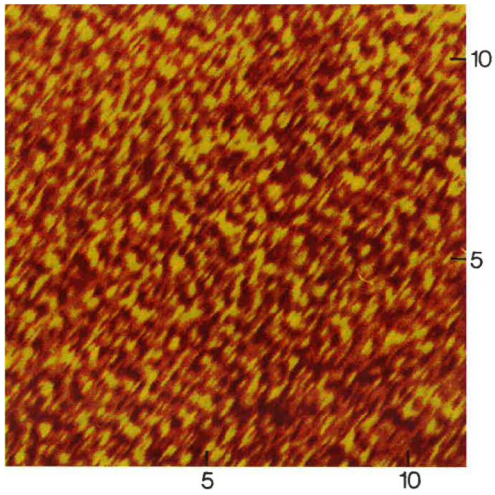

Figure 7. AFM images of *Valonia macrophysa.*

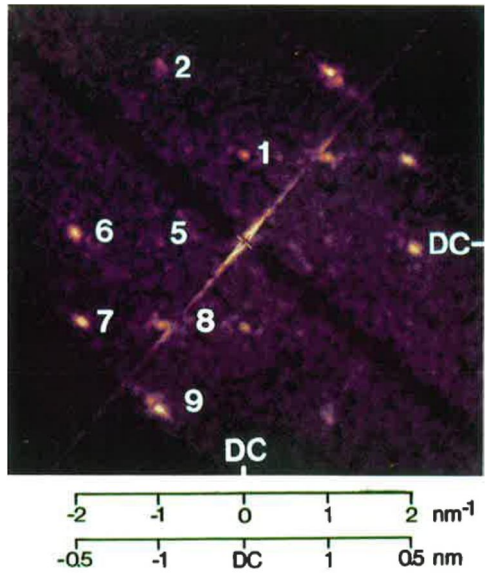

Figure 8. FFT diffractogram of *Valonia macrophysa*.

The spot numbers in Figure 8 refer to the numbers in Table 5, in which the results of the FFT diffractograms for the four artificial crystal faces are presented. The *Valonia macrophysa* sample displayed a periodicity of 1.01 nm (compared to an observed periodicity of 1.07 nm for *Valonia ventricosa* [113], close to a fibre repeat unit length of 1.036 nm containing two glucose units [30]).

3.1.1.1 Artificial AFM images based on the Connolly surfaces

The artificial AFM image of a monoclinic (110) crystal face (Figure 9) with the characteristic two- dimensional FFT spectrum is shown in Figure 10. The light spots arise from the -CH_2OH side groups pointing out from the glucose ring.

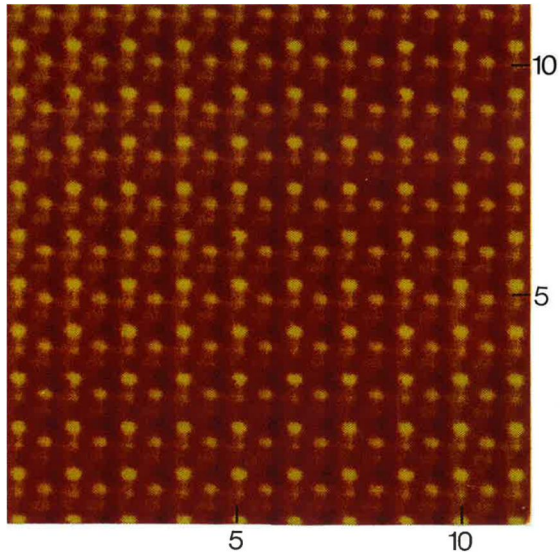

Figure 9. An artificial AFM image of a monoclinic (110) crystal face generated from the smaller Connolly surface model.

Because the artificial AFM image was based on a perfectly crystalline surface, the FFT diffractogram contains bright spots but little noise (Figure 10 A–D). Each spot was characterised by three parameters; R-value, angle and relative intensity. The R-value, in nm, indicated the period of the regularity and the angle suggested the relative direction of the regularity.

Figures 10 A–D present the FFT diffractograms of the four artificial crystal faces and in Table 5, the R-values of the spots were collected and compared with the values obtained from the experimental FFT diffractogram of *Valonia*. As could be seen, the diffractograms of the monoclinic crystal faces (110) and (1–10) were very similar (the angles and the relative intensities were almost the same) and only the R-values differed. The monoclinic (110) crystal face (Figure 10A) had slightly greater R-values than those in the monoclinic (1–10) crystal face (Figure 10 B). A clear difference was observed in the FFT diffractograms of the triclinic crystal faces. The diffractogram of *Valonia* agreed with the diffractogram of the monoclinic (1–10) crystal face. *Valonia* microfibrils also contained triclinic domains [103], but high-quality images of a triclinic surface were not obtained in this work.

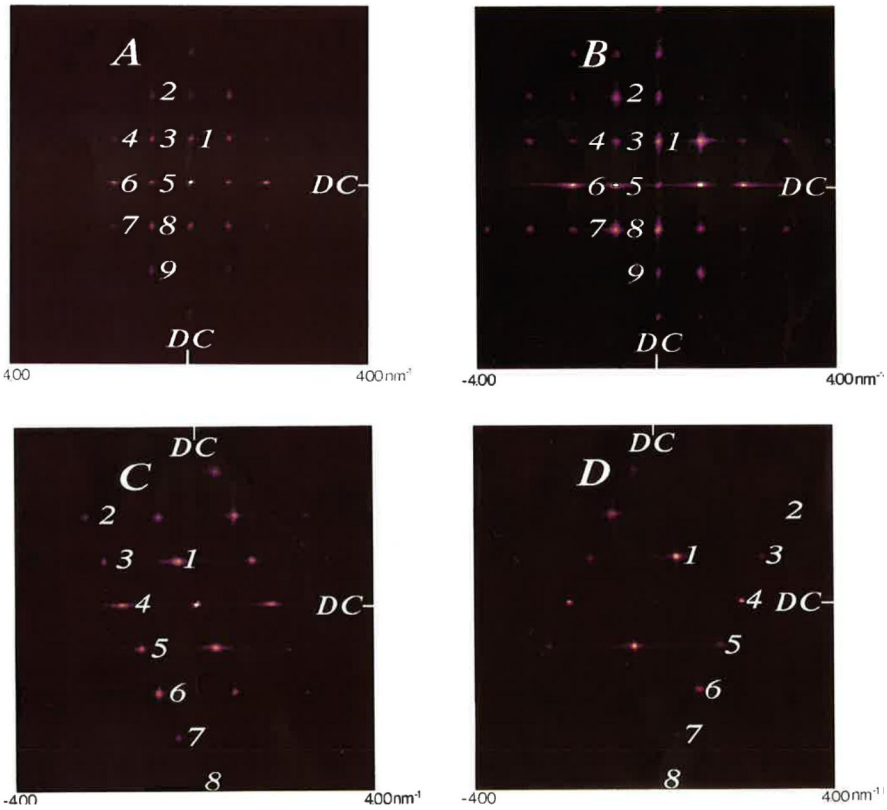

Figure 10. FFT diffractograms of the four artificial crystal faces. (**A**) monoclinic (110), (**B**) monoclinic (1–10), (**C**) triclinic (010) and (**D**) triclinic (100) crystal face. The spot numbers refer to the numbers in Table 5. The microfibril direction is parallel to the y axis. DC = direct current.

Table 5. Data collected from the FFT diffractograms of the artificial and experimental AFM images. The spot numbers refer to the numbers in Figures 10 A–D. The precision in the distances is ∓ 0.02 nm. nd = not detected.

Spot no.	*Valonia* (exp)	Mon 1–10 (model)	Mon 110 (model)	Tri 010 (model)	Tri 100 (model)
1	1.01	1.03	1.03	0.97	0.93
2	0.44	0.47	0.48	0.32	0.29
3	nd	0.75	0.79	0.44	0.39
4	nd	0.48	0.52	0.61	0.53
5	1.00	1.07	1.18	0.64	0.58
6	0.50	0.53	0.60	0.47	0.47
7	0.47	0.48	0.52	0.34	0.34
8	0.72	0.74	0.77	0.26	0.26
9	0.46	0.47	0.47		

The artificial and experimental AFM images differed mostly in the spot intensities. The artificial AFM images were generated from Connolly surfaces based only on van der Waals interactions. This gave the -CH_2OH side groups, which protrude from the glucose ring, a round and regular shape in the artificial AFM image and, in consequence, a diffractogram with symmetric spots.

3.1.1.2 Recent observations

Heiner and Teleman [114] calculated the interface between the (110) crystal face of cellulose Iβ and water by molecular dynamics simulation with cellulose coordinates refined from electron diffraction data as a starting point. Only the topmost layer in the cellulose differed in terms of structure and dynamics from the crystal bulk, but even these differences were small. At the surface approximately half of the cellulose intermolecular hydrogen bonding was lost, but this was compensated by hydrogen bonds with water molecules. Heiner [115] continued the modeling work and evaluated the reasons for the lack of high quality AFM images of triclinic surfaces. One of the suggested reasons for this has been that the triclinic faces may be softer than the monoclinic faces and therefore, so much deformed by the AFM tip that image resolution is completely lost. The fluctuation, hydrogen bonding and energy data presented in their paper suggested that the triclinic surfaces are about as hard as the monoclinic faces. Therefore, the reason for their non-observation had to be due to other factors.

High-resolution AFM of native *Valonia* cellulose I microcrystals was performed under water as well as propanol by Baker et al. [116]. They reported that the pitch of 0.52 nm along the molecule due the asymmetric glucose unit and the intermolecular spacing of ca. 0.6 nm were clearly resolved in both imaging environments. Baker et al. [117] continued the AFM measurements in water and published a paper in which was revealed the triclinic structures based on the spacing of the cellulose chains in real space.

Imai and Sugiyama [118] recorded a number of microdiffraction patterns from *Cladophora* microcrystals and proposed a model in which Iα and Iβ domains coexist either longitudinally or laterally in each microfibril (Figure 11). The surface may only be composed of the Iα phase, and there is actually very little Iβ present on the surface.

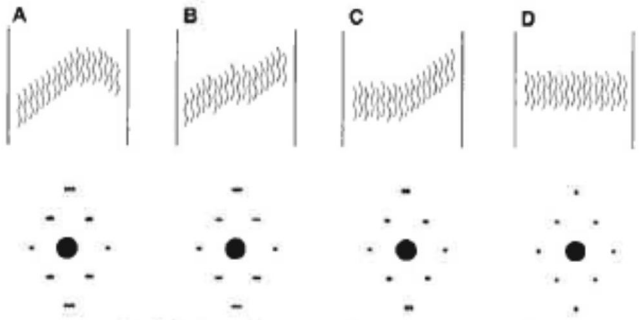

Figure 11. Probable molecular sheet packing explaining the observed differences in the diffraction patterns [118]. A: two triclinic domains with a monoclinic domain in between; B: multiple domains of triclinic and monoclinic domains, C: triclinic and monoclinic domains and D: a perfect monoclinic domain.

It has also been reported [119–120] that the Iα component was preferentially degraded by Trichoderma viride cellulase and the residual microcrystals became Iβ-rich with time. These previous results suggested that Iα is more degradable than Iβ.

Highly crystalline Iα-rich type *Cladophora* cellulose was treated with 60 wt% sulphuric acid at 100 °C, for 1–48 h. The Iα component was found to be more degraded than the Iβ component. The cellulose Iα/Iβ ratios of the samples acid-treated for 0, 24, and 48 h were about 8:2, 6:4, and 4:6, respectively. After the acid treatment, the microcrystals became narrower in width, and very sharp at their ends. These results indicate that the Iα phase is mostly located at the surface of the microcrystals, which is morphologically more susceptible to the acid treatment [121].

Li et al. [122] performed an AFM study of crystalline cellulose in the cell wall of straw. The samples were first treated and the AFM measurements were made under fresh dimethylsulfoxide (DMSO). The authors emphasized the importance of choosing a suitable liquid medium for the AFM observation of biological specimens. The crystalline regions were located and two allomorphs of crystalline cellulose were identified. In most crystalline regions, the Iα and Iβ phases were intimately associated, with the Iβ phase more abundant than the Iα phase. In some small domains only one phase with long-range order was observed. It was demonstrated that in these one-phase domains, Iα phase crystals always have their (010) plane lying parallel to the cell wall surface and Iβ phase crystals with their (110) plane lying parallel. Such orientation is different from that in primitive organisms, such in *Valonia* algae in which the cellulose crystals always have their triclinic (100) plane lying parallel to the cell wall surface [123].

Horikawa and Sugiyama [124] published an FTIR spectroscopic study combined with intracrystalline deuteration and rehydrogenation of cellulose samples to investigate the localisation of Iα and Iβ domains within a cellulose microfibril obtained from Iα-rich algae. Their conclusion was that the Iα domain localises not only on the surface but also in the central core of the cellulose microfibril, indicating that the triclinic and monoclinic domains cannot be explained only by the simple "skin-core" structure but also by a random distribution.

3.1.2 Ageing of thermoplastic starch films (Paper II)

The ageing phenomenon was characterised by AFM and FFM images, which were taken weekly during a 5 week period. Figure 12a shows a 5 µm x 5 µm AFM image of a fresh barley film (1 week old) and Figure 12b the corresponding friction force micrograph. The friction image indicated a homogeneous surface, i.e. the friction varied little within the studied surface.

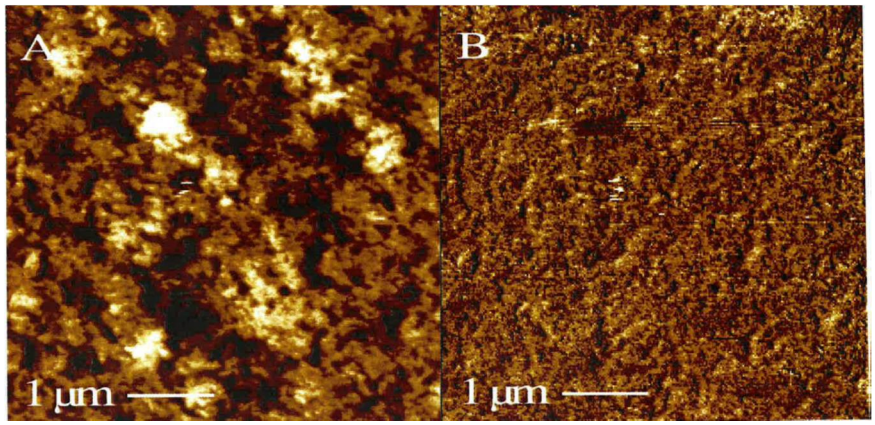

Figure 12. a) A top-view AFM image of fresh barley film (1 week old) and b) a simultaneously measured lateral force image.

The 2-week old barley film was rougher than the fresh film, but remained homogeneous. Figure 13 shows 10 µm x 10 µm micrographs of a 2 weeks old oat film. The height profile was similar to that of a one week old sample. The main change was observed in the friction image, revealing a partly heterogeneous surface structure (Figure 13b) featuring high (dark) and low (light) friction areas. The areas of low friction dominated the surface. The differences in friction were not due to changes in topography, as detected by comparing Figures 13a and 13b. The stickiness of the oat film was decreased considerably.

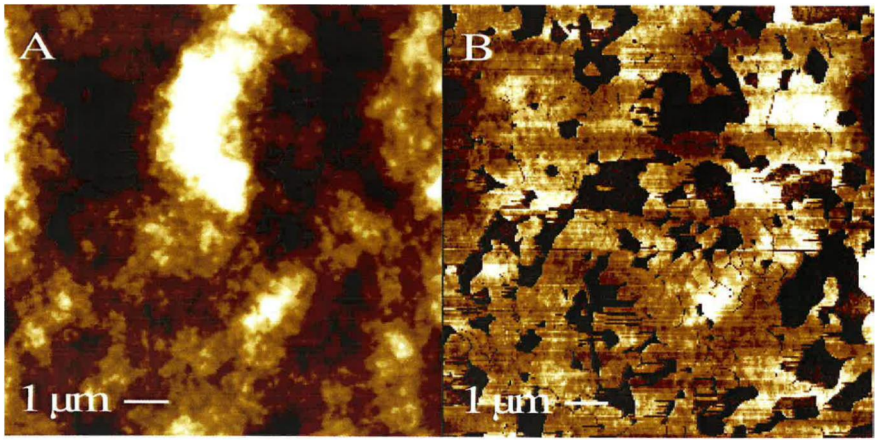

Figure 13. a) A 10 µm x 10 µm top-view AFM image of the 2 weeks old oat film and b) the respective lateral force image.

In the 3–4 weeks old oat samples, the same two-phase structure was observed on the surface. The relative amount of the low friction areas increased even further. The topography image showed small round island-like structures. The friction images captured for barley still indicated a homogeneous surface at an age of 3–4 weeks.

At 5 weeks the initial higher friction phase disappeared almost completely from the surface of the oat film, although local differences were significant. The mean roughness increased. At this age the surface structure of barley also began to change, as indicated by the friction data. The total surface roughness increased but flat areas on the surface were observed from both image types (Figures 14a and 14b). These flat areas were about 10 nm thick and often hundreds of nanometers in lateral size (Figure 15), and appeared to have a multilayer lamellar structure. These lamellae were not always straight, parallel or of uniform thickness, but typically slippery. Thus, the ageing brought about a lower friction surface in both oat- and barley-based films.

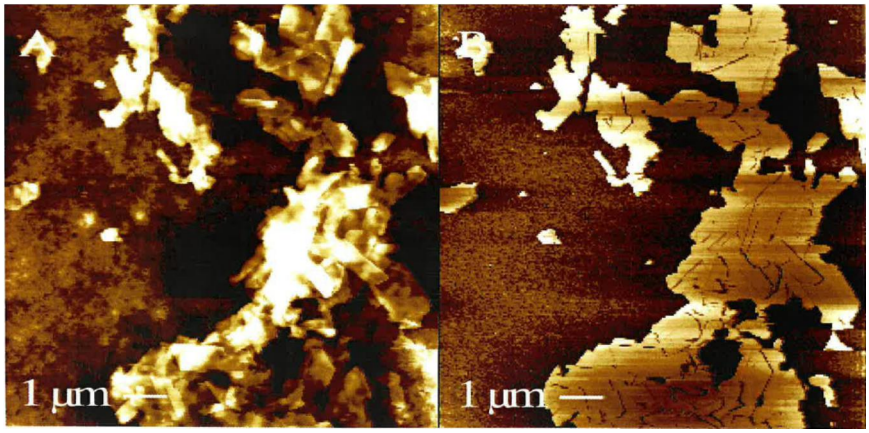

Figure 14. The 5 weeks old barley film, a) a 10 µm x 10 µm top-view AFM image and b) the respective lateral force image.

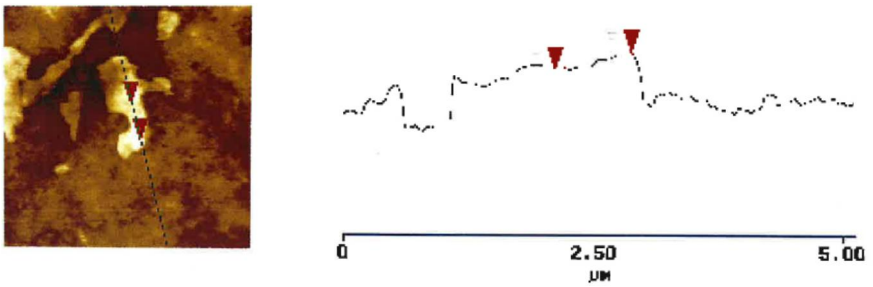

Figure 15. The section analysis of one multilayer lamellar structure in the barley film. The vertical distance between the two arrows in the figure is 7.1 nm.

During the measurements it was noticed that some part of the lamellar structure can be peeled off by the microscope tip. The fact, that the peeling occurred from the light areas but not from other topological features indicated that the flat, slippery areas are softer. Earlier results [65, 66, 125] concerning the thickness of the crystalline lamellae from different botanical sources supported our result of about 10 nm. The crystalline lamellae in barley starch films are not so-called blockets [126], which were spherical and range in diameter from 20 nm to 500 nm depending on starch type and location in the granule [127].

3.1.2.1 Crystallinity changes

Oat and barley films were found in a separate study to contain the same amount of B-type crystallinity [128]. When fresh the barley film contained a fair amount of Eh-type crystallinity, which slowly converted into Vh. The oat film contained only

Vh-type crystallinity when fresh. In connection with the results on surface changes, it appeared that the Eh-type crystallinity possibly hinders the glycerol diffusion, whereas the Vh-type does not, i.e. it allows the formation of pure glycerol patches on the film surface sooner for the oat film than for barley. It could be concluded that crystallisation and/or reorientation of amylopectin and amylose caused the ageing. Based on calorimetric transitions and on X-ray diffractograms, the major effect on failure properties have been caused by slow crystallisation of amylopectin.

3.1.2.2 Recent observations

The surfaces of solution-cast films of starch, amylose, and amylopectin were examined by Rindlay-Westling's and Gatenholm's study [129]. The surface topography visualised by SEM showed that amylopectin films were very smooth, whereas amylose and starch films were rougher. It appeared that crystallinity or phase separation in the bulk of the film affects the surface topography. AFM showed that the outermost surfaces of all films were covered with small protrusions, 15–35 nm wide and 1–4 nm high. Studies with electron spectroscopy for chemical analysis (ESCA) revealed the presence of 3–8 % nitrogen on the surfaces. Time-of-flight secondary ion mass spectrometry (ToF-SIMS) indicated that the nitrogen originates from protein because ionic fragments from amino acids and the peptide backbone were found. The proteins apparently phase separated during film formation and migrated to the surface, resulting in an extensive enrichment of proteins in the film surface, where about 8 % of the protein is present in the top 0.01 % of the film.

Myllärinen at al. [130] studied the crystallinity of amylose and amylopectin films with 0, 10 and 30 % glycerol and stored at RH 0, 54 and 91 %. Films prepared of water cast dilute solutions and dried at 70 °C were thin and transparent. Each fresh amylose film showed B-type crystalline structures, and depending on the glycerol and water contents the degree of crystallinity varied from 6 % to 32 %. No changes in the crystallinity of the amylose films were observed during storage of two months. The fresh amylopectin films were completely amorphous. After storage for two months at the highest humidity the amylopectin film with 30 % glycerol showed crystalline structure (19 %), but all other amylopectin films remained amorphous during ageing. The crystal formation in the highly plasticised amylopectin film was suggested to be due to its rubbery state under the storage conditions. Amylose films were stable in water, unlike amylopectin films that dispersed rapidly in water [128].

Ageing of normal corn starch films processed by extrusion and stored at 20–22 °C and RH 50–56 % was investigated over a period of 120 days by Pushpadass and Hanna [131]. The thermoplastic starch just after extrusion processing (≈4 h) was almost amorphous in character. However, ageing above the glass transition temperature (Tg) produced both B- and V-type crystalline structures in the TPS within 3 days of drying. As ageing continued, various conformational changes occurred in the functional groups of starch, decreasing the molecular mobility of

starch chains as well as the free volume in the film network. Further time-dependent changes in the crystalline structure were not drastic but were related to refinements of peaks and increase in crystallinity. The continuing changes in the molecular structure of TPS and film properties implied that ageing of the TPS did not reach the equilibrium state even after 120 days of storage in the stipulated conditions.

3.1.3 Morphological properties of spherical starch ester pigment (Paper III)

On the basis of experimental data, the real part of the refractive index of starch acetate was calculated to be 1.470 [132] and the calculated value was also verified by the microscopic immersion method. The optimum particle size of used materials was calculated by using complex light scattering models [87]. These models took into account the morphology, packing density, size distribution and refractive index of the used material. The optimum particle size to obtain maximum light scattering properties for starch acetate was calculated to be between 150 nm and 200 nm in diameter and the optimum particle size was dependent on the packing density.

Small spherical particles in the range 100–500 nm could be produced by the dispersion method (Figure 16). Bimodal particle size distribution (peaks at 258 nm and 893 nm) could be produced (Figure 17 A) when the dispersion was performed at room temperature and the evaporation of the solvents at low pressure and temperature (112 mbar/40 °C). The SEM images showed an indication of agglomeration of primary pigment particles.

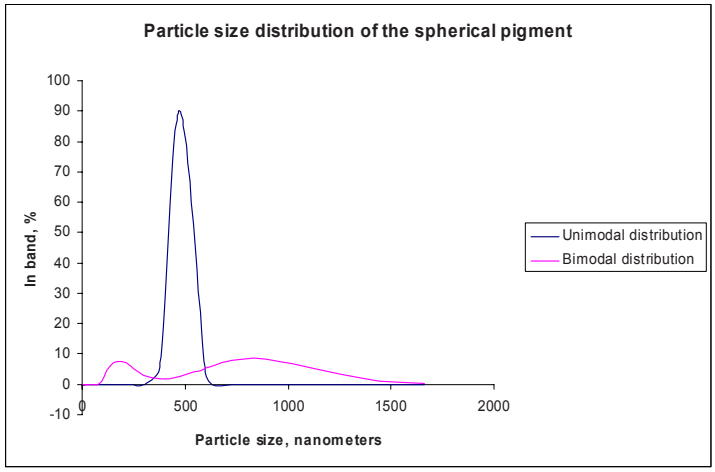

Figure 16. Particle size distribution of the spherical pigment before and after optimisation of the process.

Using the procedure of elevated temperatures a very narrow unimodal particle size distribution was obtained, in which the peak was located at 475 nm. The

reason for the better quality of the distribution was more effective removal of the organic solvents from the pigment product. Especially, the removal of acetone is important, because acetone was a very good plasticiser of starch acetate derivate and complicates optimisation of the process considerably. In the worst case, the primary particles fused and agglomerated together, as can been in Figure 17 B. Too heavy mixing during the evaporation of the solvents (over 500 rpm) also agglomerated the primary particles, which decreases the optical properties (opacity and brightness).

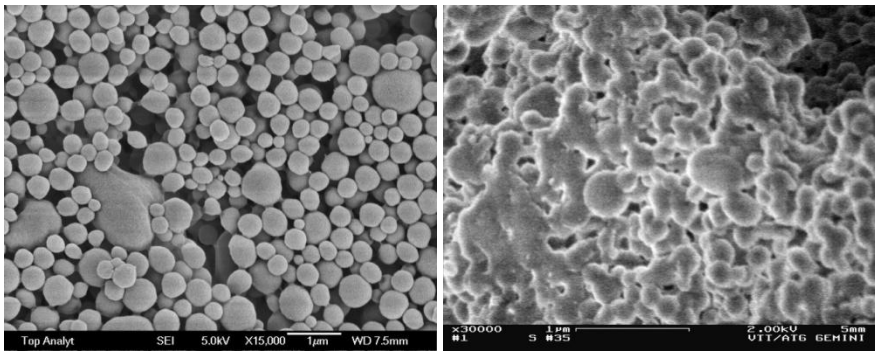

A B

Figure 17. A) Spherical pigment particles and B) fused and agglomerated primary particles.

3.1.4 Refractive properties of the hybrid materials (Paper IV)

In order to determine the effect of the hybrid materials on the optical properties, the RI studies were carried out in immersion liquids for several starting polymers, inorganic salts as such, as well as for the hybrid precipitates formed. The set for each sample contained four pictures taken in two adjacent immersion liquids in which the halo effects differ; the upper row pictures were taken in focus and the lower row pictures with increased distance from the focus. The product RI estimation was given as an interval determined by the liquid's RI (given on the top of each picture column). For pure CMS, the RI estimate was 1.50–1.55 (Figure 18, left) and similar values were observed for SPHOS, SCIT and the commercial distarch phosphates dSPHOS and adSPHOS. Calcium-containing inorganic salts gave similar RI levels, whereas for Ba-, Zn-, Zr- and Ti-containing salts, the estimates were between 1.55 and 1.65 (Figure 18, middle and right).

XRD results showed that the hybrid formed by CMS + $BaCl_2$ was amorphous and the crystalline contribution of the inorganic component was not evident. Similar amorphous indication was obtained for a hybrid formed in CMS + [$ZrO(NO_3)_2$ x H_2O] precipitation. Precipitated CMS + $Ba(OH)_2$ hybrid had an amorphous structure with some apparent crystallinity derived from the barium-containing component.

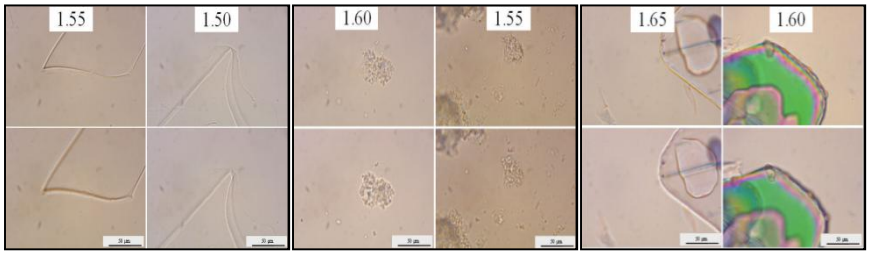

Figure 18. RI-estimation by the immersion liquid method: CMS (left) , $BaCl_2$ (middle) and $ZrO(NO_3)_2$ x H_2O (right).

Hybrid precipitates of CMS with Ca-containing salts exhibited somewhat lower RI compared to hybrids prepared with Ba- and Zr-containing salts (Figure 19). The highest RI estimates for CMS-based hybrids were in the range of 1.55–1.60.

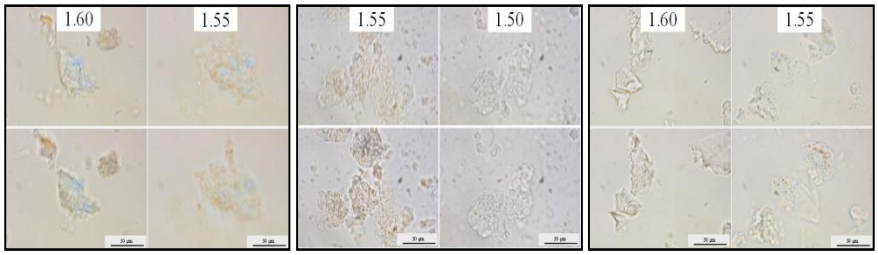

Figure 19. RI-estimation by the immersion liquid method: hybrids of CMS + $CaCl_2$ (left, in a scale of 50 µm), CMS + $BaCl_2$ (middle) and CMS + [$ZrO(NO_3)_2$ x H_2O] (right).

Some examples of hybrids based on other starch derivatives are given in Figure 20. Improved RIs were observed for SPHOS-, dSPHOS- and SCIT-based hybrids with Zr- and Ti-containing salts.

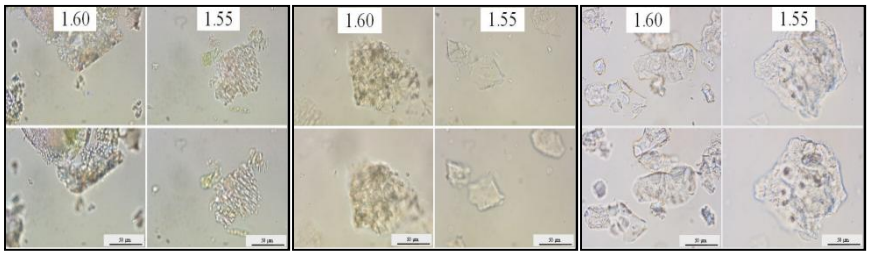

Figure 20. RI-estimation by the immersion liquid method: hybrids of SPHOS + [$Zr(NO_3)_4$ x H_2O] (left, in a scale of 50 µm l), dSPHOS + [$ZrOCl_2$ x H_2O] (middle) and SCIT + [$TiO(OCOCOOK)_2$] (right).

3.1.5 Particle composition and morphology of the hybrid materials (Paper V)

The ground samples of hybrid materials were both analysed to contain 10 wt% of water. By combustion analysis, the organic/inorganic ratio was 41/59 wt% for hybrid CMS + $BaCl_2$ and 64/36 wt% for hybrid CMS + [$ZrO(NO_3)_2$ x H_2O]. CPMAS ^{13}C nmR spectroscopy verified the assumption that complexation of CMS and inorganics was closely related to the carboxymethyl group. The obtained mean particle size was larger and the size distribution wider than considered optimal for paper fillers. Especially, in the case of milled hybrid product of CMS + $BaCl_2$, a large particle size distribution was detected (between 20 µm and 60 µm). For the hybrid of CMS + [$ZrO(NO_3)_2$ x H_2O], the size distribution averaged at around 10 µm. The relatively large particle size could be expected to affect the optical and mechanical properties of the filled sheet.

SEM analysis revealed that the milled hybrid fillers were coarse and contained some degree of porosity (Figure 21 right and Figure 22 right). A high degree of porosity is considered beneficial for the particle size reduction by grinding but also for increasing the light scattering of the fillers. The formed particle structures (Figure 21 right and Figure 22 right) resembled the starting CMS (Figure 21 left) more than the pure inorganics (Figure 21 middle and Figure 22 left).

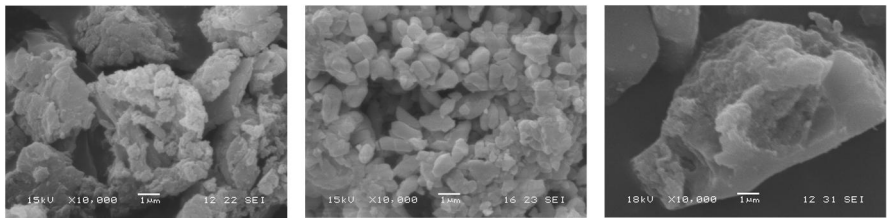

Figure 21. SEM images: pure CMS (left), $ZrO(NO_3)_2$ x H_2O (middle) and milled hybrid product of CMS + [$ZrO(NO_3)_2$ x H_2O] (right).

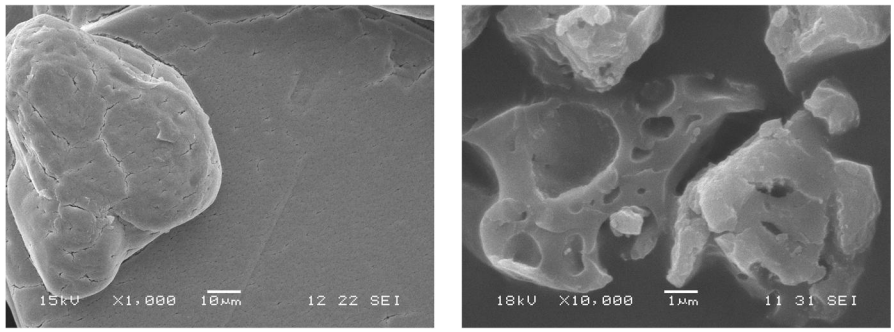

Figure 22. SEM images: $BaCl_2$ (left) and milled hybrid product of CMS + $BaCl_2$ (right).

Dispersability of the particles into distilled water appeared to be satisfactory and not to cause softening or swelling even after several weeks of storage, although sedimentation of the filler powders of formed particle size was rapid without any dispersing additives. However, pH- induced (re)precipitation of the inorganics was not observed, indicating a stable bonding between the polymer and inorganic constituents.

3.1.6 Flocculation efficiency in papermaking (Paper V)

The flocculation and retention capabilities of the polymers were evaluated using an image analysis technique. Polymer C (Table 4) was able to increase the flocculation level at high dosage and slow flow velocity, but when the velocity was doubled and the dosage halved the floc size remained almost unchanged. Furthermore, the intensity quantities indicated that a major part of the fillers remain in the water phase. Figure 23 shows an example of the acquired images for each case. Clear flocculation into localised mass concentrations (variations in gray levels) was observed for pulp treated with polymer F, whereas the flocculation pattern produced by polymer C was rather close to that of the reference pulp without additives.

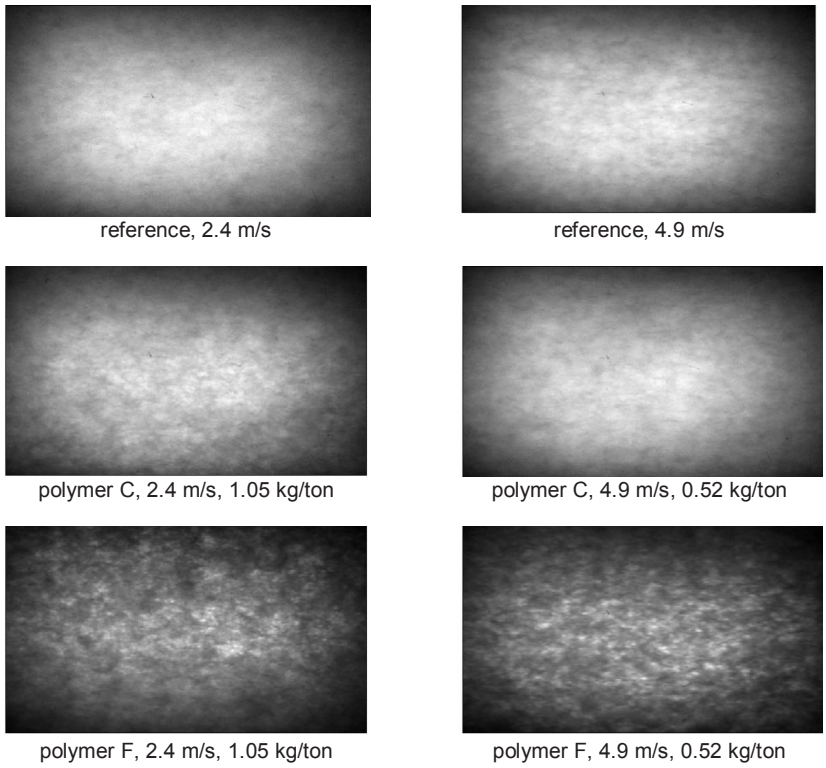

Figure 23. Transilluminated photos of the flow in the channel with different flow conditions and polymer dosages.

3.2 Optical properties of the selected polysaccharides systems

3.2.1 Spherical starch ester pigments (Paper III)

The opacity results of the different coating pigments are shown in Figure 24 and the corresponding ISO-brightness results in Figure 25. Precipitated calcium carbonate (PCC) filler was used as a reference pigment and the used paper was uncoated book paper (62 % ISO-brightness and 96 % opacity). Commercial PCC was somewhat superior in both properties (brightness and opacity), but not drastically. The differences in the values of ISO-brightness and opacity of the starch acetate pigments (AP2-2 and AT60-1) were mainly dependent on dry matter content and the drying method. Some samples were in the form of a slurry dewatered by centrifugation and some were in form of a spray-dried powder. The final form of the pigment product influenced the particle size distribution and also the degree of agglomeration of the primary pigment particle. As size distribution can be narrowed and brightness of the starch product increased, these starch-based pigments are potential alternatives to PCC. The ISO-brightness results for the starch acetate pigment in standard compressed sample tablet form was as its best as good as 94.4 %. The most important factor for the superiority of PCC fillers was their low price in addition to good optical properties.

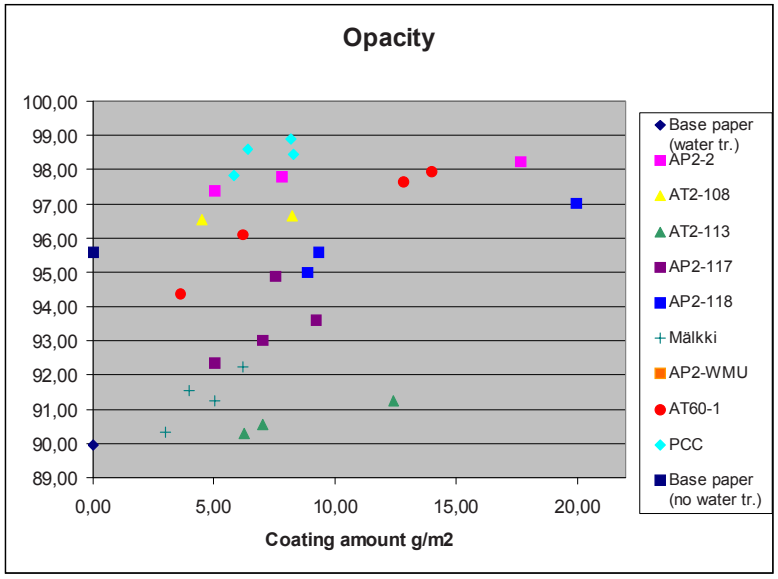

Figure 24. Opacity values of pigments and reference PCC coated on 52 g/m^2 book grade.

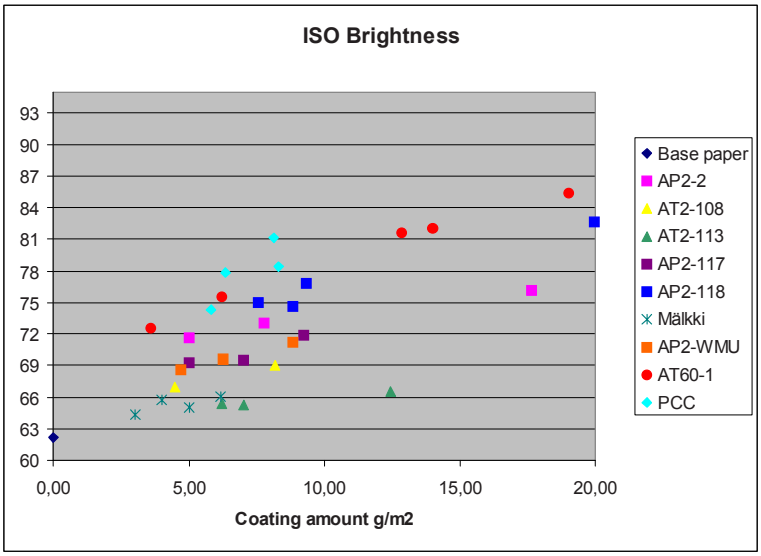

Figure 25. ISO-brightness values of experimental pigments and reference PCC coated on 52 g/m^2 book grade.

3.2.2 Optical and mechanical properties of the filled sheets (Paper IV)

CMS + $BaCl_2$ and CMS + [$ZrO(NO_3)_2$ x H_2O] could conveniently be incorporated in the paper as fillers using the conventional forming procedure. According to the measurements, the CMS + [$ZrO(NO_3)_2$ x H_2O] hybrid filler had some contribution to opacity at high filler content, although generally the light scattering properties of the handsheets were not significantly affected (Figures 26–27). The sheets filled with the CMS + $BaCl_2$ hybrid attached strongly to the blotting boards. Impaired scattering properties were anticipated to be due to a strong tendency to increase the internal bonding of the sheets, also observed as the low bulk (Figure 27 right). Only the A-PCC and CMS + [$ZrO(NO_3)_2$ x H_2O] hybrid provided higher bulk than the sheets without fillers (Figure 27 right).

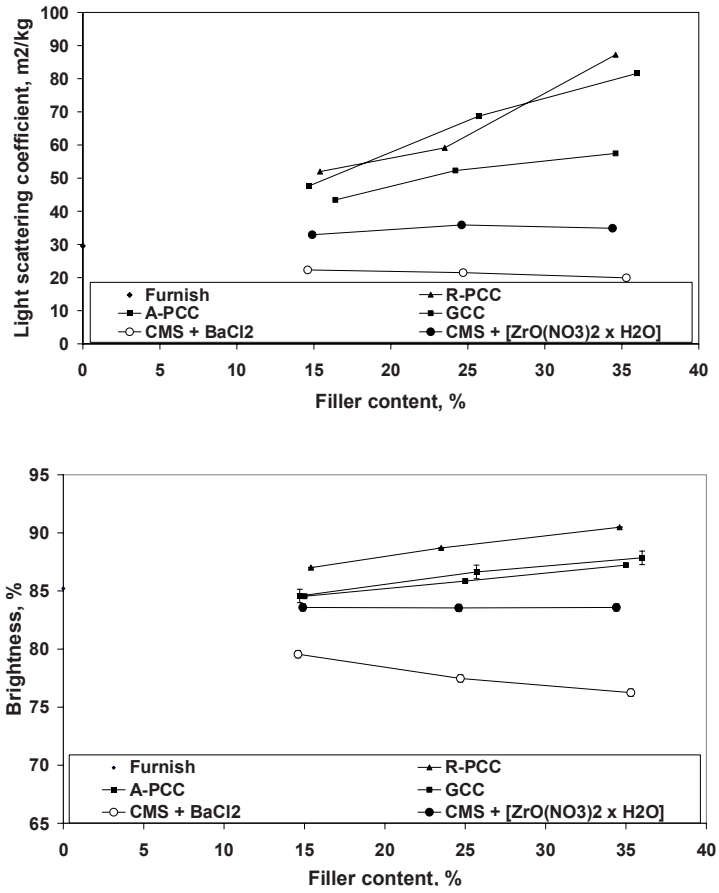

Figure 26. The light scattering coefficient of unfilled and filled sheets at varying filler contents (left) and brightness of unfilled and filled sheets at varying filler contents, prior to calendaring (right).

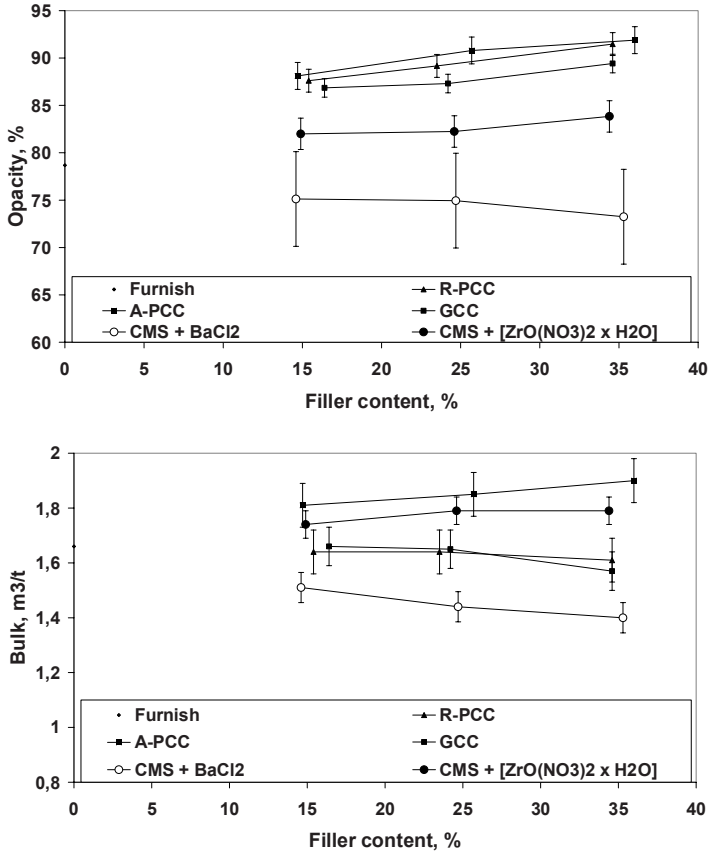

Figure 27. Opacity of unfilled and filled sheets at varying filler contents (left) and the bulk of unfilled and filled sheets at varying filler contents, prior to calendaring (right).

Both CMS + $BaCl_2$ and CMS + [$ZrO(NO_3)_2$ x H_2O] hybrid fillers yielded higher tensile strength indices and the Huygen bond energies than the sheets prepared with the reference fillers. CMS + [$ZrO(NO_3)_2$ x H_2O] hybrid yielded better property combinations than CMS + $BaCl_2$. After calendering the CMS + [$ZrO(NO_3)_2$ x H_2O] hybrid gave the highest bulk. The benefit was the most significant at 25 % filler content, at which concentration an improvement of 10–20 % was observed compared to the other fillers.

The scattering properties of the hybrids must be optimised using existing knowledge in the field of starch-based pigments, e.g. an improved milling response is required.

3.2.3 Turbidity of pre-tested and further developed polymers (Paper V)

3.2.3.1 Jar test

Together 30 flocculants were selected randomly from other projects for the jar test. As a general observation from the studies (Table 6) it could be said that products that are subjected to anionic modifications, such as cross-linked and cationised CMC-flocculants, act as dispersing agents. An increasing degree of acetylation and nitrogen content improved the efficiency of the flocculant. Lowering of the pH of the suspension also improved the efficiency of the flocculants.

Table 6. Turbidity results of the jar test study. Symbol values : +++ = under 5, ++ = 6 to 20, + = 20 to 49, - = 50 to 100, - - = 101 to 199 and - - - = over 200 NTU (NTU = Nephelometric Turbidity Units).

	TMP fines		Kaolin	
	1 ppm	2 ppm	1 ppm	2 ppm
5 x cationised potato starch	++	++	++	+
2 x cationised maize starch	++	+++	+	- -
2 x enzymatic + cationised barley	+	-	++	- -
9 x cationised + modified starch	-	-	++	++
3 x cationised CMC	--	-	- -	- -
3 x acetylated starch	+	+++	+	- -
cationised starch acetate	-	++	+	-
cationised chitosan	+	+++	-	- - -
commercial cationised starch	++	+++	+	- -
3 x commercial cationised PAM	+++	+++	+	+
2 x cationised hydroxyethyl cellulose	++	++	+	- - -
cationised lignin	-	-	-	- - -

The influence of the side chain of modified starch (HPS) on the effectiveness of TMP fines flocculation can be seen from Figure 28. The larger the side chain was, from methyl to stearyl, the more ineffective was the flocculation. The comparison of the best flocculants to commercial flocculants revealed that at low dosage the commercial flocculants performed better than the modified starches.

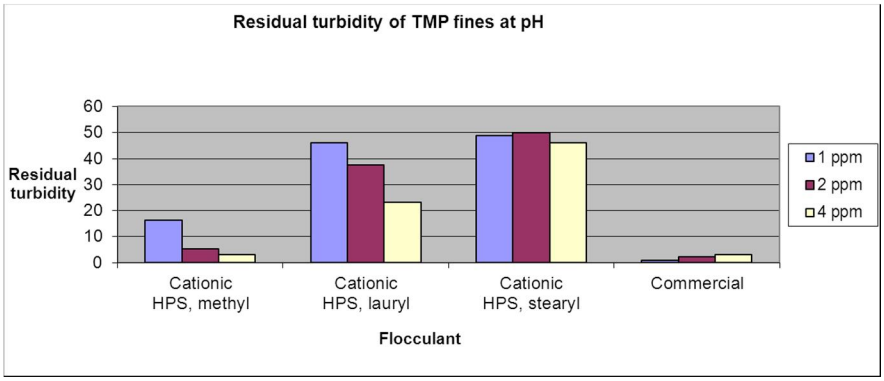

Figure 28. Effect of the side chain of modified starch on the flocculation of TMP fines at pH 4.

The conclusion from the jar test results was that the optimisation parameters for the polymer were increased molecular mass and nitrogen content. Table 4 lists information pertaining to the modified polymers considered during the project. The jar test data of the modified polymers revealed that the best flocculants reached almost the same efficiency level as the commercial products (Figure 29).

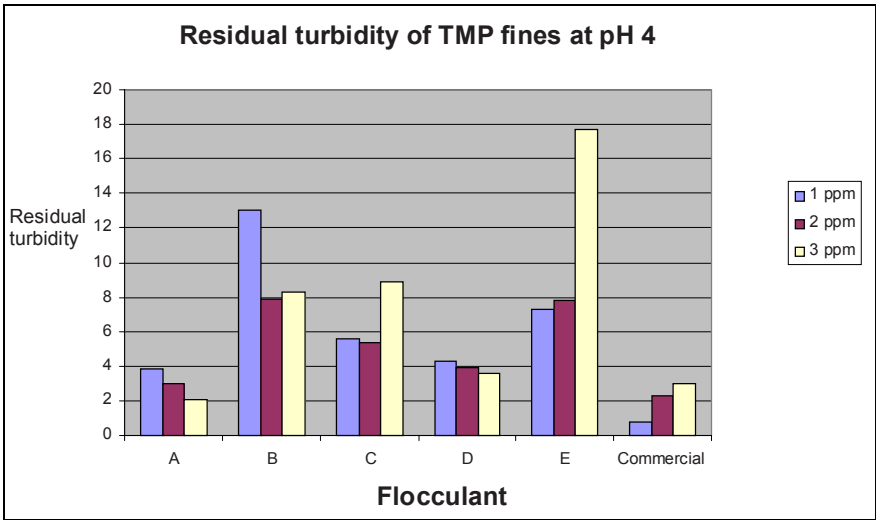

Figure 29. Comparison of modified flocculants compared to a commercial flocculant.

3.2.3.2 Sludge treatment

In order to evaluate the effectiveness of the developed flocculants, more realistic sludge matrices were chosen. Cellulose-based polymers did not produce visible

flocs in sludge applications. The tested D polymer, which was a cross-linked starch-based polymer, performed the best of all the developed polymers in this application (Table 7). It also had the highest molecular mass of the developed polymers (M_w = 2 080 000 g/mol). The most satisfactory flocs for further dewatering tests were obtained using the commercial flocculant H with a molecular mass of 9 500000 g/mol. The use of ferric sulphate produced better flocs only with flocculants C and I.

Table 7. Visual estimation of floc appearance. Polymer dose (kg dry solids/t sludge) in parentheses. For the symbols A–I, see Table 4.

No flocs	Minor flocs	Good flocs	Excellent flocs
Reference (0)	C (15) + ferric	I (4) + ferric	H (8)
Reference (0) + ferric	D (8)	I (8) + ferric	H (8)
A (4)	D (15)	I (15) + ferric	
A (8)	D (15) + ferric	H (4) + ferric	
A (15)	I (4)	H (4) + ferric	
C (4) + ferric	I (8)		
C (4)	I (15)		
C (15)			
D (4)			
D (4) + ferric			
D (8) + ferric			

The filtration tests gave similar results to those of the visual estimation of floc appearance. There was no cake on the filter when filtering sludge flocculated using cellulose-based polymers, and the filtrates had similar total solids (TS) content to the reference with no flocculant addition. Starch-based polymers produced better filtration results. When the sludge was flocculated using the polymer D (polymer dose 15 g/t TS), the dry solid content of the cake obtained was rather good, 4.3 %. However, the filtrate was turbid and the TS of the filtrate was high (> 0.6%). The TS of the cakes when using either of the commercial polymers were > 5.0 %. The filtrates were clearer (TS < 0.4 %) than when using the starch-based polymers.

The continuous belt filtering was carried out with the starch-based polymer D and the commercial polymer H. The TS 10 % obtained using polymer D was rather good. However, the TS with polymer H was somewhat higher at 12 % and the filtrate was clearer. The amount of polymer needed for flocculation was 1.5-fold for the polymer D compared to polymer H.

3.2.3.3 Drainage and flocculation efficiency in papermaking

To study the free water removal rate from the furnish, the cumulative filtrate mass was analysed as a function of time during the dewatering process. The total filtration times when the maximum amount of filtrate was achieved are presented in Table 8. All flocculants increased the dewatering rate of the furnish, because all the used polymers were cationic and therefore flocculation was expected at least due to electrostatic attraction. A decrease in specific surface area of the pulp through flocculation of fines and fillers onto fibres leads to increase in porosity of the consolidating pulp layer during the dewatering process.

Table 8. Total filtration times (seconds) of the pulp samples (time to maximum filtrate volume).

Sample	500 g/ton	1000 g/ton
Reference	26.5	26.5
F (C-PAM)	15	14
G (C-PAM)	20	16.5
C (starch)	20.5	20
D (starch)	21	20.5
E (cellulose)	27	28.5

Despite the similar charge density and molecular mass of polymers C and G, the commercial C-PAM-based polymer G outperformed the starch-based polymer C in dewatering efficiency. The starch-based polymers C and D achieved almost identical dewatering behaviour, despite the noticeable difference in both charge density and molecular mass. The highest dewatering rate was achieved with C-PAM having relatively low charge density but very high molecular mass. The performance of the cellulose-based polymer was very weak.

Filtrate turbidity values are presented relative to the value of reference pulp in Figure 30. The commercial C-PAMs F and G were able to reduce the turbidity to 20 % of the reference. The tailored starch-based polymers C and D decreased turbidity to 30 % of the reference, whereas the cellulose-based polymer E only yielded turbidity that was approximately 65 % of the reference. The reason for the poorer performance of the cellulose-based polymer in dewatering and retention might be the significantly lower charge density and somewhat lower molecular mass.

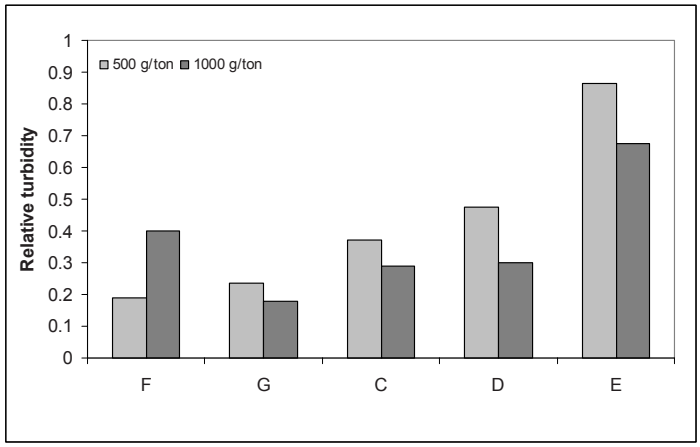

Figure 30. Filtrate turbidities relative to the reference pulp filtrate.

The starch-based flocculant C and the commercial flocculant F were selected for studies in a laboratory flow loop system. The images analysis was discussed in Section 3.1.5. The cross-sectional area of the flocs produced by the different polymers relative to the reference without additives is shown in Figure 31. The commercial polymer F produced ,compared to the reference, 1.9 to 2.3 times larger flocs, depending on the flow conditions and polymer dosage. The increase in intensity and deviation of intensity indicated that filler particles are attached onto fibres.

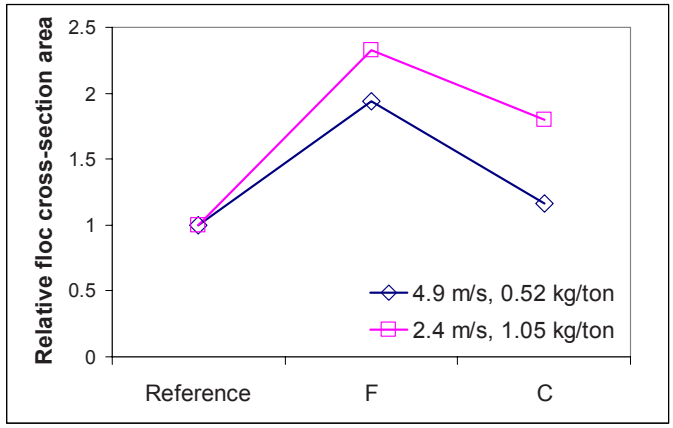

Figure 31. Cross-sectional area of the flocs relative to the reference pulp. Similar flow conditions and polymer dosage are connected with a line.

4. Conclusions

The differences in supermolecular structures, the capability to form extensive hydrogen bond systems and differences in interactions with water are the main reasons why cellulose and starches behave differently in many applications. For example, cellulose is of the order of 100 times more difficult to hydrolyse than starch.

It was demonstrated how to interpret and identify the experimental AFM images of crystalline cellulose by comparing to modeled ones. Highly crystalline cellulose samples have very strong hydrogen bond systems. *Valonia* celluloses contain 60 % to 70 % of the Iα crystalline phase. However, only the Iβ monoclinic phases were found on the surface with a lateral resolution of about 4 Å. This finding means that there is an experimental problem. In a dry environment the water molecules cannot penetrate, thus disturbing the surface structure of monoclinic cellulose. The AFM measurements without liquid cell disturb the surface structure so that the detection of lateral resolution is no longer possible at the molecular level for triclinic cellulose. It is important to know the cellulose surface structures when planning applications where highly crystalline cellulose's strength and light weight is utilized in high-performance products comparable to Kevlar fibre applications.

The crystal forms of starch are dependent on the relative ratio of amylose and amylopectin. In the ageing process of TPS films many supermolecular changes take place. In oat starch films, the glycerol plasticiser diffuses from the starch-glycerol-water matrix to the surface of thermoplastic starch. Fresh barley film contains, in turn, a considerable amount of Eh-type crystallinity, which is slowly converted into Vh-type crystallinity. The reason in barley starch films appears to be at first short range reorientation of starch and finally the crystallisation of starch. The amylopectin branches form helical crystal structures, which seem to be a rather soft material. The results of some recent publications also support this conclusion.

Chemical cleaving of the molecular chains is important for the processability of the polysaccharides in the preparation of ideally spherical particles. Particle shape and desired size take form spontaneously due to the free mobility of the modified starch chains when the process is optimised. The products are rigid, water insoluble particles with a diameter of about half the wavelength of visible light. The optimum particle size of the materials used can be calculated by using complex light scattering models. The effective removal of organic solvents from the particle products must be performed very carefully. Otherwise the primary particles ag-

glomerate together and the particles lose their optical performance. These starch-based pigments are good alternatives to PCC.

Polymer derivatives selected from the group of starch phosphates, acetylated starch phosphates, starch citrate and carboxymethyl starch were combined with water-soluble inorganic salts to form insoluble starch-hybrid fillers. The inorganic components can be selected from the group of calcium-, barium-, zirconium-, zinc- and titanium-based compounds. The criteria for the selection includes the efficiency of polymer functionalization as well as its insolubility, yield and optical properties of the hybrid structures. The results of NMR measurements indicate that the complexation of CMS and inorganics is closely related to the carboxymethyl group in the starch-based hybrid pigmented materials. XRD results show that the formed hybrids are mostly amorphous and that the crystalline contribution of the inorganic component is not evident. The resulting precipitates exhibit composite structures and improved refractive indices depending on the inorganic constituent.

The properties of the starch-based polymers in flocculation test are sufficient in shearless dewatering conditions compared to the studied commercial polyacrylamide-based polymers. When the flow studies are performed in more realistic conditions at higher shear conditions, the starch-based polymers cannot produce a flocculation level which can be expected to maintain sufficient retention properties, at least with the studied dosages. The performance of the cellulose-based polymer as flocculating agent is less efficient. The reasons for the weak performance of polysaccharide-based flocculants are probably too low molecular mass especially in the case of cellulose and the charge density distribution. The used cross-linking method to increase the molecular mass of the optimised polysaccharide-based flocculants is not optimal when considering the hydrodynamic properties. Better understanding of how to improve the hydrodynamic properties of bio-based polymers by controlling their molecular size, shape or internal rigidity, will be essential when planning new bio-based flocculants.

References

1. Netravali, A.N., Chabba, S. Composites get greener. Materials Today 2003, 6(4), pp. 22–29.

2. Groombridge B., Jenkins M.D. Global biodiversity: Earth's living resources in the 21st century. World Conservation Press, Cambridge, UK, 2000.

3. Field, C.B., Behrenfeld, M.J., Randerson, J.T., Falkowski, P. Primary production of the biosphere: Integrating terrestrial and oceanic components. Science 1998, 281, pp. 237–240.

4. Parikka, M. Global biomass fuel resources. Biomass Bioenergy 2004, 27, pp. 613–620.

5. FAO, FAOSTAT-database 2002, http://www.fao.org.

6. FAO, State of World's Forest-2001, http://www.fao.org.

7. Thrän, D., Kaltschmitt, M. Biomass for a sustainable energy provision systems—state of technology, potentials and environmental aspects. In: Sayigh, A. (Ed.). Workshop Proceedings, World Renewable Energy Congress, June 29 – July 5, 2002, Cologne, Germany.

8. Kaltschmitt, M., Neubarth, J. Biomass for energy – an option for covering the energy demand and contributing to the reduction of GHG emissions? Workshop Proceedings, Workshop on Integrating Biomass Energy with Agriculture, Forestry and Climate Change Policies in Europe, Imperial College, London, UK, 2000.

9. Zoebelin, H. (Ed.). Dictionary of Renewable Resources. Wiley-VCH, Weinheim, Germany, 2001.

10. Shen, L., Haufe, J., Patel, M. Product overview and market projection of emerging bio-based plastics PRO-BIP 2009. Universiteit Utrecht, Netherlands, 2009.

11. FAOSTAT Resources 2009, ResourcesSTAT data archives, Land. Updated 30 April 2009. http://faostat.fao.org/site/377/default.arpx#ancor.

12. European Biomass Industry Association 2007. http://www.eubia.org/215.0.html.

13. World Energy Council, Survey of Energy Resources 2001. http://www.worldenergy.org/documents/ser_sept2001.pdf.

14. International Energy Agency 2009. http://www.iea.org/textbase/nppdf/free/2009/key_stats_2009.pdf.

15. Alen, R. (Ed.) Biorefinery of Forest Resources. Paperi ja Puu Oy, Helsinki, Finland, 2011.

16. Gruell, D., Jetzinger, F., Kozich, M., Wastyn, M.M., Wittenberger, R. Industrial starchplatform – Status quo of production, modification and application. In: Kamm, P., Gruber, P.R., Kamm, M. (Eds.). Biorefineries – Industrial Processes and Products, Wiley-VCH, Weinheim, Germany, 2006.

17. Lampke, T.H. Beitrag zur Charakterisierung naturfaserverstärkter Verbundwerkstoffe mit hochpolymerer. Doctoral thesis, Technische Universität Chemnitz, Germany, 2001.

18. Alen, R. Structure and chemical composition of wood. In: Stenius, P. (Ed.). Forest Products Chemistry. Book 3. Fapet Oy, Helsinki, Finland, 2000. Pp. 11–57.

19. Swatloski, R.P., Spear, S.K.H., Rogers, R.D. Dissolution of cellose with ionic liquids. J. Am. Chem. Soc. 2002, 124, pp. 4974–4975.

20. Meyer, K.H., Misch, L. Positions des atomes dans le nouveau modèle spatial de la cellulose. Helvetica Chimica Acta, 1937, 20, pp. 232–244.

21. Honjo, G., Watanabe, M. Examination of cellulose fibre by the low-temperature specimen method of electron diffraction and electron microscopy. Nature 1958, 181, pp. 326–328.

22. Gardner, K.H., Blackwell, J. The structure of native cellulose. Biopolymers 1974, 13, pp. 1975–2001.

23. Sarko, A., Muggli, R. Packing analysis of carbohydrates and polysaccharides. III. Valonia cellulose and cellulose II. Macromolecules 1974, 7, pp. 486–494.

24. Atalla, R.H., VanderHart, D.L. Native Cellulose: A Composite of Two Distinct Crystalline Forms. Science 1984, 223, pp. 283–285.

25. Horii, F., Hirai, A., Kitamaru, R. CP/MAS carbon-13 NMR spectra of the crystalline components of native celluloses. Macromolecules 1987, 20, pp. 2117–2120.

26. Sugiyama, J., Persson, J., Chanzy, H. Combined infrared and electron diffraction study of the polymorphism of native celluloses. Macromolecules 1991, 24, pp. 2461–2466.

27. Horii, F., Yamamoto, H., Kitamaru, R., Tanahashi, M., Higuchi, T. Transformation of native cellulose crystals induced by saturated steam at high temperatures. Macromolecules 1987, 20, pp. 2946–2949.

28. Yamamoto, Y., Horii, F., Odani, H. Structural changes of native cellulose crystals induced by annealing in aqueous alkaline and acidic solutions at high temperatures. Macromolecules 1989, 22, pp. 4130–4132.

29. Belton, P.S., Tanner, S.F., Cartier, N., Chanzy, H. High-resolution solid-state carbon-13 nuclear magnetic resonance spectroscopy of tunicin, an animal cellulose. Macromolecules 1989, 22, pp. 1615–1617.

30. Sugiyama, J., Vuong, R., Chanzy, H. Electron diffraction study on the two crystalline phases occurring in native cellulose from an algal cell wall. Macromolecules 1991, 24, pp. 4168–4175.

31. Nishiyama, Y., Sugiyama, J., Chanzy, H., Langan, P. Crystal structure and hydrogen bonding system in cellulose I_α from synchrotron X-ray and neutron fiber diffraction. J. Am. Chem. Soc. 2003, 125, pp. 14300–14306.

32. O'Sullivan, A.C. Cellulose: the structure slowly unravels. Cellulose, 1997, 4, pp. 173–207.

33. Marchessault, R.H., Sarko, A. X-ray structure of polysaccharides. In: Wolfrom, M.L. (Ed.). Advanced Carbohydrate Chemistry, New York: Academic Press, USA, 1967. Pp. 421–483.

34. Marchessault, R.H., Sundararajan, P.R. Cellulose, in the Polysaccharides. Academic Press, New York, USA, 1983. Pp. 11–95.

35. Kolpak, F.J., Blackwell, J. Determination of the structure of cellulose II. Macromolecules 1976, 9, pp. 273–278.

36. Langan, P., Nishiyama, Y., Chanzy, H. A revised structure and hydrogen-bonding system in cellulose II from a neutron fiber diffraction analysis. J. Am. Chem. Soc. 1999, 121, pp. 9940–9946.

37. Marrinan, M., Mann, J. Infrared spectra of the crystalline modifications of cellulose. J. Polym Sci. 1956, 21, pp. 301–311.

38. Hayashi, J., Sufoka, A., Ohkita, J., Watanabe, S. The confirmation of existences of cellulose III_I, III_{II}, IV_I, and IV_{II} by the X-ray method. J. Polym. Sci., Polym. Lett. Ed. 1975, 13, pp. 22–27.

39. Sarko, A., Southwick, J., Hayashi, J. Packing analysis of carbohydrates and polysaccharides. 7. Crystal structure of cellulose IIII and its relationship to other cellulose polymorphs. Macromolecules 1976, 9, pp. 857–863.

40. Sarko, A. In Wood and Cellulosics: Industrial utilization, biotechnology, structure and properties. In: Kennedy, J.F. (Ed.). Chichester, Ellis Horwood, UK, 1987. Pp. 55–70.

41. Gardiner, E.S., Sarko, A. Packing analysis of carbohydrates and polysaccharides. 16. The crystal structures of celluloses IV_I and IV_{II}. Can. J. Chem.1985, 63, pp. 173–180.

42. Sarko, M., Muggli, R. Packing analysis of carbohydrates and polysaccharides. III. Valonia cellulose and cellulose II. Macromolecules 1974, 7, pp. 486–494.

43. Kolpak, F.J., Blackwell, J. Determination of the structure of cellulose II. Macromolecules 1976, 9, pp. 273–278.

44. Stipanovic, A.J., Sarko, A. Packing analysis of carbohydrates and polysaccharides. 6. Molecular and crystal structure of regenerated cellulose II. Macromolecules 1976, 9, pp. 851–857.

45. Taipale, T. Interactions of microfibrillated cellulose and cellulosic fines with cationicpolyelectrolytes. Doctoral thesis, Aalto University School of Science and Technology, Finland, 2010.

46. Turbak, A.F., Snyder, F.W., Sandberg, K.R. Microfibrillated cellulose, a new cellulose product: properties, uses, and commercial potential. J. Appl. Polym. Sci. 1983, 37, pp. 815–827.

47. Wågberg, L., Decher, G., Norgren, M., Lindström, T., Ankerfors, M., Axnäs, K. The build-up of polyelectrolyte multilayers of microfibrillated cellulose and cationic polyelectrolytes. Langmuir, 2008, 24(3), pp. 784–795.

48. Cranston, E.D., Gray, D.G. Morphological and optical characterization of polyelectrolyte multilayers incorporating nanocrystalline cellulose. Biomacromolecules 2006, 7(9), pp. 2522–2530.

49. Eichhorn, S.J., Dufresne, A., Aranguren, M., Marcovich, N.E., Capadona, J.R., Rowan, S.J., Weder, C., Thielemans, W., Toman, M., Renneckar, S., Gindl, W., Veigel, S., Keckes, J., Yano, H., Abe, K., Nogi, M., Nakagaito, A.N., Mangalam, A., Simonsen, J., Benight, A.S., Bismarck, A., Berglund, L.A., Peijs, T. Current international research into cellulose nanofibres and nanocomposites. J. Mater. Sci. 2010, 45(1), pp. 1–33.

50. Pääkkö, M., Ankerfors, M., Kosonen, H., Nykänen, A., Ahola, S., Österberg, M., Ruokolainen, J., Laine, J., Larsson, P.T., Ikkala, O., Lindström, T. Enzymatic hydrolysis combined with mechanical shearing and high-pressure homogenization for nanoscale cellulose fibrils and strong gels. Biomacromolecules, 2007, 8(6),pp. 1934–1941.

51. Siró, I., Plackett, D. Microfibrillated cellulose and new nanocomposite materials: a review. Cellulose, 2010, 17(3), pp. 459–494.

52. Ding, S.-Y., Himmel, M. The maize primary cell wall microfibril: A new model derived from direct visualization. J. Agric. Food. Chem. 2006, 54(3), pp. 597–606.

53. Jakob, H.F., Fengel, D., Tschegg, S.E., Pratzl, P. The elementary cellulose fibril in Picea abies: Comparison of transmission electron microscopy, small-angle X-ray scattering, and wide-angle X-ray scattering results. Macromolecules 1995, 28(26), pp. 8782–8787.

54. Davies, L.M., Harris, P.J. Atomic force microscopy of microfibrils in primary cell walls. Planta 2003, 217(2), pp. 283–289.

55. Somerville, C., Bauer, S., Brininstool, G., Facette, M., Hamann, T., Milne, J., Osborne, E., Paredez, A., Persson, S., Raab, T., Vorwerk, S., Youngs, H. Toward a Systems Approach to Understanding Plant Cell Walls. Science 2004, 306(5705), pp. 2206–2211.

56. Wada, M., Sugiyama, J., Okano, T. Native celluloses on the basis of two crystalline phase (Iα/Iß) system. J. Appl. Polym. Sci. 1993, 49, pp. 1491–1496.

57. Kontturi, E. Surface chemistry of cellulose from natural fibres to model surfaces. Doctoral thesis. Eindhoven University of Technology, the Netherlands, 2005.

58. http://en.wikipedia.org/wiki/Nanocellulose.

59. de Vlieger, J.J. Green plastics for food packaging, Novel food packaging techniques. In: Ahvenainen, R. (Ed.). Woodhead Publishing Limited, UK, 2003. Pp. 519–534.

60. Zobel, H.F. Starch granule structure. In: Developments in Carbohydrate Chemistry, American Association of Cereal Chemists 1992. Pp. 1–36.

61. Imberty, A., Buleon, A., Tran, V., Perez, S. Recen advances in knowledge of strach structure. Starch 1991, 43, pp. 375–384.

62. Imberty, A., Chanzy, H., Perez, S., Buleon, A., Tran, V.J. The double helical nature of the crystalline part of A-starch. Mol. Biol. 1988, 201, pp. 365–378.

63. Imberty, A., Perez, S. A revisit to the three-dimensional structure of B- type starch. Biopolymers 1988, 27, pp. 1205–1221.

64. Sarko, A., Wu, H.-C.H. Crystal Structures of A-, B- and C-Polymorphs of Amylose and Starch. Starch 1978, 30, pp. 73–78.

65. Kassenbeck, P. Electron microscope contribution to the study of fine structure of wheat starch. Starch/Stärke 1975, 27, pp. 217–227.

66. Kassenbeck, P. Beitrag zur Kenntnis der Verteilung von Amylose und Amylopektin in Stärkekörnern. Starch/Stärke 1978, 30, pp. 40–46.

67. van Soest, J.J.G. Starch plastics: structure-property relationships. Doctoral thesis, Utrecht University, the Netherlands, 1996. 168 p.

68. Shogren, R.L., Swanson, C.L., Thomson, A.R. Extrudates of cornstarch with urea and glycols: Structure/mechanical property relations. Starch/Stärke 1992, 44, pp. 335–338.

69. Sala, R., Tomka, I. Water uptake in partially frozen and plastisized starch. In: Blanshard, J.M.V., Lillford, P.J. (Eds.). The glassy state in foods, Nottingham University Press, UK, 1993. Pp. 483–489.

70. Forssell, P.M., Hulleman, S.H.D., Myllärinen, P., Moates, G.K.M., Parker, R. Ageing of rubbery thermoplastic barley and oat starches. Carbohydrate Polymers 1999, 39, pp. 43–51.

71. van Soest, J.J.G., Hulleman, S.H.D., de Wit, D., Vliegenhart, J.F.G. Crystallinity in starch bioplastics. Ind. Crops Prod. 1996, 5, pp. 11–22.

72. Elias, H.-G. Macromolecules 2: Synthesis, materials and technology. Plenum press, New York, USA, 1984.

73. Lenzinger Bericte, 89, Lenzing, Austria, 2011.

74. http://en.wikipedia.org/wiki/Microcrystalline_cellulose.

75. http://en.wikipedia.org/wiki/Lyocell.

76. Majewicz, T.G., Erazo-Majewicz, P.E., Podlas, T.J. Polyethers. In: Kirk-Othmer Encyclopedia of Chemical Technology. John Wiley & Sons, New York, USA, 2001. Pp. 507–532.

77. Whistler, R.L., Bemiller, J.N., Pashall, E.F. Starch: Chemistry and Technology. Academic Press, Orlando, USA, 1984.

78. http://en.wikipedia.org/wiki/Cellulose.

79. http://en.wikipedia.org/wiki/Starch.

80. http://en.wikipedia.org/wiki/Amylose.

81. Hagemeyer, R.W. Paper coating. In: Hagemeyer, R.W. (Ed.). Pigments on paper. TAPPI Press, Atlanta, USA, 1984.

82. Patel, M. Minerals in paper manufacturing. Industry Paper Publications, Sambalpur, India, 2007.

83. Varjos, P., Mikkonen, H., Kataja, K., Kuutti, L., Luukkainen, S., Peltonen, S., Qvintus-Leino, P. In: PulPaper 2004 Conferences Coating Proceedings, The Finnish Paper Engineers Association, Helsinki, Finland, 2004. Pp. 131–134.

84. Peltonen, S., Mikkonen, H., Qvintus-Leino, P., Varjos, P., Kataja, K. Pigment and filler and a method of manufacturing it. Pat. WO2005030844, 2005.

85. Saari, J., Kataja, K., Qvintus-Leino, P., Kuutti, L., Peltonen, S., Mikkonen, H., Joyce, M. In: TAPPI 2005 Coating Conference and Exhibit Proceedings. TAPPI Press, Toronto, Canada, 2005. Pp. 271–276.

86. Johansson, A., Qvintus-Leino, P., Varjos, P., Peltonen, S., Mikkonen, H., Miettinen, M., Luukkainen, S. Porous filler or coating pigment of paper and cardboard and a method of manufacturing it. Pat. WO2005030847, 2005.

87. Penttilä, A., Lumme, K., Kuutti, Light-scattering efficiency of starch acetate pigments as a function of size and packing density. L. Appl. Opt. 2006, 45(15), pp. 3501–3509.

88. Monte, M.C., Fuente, E., Blanco, A., Negro, C. Waste management from pulp and paper production in the European Union. Waste Management 2009, 29(1), pp. 293–308.

89. Verordnung über das In Verkehr bringen von Düngemitteln, Bodenhilfsstoffen, Kultursubstraten und Pflanzenhilfsmitteln (Düngemittelverordnung – DüMV) vom 26. November 2003, Bundesgesetzblatt Jahrgang 2003 Teil I Nr. 57, ausgegeben zu Bonn am 4. Dezember 2003.

90. Heinze, T., Haack, V., Rensing, S. Starch derivatives of high degree of functionalization. 7. Preparation of Cationic 2-Hydroxypropyltrimethylammonium Chloride starches. Starch/Stärke, 2004, 56, pp. 288–296.

91. Pavlovic, S., Brandao, P.R.G. Adsorption of starch, amylose, amylopectin and glucose monomer and their effect on the flotation of hematite and quartz. Minerals Engineering 2003, 16, pp. 1117–1122.

92. Ott, G., Schempp, W., Krause, T. : Preparation of cationic cellulose with high degree of substitution in lithium chloride/dimethylacetamide. Papier 1989, 43(12), pp. 694–699.

93. Ashmore, M., Hearn, J. Flocculation of model latex particles by chitosans of varying degrees of acetylation. Langmuir 2000, 16(11), pp. 4906–4911.

94. Roussy, J., Van Vooren, M., Guibal, E. Chitosan for the Coagulation and Flocculation of Mineral Colloids. J. Dispersion Sci. Tech. 2004, 25(5), pp. 663–677.

95. Xie, C., Feng, Y., Cao, W., Xia, Y., Lu, Z. Novel biodegradable flocculating agents prepared by phosphate modification of Konjac. Carb. Polym. 2007, 67, pp. 566–571.

96. Nayak, B.K., Singh, R.P. Comparative studies on the flocculation characteristics of polyacrylamide grafted guar gum and hydroxypropyl guar gum-Polym. Int. 2001, 50(8), pp. 875–884.

97. Biswal, D.R., Singh, R.P. Characterisation of carboxymethyl cellulose and polyacrylamide graft copolymer. Carb. Polym. 2004, 57, pp. 379–387.

98. Oelmeyer, G., Krentz, O., Kuliche, W.-M. Chem. Combined Flocculant Systems with Cationic Starches in the Solid/Liquid Separation of Harbor Sediments. Eng. Technol. 2002, 25, pp. 47–50.

99. Bratskaya, S., Schwartz, S., Liebert, T., Heinze, Th. Starch derivatives of high degree of functionalization: 10. Flocculation of kaolin dispersions. Coll. Surf. A. 2005, 254, pp. 75–80.

100. Peltonen, S., Tiitola, P., Vuorenpää, J., Happonen, H., Törmälä, P. Hydroxyalkylated starch ester and preparation and use thereof. Pat. WO9829456, 1998.

101. Peltonen, J.P.K., Pingsheng, H., Rosenholm, J.B. Order and defects of Langmuir-Blodgett films detected with the atomic force microscope. J. Am. Chem. Soc. 1992, 114, pp. 7637–7642.

102. Mate, C.M., McClelland, G.M., Erlandsson, R., Chiang, S. Atomic-scale friction of a tungsten tip on a graphite surface. Phys. Rev. Lett. 1987, 59, pp. 1942–1945.

103. Meyer, G., Amer, N.M. Simultaneous measurement of lateral and normal forces with an optical-beam-deflection atomic force microscope. Applied Physics Letter 1990, 57, pp. 2089–2091.

104. Bhushan, B., Israelachvili, J.N., Landman, U. Nanotribology: friction, wear and lubrication at the atomic scale. Nature 1995, 374, pp. 607–616.

105. Overney, R.M., Meyer, E., Frommer, J., Brodbeck, C., Lüthi, R., Howald, L., Güntherodt, H.-J., Fujihira, M., Takano, H., Gotoh, Y. Friction measurements on phase-separated thin films with a modified atomic force microscope. Nature 1992, 359, pp. 133–135.

106. Connolly, M.L. Analytical molecular surface calculation. Int. Appl. Cryst. 1983, 16(5), pp. 548–558.

107. Sugiyama, J., Chanzy, H. personal communication 1992.

108. Discover program, Biosym Technologies Inc., San Diego, USA.

109. Nesse, W.D. Introduction to Optical Mineralogy. Oxford University Press, UK, 2012.

110. Kellomäki, M., Karema, H., Kataja, M., Salmela, J., Selenius, P. Fiber flocculation measurement in pipe flow by digital image analysis. In: Proc. TAPPI Intl. Paper Physics Conf., 1999. Pp. 461–463.

111. Karema, H., Salmela, J. Predication of paper formation by fluidization and reflocculation experiments. 12th Fundamental Research Symposium, UK, 2001. Pp. 559–589.

112. Salmela, J., Kataja, M. Floc rupture and re-flocculation in turbulent shear flow. 13th Fundamental Research Symposium, Cambridge, UK, 2005. Pp. 35–50.

113. Hanley, S.J., Giasson, J., Revol, J.-F., Gray, D.G. Atomic force microscopy of cellulose microfibrils: comparison with transmission electron microscopy. Polymer 1992, 33, pp. 4639–4642.

114. Heiner, A.P., Teleman, O. Interface between monoclinic crystalline cellulose and water: Breakdown of the odd/even duplicity. Langmuir 1997, 13, pp. 511–518.

115. Heiner, A.A., Kuutti, L., Teleman, O. Comparison of the interface between water and four surfaces of native crystalline cellulose by molecular dynamics simulations. Carb. Res. 1998, 306, pp. 205–220.

116. Baker, A.A., Helbert, W., Sugiyama, J., Miles, M.J. High-resolution atomic force microscopy of native valonia cellulose I microcrystals. J. Struct. Biol. 1997, 119, pp. 129–138.

117. Baker, A.A., Helbert, W., Sugiyama, J., Miles, M.J. New insight into cellulose structure by atomic force microscopy shows the i(alpha) crystal phase at near-atomic resolution. Biophys. J. 2000, 79, pp. 1139–1145.

118. Imai, T., Sugiyama, J. Nanodomains of I_α and I_β Cellulose in Algal Microfibrils. Macromolecules 1998, 31, pp. 6275–7279.

119. Hayashi, N., Sugiyama, J., Okano, T., Ishihara, M. Selective degradation of the cellulose Iα component in *Cladophora* cellulose with *Trichoderma viride* cellulase. Carb. Res. 1998, 305, pp. 109–116.

120. Hayashi, N., Sugiyama, J., Okano, T., Ishihara, M. The enzymatic susceptibility of cellulose microfibrils of the algal-bacterial type and the cotton-ramie type. Carb. Res. 1998, 305, pp. 261–269.

121. Wada, M., Okano, T. Localization of Iα and Iβ phases in algal cellulose revealed by acid treatments. Cellulose 2001, 8, pp. 183–188.

122. Li, W., Yan, L., Yang J. AFM study of crystalline cellulose in the cell walls of straw. Polym Int. 2006, 55, pp. 87–92.

123. Sugiyama, J., Chanzy, H., Revol, J.F. On the polarity of cellulose in the cell wall of *Valonia*. Planta 1994, 193, pp. 260–265.

124. Horikawa, Y., Sugiyama, J. Localization of Crystalline Allomorphs in Cellulose Microfibril. Biomacromolecules 2009, 10, pp. pp. 2235–2239.

125. Jenkins, P.J., Cameron, R.E., Donald, A.M. A universal feature in the structure of starch granules from different botanical sources. Starch / Stärke 1993, 45, pp. 417–420.

126. Gallant, D.J., Bouchet, B., Baldwin, P.M. Microscopy of starch: evidence of a new level of granule organization. Carb. Polym. 1997, 32, pp. 177–191

127. Baldwin, P. Studies on the surface chemistry, minor component composition and structure of granular starches. PhD Thesis, The University of Nottingham, U.K., 1995.

128. Forssell, P.M., Hulleman, S.H.D., Myllärinen, P., Moates, G.K.M., Parker, R. Ageing of rubbery thermoplastic barley and oat starches. Carb. Polym. 1999, 39, pp. 43–51.

129. Rindlav-Westling, Å., Gatenholm, P. Surface composition and morphology of starch, amylose, and amylopectin films. Biomacromolecules 2003, 4, pp. 166–172.

130. Myllärinen, P., Buleon, A., Lahtinen, R., Forsell, P. The crystallinity of amylose and amylopectin films. Carb. Polym. 2002, 48, pp. 41–48.

131. Puspadass, H., Hanna, M. Age-Induced Changes in the Microstructure and Selected Properties of Extruded Starch Films Plasticized with Glycerol and Stearic Acid. Ind. Eng. Chem. Res. 2009, 48, pp. 8457–8463.

132. Karvinen, P., Oksman, A., Silvennoinen, R., Mikkonen, H. Complex refractive index of starch acetate used as a biodegradable pigment and filler of paper. Opt. Mater. 2007, 29, 1171–1176.

PUBLICATION I

Identification and surface structure of crystalline cellulose studied by atomic force microscopy

In: Journal of Microscopy, 1995, 178, pp. 1–6.

Journal of Microscopy, Vol. 178, Pt 1, April 1995, pp. 1–6.
Received 30 August 1994; accepted 18 December 1994

Identification and surface structure of crystalline cellulose studied by atomic force microscopy

L. KUUTTI,* J. PELTONEN,† J. PERE* & O. TELEMAN*
*VTT, Biotechnology and Food Research, PO Box 1503, FIN-02044 Espoo, Finland
†Department of Physical Chemistry, Åbo Akademi University, Porthaninkatu 3–5, FIN-20500 Turku, Finland

Key words. AFM, crystalline cellulose, molecular modelling, Connolly surface.

Summary

A combination of molecular modelling and atomic force microscopy (AFM) techniques was used to study the surface structure of crystalline cellulose. Two-dimensional Fourier analysis of the AFM raw data gave crystal parameters as well as a highly filtered inverse-transformed image. Molecular modelling was used to generate Connolly surfaces based on electron diffraction data for crystalline cellulose. The modelled surfaces were used to interpret the experimental AFM images. Monoclinic ($1\bar{1}0$) crystal faces were identified. The method used enables the structural analysis of cellulose surfaces at the molecular level, where all biological processes involving cellulose take place.

1. Introduction

Although cellulose is the most abundant renewable organic compound in the biosphere, its molecular structure is still incompletely known. The three-dimensional structure of crystalline cellulose has been the focus of several investigations (Meyer & Misch, 1937; Honjo & Watanabe, 1958; Gardner & Blackwell, 1974; Sarko & Muggli, 1974). Atalla & VanderHart (1984) showed by high-resolution solid-state ^{13}C cross-polarization magic-angle nuclear magnetic resonance (CP/MAS NMR) spectroscopy that two phases, cellulose I_α and cellulose I_β, coexist in several native celluloses. The ratio I_α/I_β varies greatly depending on the cellulose substrate. Also by ^{13}C CP/MAS NMR spectroscopy it has been shown that the I_α phase is metastable and can be converted into the thermodynamically stable I_β phase by hydrothermal annealing (Horii *et al.*, 1987; Yamamoto *et al.*, 1989). Pure I_β cellulose has been isolated from animal cellulose (Belton *et al.*, 1989), but no pure I_α cellulose has been found or prepared so far. The unit-cell parameters of both crystalline phases were published in 1991 (Sugiyama *et al.*, 1991).

Atomic force microscopy (AFM) (Binnig *et al.*, 1986; Hansma *et al.*, 1988) has been used to image a wide variety of surfaces with atomic resolution by scanning a flexible cantilever tip over the studied surface. AFM can be applied directly to non-conducting surfaces and the AFM images are interpreted as maps of the total interaction including sterics and electrostatics (Binnig *et al.*, 1987; Meyer *et al.*, 1991). Cellulose microfibrils have also been studied by AFM (Hanley *et al.*, 1992), but as is often the case for biological surfaces, AFM images have only provided an idea of the surface topology (Hanley *et al.*, 1992; Bustamante *et al.*, 1993; Rees *et al.*, 1993).

We present here (i) an atomic force microscopy study at the molecular level of highly crystalline *Valonia macrophysa* vesicles; (ii) the generation of artificial AFM images from Connolly model surfaces (Connolly, 1983) of crystalline cellulose for the monoclinic (110 and $1\bar{1}0$) and the triclinic (010 and 100) crystal faces (Wada *et al.*, 1993) and (iii) a comparison of artificial and experimental images providing the means to identify the crystal faces of the studied celluloses. Finally, we discuss the differences between the experimental and artificial AFM images.

2. Experimental

Valonia celluloses contain 60–70% of the I_α crystalline phase (Atalla & VanderHart, 1984). In *Valonia macrophysa*, the cellulose microfibrils are highly organized, being packed in parallel within the wall layers. Prior to imaging, *Valonia macrophysa* vesicles were pretreated with dilute alkali and an excess of distilled water to remove residual hemicellulose. Small vesicle pieces (2 × 2 mm) were cut and placed on sample stubs. A Nanoscope II (Digital Instruments, Inc., Santa Barbara, CA, U.S.A.) AFM with a 100-μm cantilever tip with a spring constant of $k = 0{\cdot}38$ N m^{-1} was used to image the samples (Peltonen *et al.*, 1992). All images (400 × 400 pixels) were measured in air. Both height (constant deflection) and force (tip deflection is recorded according to the topographical changes on the sample surface) modes were used. The measuring unit was placed on a vibration-

isolating table to eliminate external noise. In addition, high-pass filtering via both the electronics and software was used to cut off low-frequency noise.

The Connolly algorithm was used to generate the solvent accessible surfaces for crystalline cellulose faces, starting from the atomic coordinates (J. Sugiyama *et al.*, pers. comm., 1992). The Connolly surface is the surface described by the centre of a probe sphere rolling over the actual surface and was calculated with the *Discover* program (Biosym Technologies Inc., San Diego, CA, U.S.A.). A value of 0·2 nm was used as the radius of the probe (solvent) molecule and the point density of the surface was 0·2 dots nm^{-2}. The maximum number of atoms in the calculation was below 2000 and all the calculations were performed as background processes. The calculations took from one to six CPU hours on a Silicon Graphics 4D/35 workstation depending on the radius of the probe and the point density of the surface. Two sets of atomic coordinates were used, namely those for triclinic (I_α) and monoclinic (I_β) cellulose. The coordinates for heavy atoms are based on electron diffraction data for fibres (J. Sugiyama *et al.*, pers. comm., 1992), and hydrogen atoms were modelled by *Insight II* (Biosym Technologies Inc.). The torsion angle H6-O6-O5-C5 was set to 180°. We generated four crystal faces by our own software, namely the monoclinic (110) and the triclinic (010) faces, which are equivalent faces of the microfibril, and the monoclinic ($1\bar{1}0$) and the triclinic (100) faces, which are also equivalent faces of the microfibril. Since the *d*-spacings are different on the two faces of the microfibril (monoclinic (110) 0·535 nm, triclinic (010) 0·528 nm versus monoclinic ($1\bar{1}0$) 0·607 nm, triclinic (100) 0·621 nm) (Wada *et al.*, 1993), the differences in the surface structure are mainly caused by the positions of the cellulose chains with respect to each other.

The artificial AFM images were generated from the crystal faces, i.e. one layer of cellulose chains containing 7–9 chains each with 9–12 glucose units depending on the crystal face. Each crystal face was rotated into the *xy*-plane with the cellulose chains parallel to the *y*-axis. The generated crystal face was rectangular (dimensions of the order of 2–4 nm) and typically limited by four glycosidic oxygens. The *z*-coordinate as a function of *x*- and *y*-coordinates was extracted from the Connolly surface and copied until the desired image size (13–14 nm) and resolution (200 × 200) were reached. Finally we scaled the height information to the vertical scale used in the AFM image (from 0 to 1·36 nm).

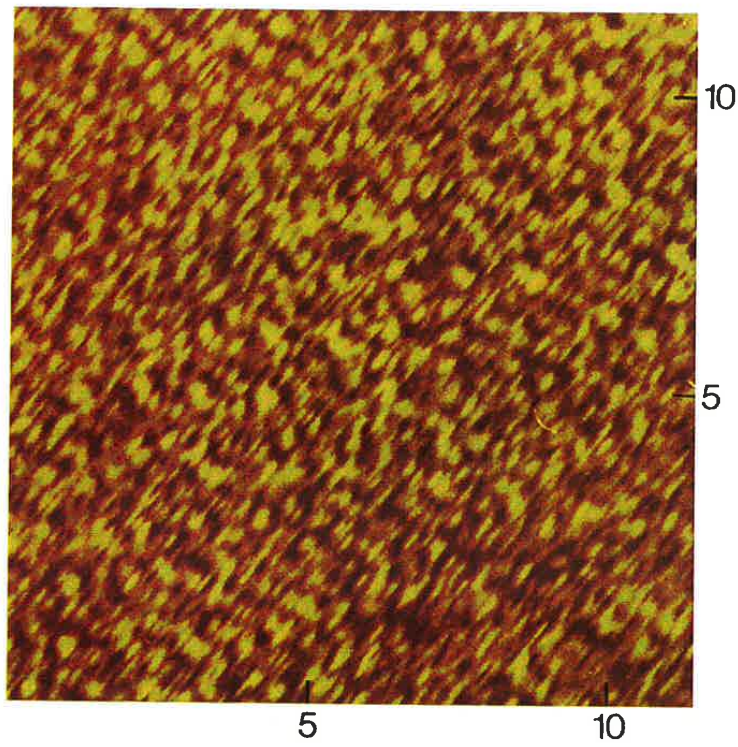

Fig. 1. AFM image of *Valonia macrophysa*. The image size is 11 × 11 nm^2 and the black-to-white colour scale (*z*-scale) is 0–1·7 nm. The microfibril direction is parallel to the *y*-axis. The height difference between light and dark spots in the middle of the image is between 0·25 and 0·4 nm.

3. Results and conclusions

The typical microcrystal width was 100 nm (measured by height mode) which is clearly greater than the average diameter of 20 nm observed by transmission electron microscopy (TEM) (Chanzy *et al.*, 1984). This broadening of the object is due to the convolution induced by the tip geometry (Hanley *et al.*, 1992). In a simple model (Butt *et al.*, 1992; Zenhausern *et al.*, 1992) the apparent lateral dimension (L) of the object is given by the expression

$$L = 4(Rr)^{1/2}$$

where R is the tip radius and r is the object radius. With the values R = 50 nm (Hanley *et al.*, 1992) and L = 100 nm, the width of one microcrystal becomes 25 nm. This result agrees with the experimental data obtained by TEM, but should only be considered as an estimate because the shape and dimensions of the tip are only assumptions and vary from one tip to another. Furthermore, the width and the cross-sectional shape of microcrystals depend on the scanning mode and the scan rate used (Hanley *et al.*, 1992). The AFM images indicate that a better dynamic response can be obtained on the micrometre scale when imaging in the force mode.

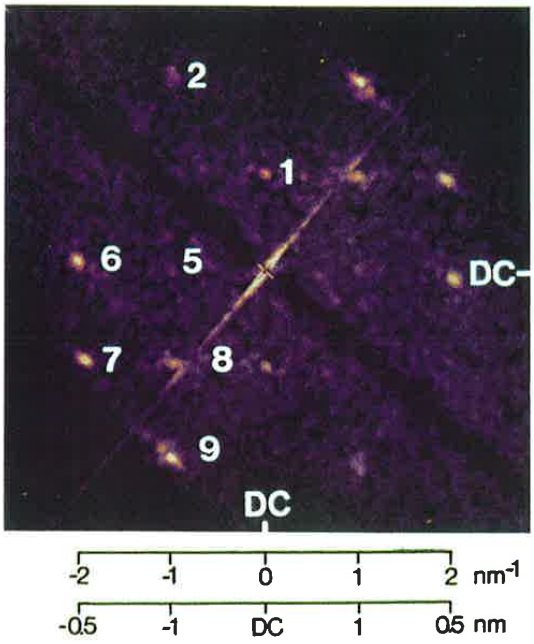

Fig. 2. FFT diffractogram of *Valonia macrophysa*. The spot numbers refer to the numbers in Table 1. The microfibril direction is parallel to the y-axis. The x-axis scale is given in two versions. The upper scale gives the spatial frequencies in nm^{-1}, while the lower is the inverted real space scale as given by most AFM instruments. Throughout this work we will use the physically correct spatial frequency scale in the images. The vertical scale is identical to the horizontal. DC = direct current. The light and dark diagonals correspond to DC parallel and perpendicular to the scanning direction of the microscope tip and are thus artefacts.

High-resolution images of the cellulose substrate were also obtained repeatedly by using the height mode. Figure 1 shows the membrane surface of a *Valonia macrophysa* vesicle (11 × 11 nm^2) with a surface roughness less than 1·7 nm. The two-dimensional fast Fourier transform (FFT) of the raw data (Fig. 2) gave crystal parameters as well as a highly filtered inverse-transformed image (not shown). The FFT spectra contained several bright spots revealing the periodicities and regularities of the surface. The *Valonia macrophysa* sample displayed a periodicity of 1·01 nm (compared to an observed periodicity of 1·07 nm for *Valonia ventricosa*; Hanley *et al.*, 1992), close to the fibre repeat unit length of 1·036 nm containing two glucose units (Sugiyama *et al.*, 1991).

The artificial AFM image of a monoclinic (110) crystal face with the characteristic two-dimensional FFT spectrum is shown in Figs. 3 and 4(A). The light spots in Fig. 3 arise from the $-CH_2OH$ side groups pointing out from the glucose ring. Because the artificial AFM image is based on a perfectly crystalline surface, the FFT diffractogram contains bright spots but little noise (Fig. 4A). Each spot is characterized by three parameters; R-value, angle and relative intensity. The R-value, in nm, indicates the period of the regularity and the angle indicates the relative direction of the regularity. Figure 4(A–D) present the FFT diffractograms of the four artificial crystal faces and in Table 1, the R-values of the spots have been collected and compared with the values obtained from the experimental FFT diffractogram of *Valonia*. As can be seen, the diffractograms of the monoclinic crystal faces (110) and ($1\bar{1}0$) are very similar (the angles and the relative intensities are almost the same) and only the R-values differ. The monoclinic (110) crystal face (Fig. 4A) has slightly greater R-values than those in the monoclinic ($1\bar{1}0$) crystal face (Fig. 4B). A clear difference is observed in the FFT diffractograms of the triclinic crystal faces. The diffractogram of *Valonia* agrees with the diffractogram of the monoclinic ($1\bar{1}0$) crystal face. *Valonia* microfibrils also contain triclinic domains (J. Sugiyama *et al.*, pers. comm., 1992), but hitherto we have not been able to obtain high-quality images of a triclinic surface.

The artificial and experimental AFM images differ mostly in the spot intensities. The artificial AFM images were generated from Connolly surfaces based only on van der Waals' interactions. This gave the $-CH_2OH$ side groups, which protrude from the glucose ring, a round and regular shape in the artificial AFM image and, in consequence, a diffractogram with symmetric spots. We believe that if the

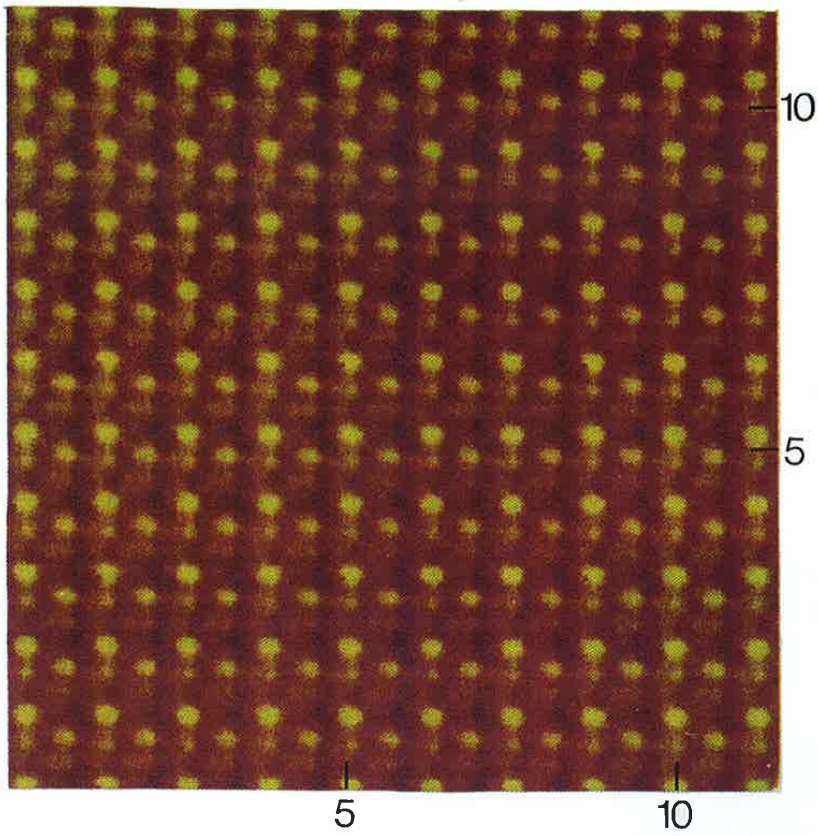

Fig. 3. An artificial AFM image of the monoclinic (110) crystal face. The image size is 11 × 11 nm^2. The black-to-white colour scale (*z*-scale) is 0–1·4 nm. The height difference between light and dark spots is between 0·2–0·3 nm. The microfibril direction is parallel to the *y*-axis.

artificial AFM images were generated from a more realistic interaction including electrostatics, the relative spot intensities would approach those obtained experimentally.

In conclusion, we have demonstrated how to interpret and identify the experimental AFM image of crystalline cellulose by comparing it to the artificial AFM image in reciprocal space. The differences in the comparison are mainly caused by modelling only the van der Waals' properties of the surface atoms, whereas the experimental AFM image represents both van der Waals' and electrostatic

Table 1. *R*-values (nm) collected from the FFT diffractograms of the artificial and experimental AFM images. The spot numbers refer to the numbers in Fig. 4. The precision in the distances is ± 0·02 nm. nd = not detected.

Spot no.	*Valonia* (exp)	Mon $1\bar{1}0$ (model)	Mon 110 (model)	Tri 010 (model)	Tri 100 (model)
1	1·01	1·03	1·03	0·97	0·93
2	0·44	0·47	0·48	0·32	0·29
3	nd	0·75	0·79	0·44	0·39
4	nd	0·48	0·52	0·61	0·53
5	1·00	1·07	1·18	0·64	0·58
6	0·50	0·53	0·60	0·47	0·47
7	0·47	0·48	0·52	0·34	0·34
8	0·72	0·74	0·77	0·26	0·26
9	0·46	0·47	0·47		

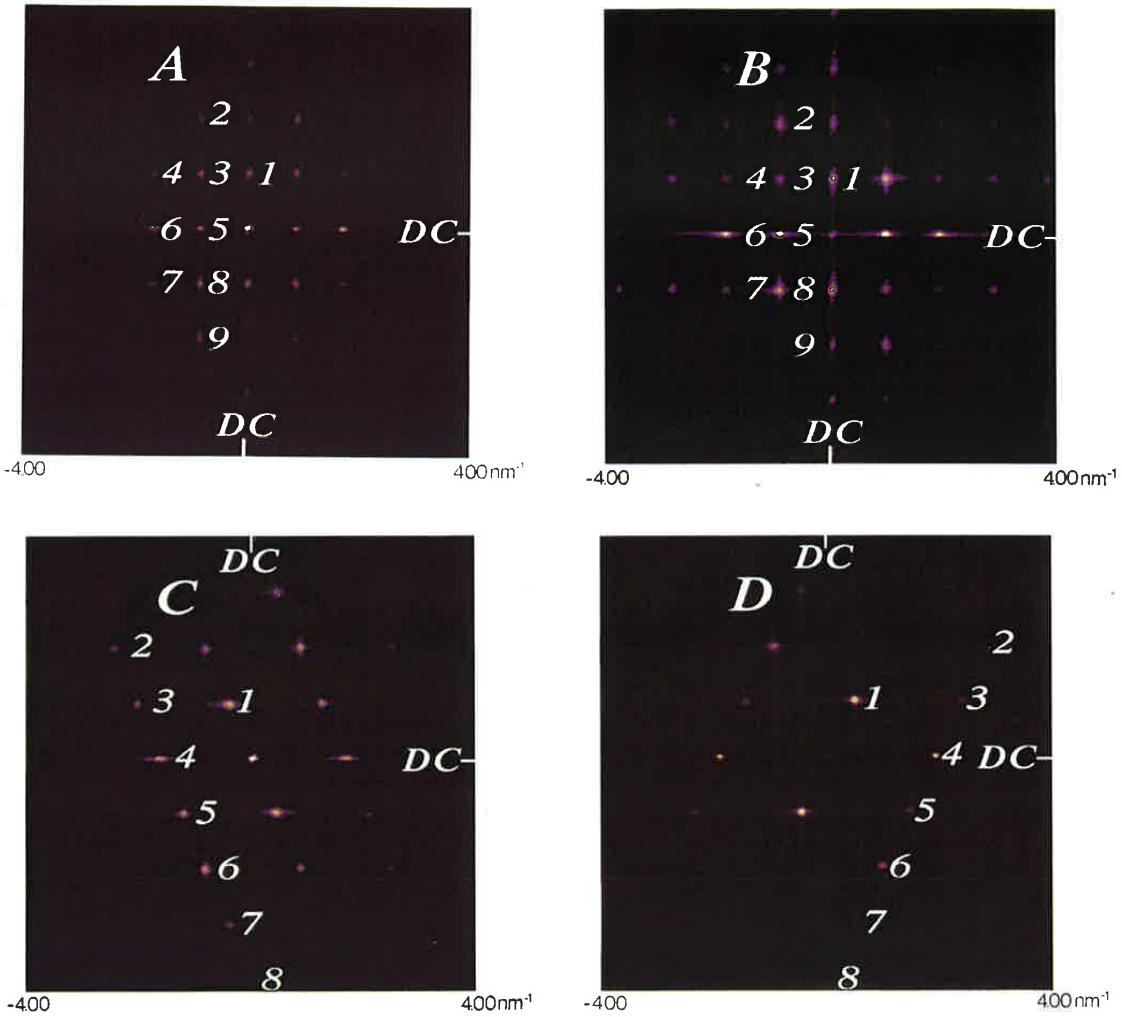

Fig. 4. FFT diffractograms of the four artificial crystal faces. (A) Monoclinic (110), (B) monoclinic ($1\bar{1}0$), (C) triclinic (010) and (D) triclinic (100) crystal face. The spot numbers refer to the numbers in Table 1. The microfibril direction is parallel to the y-axis. DC = direct current.

forces (Chen, 1991). Despite the differences, our results corroborate the fibre diffraction structure of the monoclinic phase and show that AFM can be used to study cellulose surfaces with a lateral resolution of about 0·4 nm. The possibility to access the microfibril surface directly is particularly important since all biologically important interactions involving cellulose occur at these surfaces.

Acknowledgments

We thank L. Laaksonen for helpful advice and discussion, J. Rosenholm for providing the use of the microscope, J. Sugiyama and H. Chanzy for providing their structural data before publication, and A. P. Heiner for useful critical discussion. Financial support by the VTT Research Programme on Biodegradable Plastics is gratefully acknowledged.

References

Atalla, R.H. & VanderHart, D.L. (1984) Native cellulose: a composite of two distinct crystalline forms. *Science*, **223**, 283–285.

Belton, P.S., Tanner, S.F., Cartier, N. & Chanzy, H. (1989) High-resolution solid-state ^{13}C nuclear magnetic resonance spectroscopy of tunicin, an animal cellulose. *Macromolecules*, **22**, 1615–1617.

Binnig, G., Quate, C.F. & Gerber, C. (1986) Atomic force microscope. *Phys. Rev. Lett.* **56**, 930–933.

Binnig, G., Gerber, C., Stoll, E., Albrecht, T.R. & Quate, F. (1987) Atomic resolution with atomic force microscope. *Europhys. Lett.* **3**, 1281–1286.

Bustamante, C., Keller, D. & Yang, G. (1993) Scanning force microscopy of nucleic acids and nucleoprotein assemblies. *Current Opinion in Structural Biology*, **3**, 363–372.

Butt, H.-J., Guckengerber, R. & Rabe, J.P (1992) Quantitative scanning tunneling microscopy and scanning force microscopy of organic materials. *Ultramicroscopy*, **46**, 375–393.

Chanzy, H., Henrissat, B. & Vuong, R. (1984) Colloid gold labelling of 1,4-β-D-glucan cellobiohydrolase adsorbed on cellulose substrates. *FEBS Lett.* **172**, 193–197.

Chen, C.J. (1991) Attractive interatomic force as a tunneling phenomenon *J. Phys.: Condensed Matter*, **3**, 1227–1245.

Connolly, M.L. (1983) Solvent-accessible surfaces of proteins and nucleic acids. *Science*, **221**, 709–713.

Connolly, M.L. (1984) *QCPE Program # 429*, Indiana University.

Gardner, K.H. & Blackwell, J. (1974) The structure of native cellulose. *Biopolymers*, **13**, 1975–2001.

Hanley, S.J., Giasson, J., Revol, J.-F. & Gray, D.G. (1992) Atomic force microscopy of cellulose microfibrils: comparison of transmission electron microscopy. *Polymer*, **33**, 4639–4642.

Hansma, P.K., Elings, V.B., Marti, O. & Bracker, C.E. (1988) Scanning tunneling microscopy and atomic force microscopy: application to biology and technology. *Science*, **242**, 209–216.

Honjo, G. & Watanabe, M. (1958) Examination of cellulose fibre by the low-temperature specimen method of electron diffraction and electron microscopy. *Nature*, **181**, 326–328.

Horii, F., Yamamoto, H., Kitamaru, R., Tanahashi, M. & Higuchi, T. (1987) Transformation of native cellulose crystals induced by saturated steam at high temperatures *Macromolecules*, **20**, 2946–2949.

Meyer, E., Heinzelmann, H., Brodbeck, D., Overney, G., Overney, R., Howald, L., Hug, H., Jung, T., Hidber, H.-R. & Güntherodt, H.-J. (1991) Atomic resolution on the surface of LiF (100) by atomic force microscopy. *J. Vac. Sci. Technol.* **B2**, 1329–1332.

Meyer, K.H. & Misch, L. (1937) Positions des atomes dans le nouveau modèle spatial de la cellulose. *Helv. Chim. Acta*, **20**, 232–244.

Peltonen, J.P.K., Pingsheng, H. & Rosenholm, J.B. (1992) Order and defects of Langmuir–Blodgett films detected with the atomic force microscope. *J. Am. Chem. Soc.* **114**, 7637- 7642.

Rees, W.A., Keller, R.W., Vesenka, J.P. Yang, G. & Bustamante, C. (1993) Evidence of DNA bending in transcription complexes imaged by scanning force microscopy. *Science*, **260**, 1646–1649.

Sarko, A. & Muggli, R. (1974) Packing analysis of carbohydrates and polysaccharides III. Valonia cellulose and cellulose II. *Macromolecules*, **7**, 486–494.

Sugiyama, J., Vuong, R. & Chanzy, H. (1991) Electron diffraction study of two crystalline phases occuring in native cellulose from an algal cell wall. *Macromolecules*, **24**, 4168–4175.

Wada, M., Sugiyama, J. & Okano, T. (1993) Native cellulose on the basis of two crystalline phase (I_α/I_β) system. *J. Appl. Polym. Sci.* **49**, 1491–1496.

Yamamoto, Y., Horii, F. & Odani, H. (1989) Structural changes of native cellulose crystals induced by annealing in aqueous alkaline and acidic solutions at high temperatures *Macromolecules*, **22**, 4130–4132.

Zenhausern, F., Adrian, M., ten Heggeler-Bordier, B., Eng, L.M. & Descouts, P. (1992) DNA and RNA Polymerase/DNA complex imaged by scanning force microscopy: influence of molecular-scale friction. *Scanning*, **14**, 212–217.

PUBLICATION II

AFM in studies of thermoplastic starches during ageing

In: Carbohydrate Polymers, 1998, 37,
pp. 7–12.

ELSEVIER

Carbohydrate Polymers 37 (1998) 7–12

Carbohydrate Polymers

AFM in studies of thermoplastic starches during ageing

L. Kuutti[a], J. Peltonen[b], P. Myllärinen[c], O. Teleman[c], P. Forssell[c,*]

[a]*VTT, Chemical Technology, PO Box 1401, FIN-02044 Espoo, Finland*
[b]*Department of Physical Chemistry, Åbo Akademi University, Porthaninkatu 3-5, FIN-20500 Turku, Finland*
[c]*VTT, Biotechnology and Food Research, PO Box 1503, FIN-02044 Espoo, Finland*

Received 16 January 1998; revised 21 April 1998; accepted 5 May 1998

Abstract

Atomic force microscopy (AFM) and friction force microscopy (FFM) have been used to characterize the ageing of thermoplastic starch (TPS) films prepared by the extrusion technique, using water and glycerol as plasticizers. The fresh oat and barley starch films (1 week after extrusion) have flat and homogeneous surfaces. In the older starch films (2–5 weeks), the surface roughness has changed and the friction images reveal surface heterogeneity. The structural changes are supported by the tip-sample force–distance curve analysis. The changes in the structural properties during ageing i.e. starch–glycerol phase separation, crystallization of starch, or reorientation of polymers, are discussed.

Keywords: Starch; Atomic force microscopy; Friction force microscopy

1. Introduction

Starch can be processed to mouldable thermoplastic material at high temperatures under shear (Shogren et al., 1992; Sala and Tomka, 1993). During processing the semi-crystalline structure is lost and the molecules are partially depolymerized. If water is used as the plasticizer the product is brittle, but in the presence of another plasticizer, such as glycerol, materials with varying mechanical properties can be prepared. Even if stored at constant humidity and temperature, the mechanical properties of thermoplastic starch (TPS) films change with time (Forssell et al., 1998).

Starch occurs as semi-crystalline small particles, which are insoluble in water at room temperature. Starch is a homopolymer of glucose consisting of α (1,4)-linked, essentially linear and α (1,4)- and α (1,6)-linked amylopectin, with a highly branched structure. The chains of amylose easily form single or double helices (Zobel, 1992). The linear outer chains of the amylopectin form left-handed double helical structures, with strong hydrogen bonding of the hydroxyl groups. The crystalline regions are arranged as thin lamellar domains (Kassenbeck, 1975; Kassenbeck, 1978).

The atomic force microscope (AFM) (Binnig et al., 1986) creates a surface image by scanning a flexible cantilever mounted tip over the sample. AFM is now an established technique (see e.g. Hansma et al., 1988; Drake et al., 1989; Hansma et al., 1991; Butt et al., 1992; Peltonen et al., 1992; Bustamante and Keller, 1995; Zasadzinski, 1996) and will not be described in detail here. When the tip is scanned sideways, the friction force causes a torsion in the tip cantilever. A micrograph showing this torsion is termed friction force microscopy (FFM) (Mate et al., 1987; Meyer and Amer, 1990; Bhushan et al., 1995), and can be used, for example, to resolve different phases in phase-separated thin films (Overney et al., 1992).

AFM has been used directly in the structural investigation of biological specimens (Bustamante et al., 1994, Yang and Shao, 1995) and surfaces. Hanley and Gray applied the technique to cellulose microfibrils (Hanley et al., 1992; Hanley et al., 1994), and obtained information on the microfibril morphology at the 100 nm scale. More recently, we achieved a resolution of 4 Å in AFM micrographs of crystalline cellulose surfaces (Kuutti et al., 1995), and demonstrated that they corroborate the three-dimensional crystalline cellulose structures derived from electron diffraction experiments (Wada et al., 1993; Sugiyama et al., personal communication, 1992). AFM has also been applied to image real-time enzymatic degradation of starch granules (Thomson et al., 1994) and the surface structures of a starch–zein thermoplastic polymer (Gauldie et al., 1994).

* Corresponding author. Tel: 00 358 94565212; Fax: 00 358 94552103; e-mail: pirkke.forssell@vtt.fi

0144–8617/98/$ - see front matter
PII S0144-8617(98)00042-3

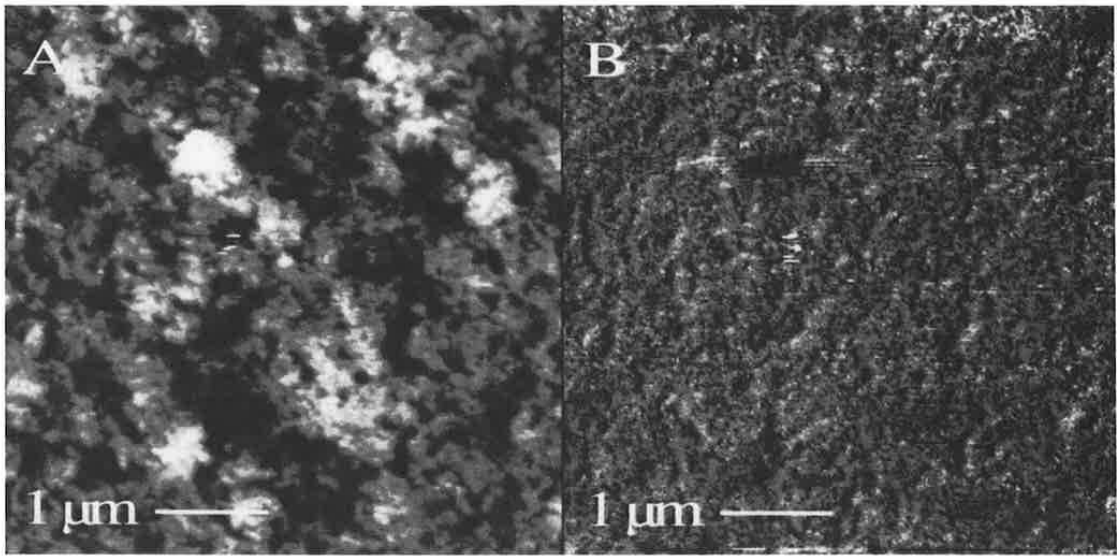

Fig. 1. (a) A top-view AFM image of the fresh barley film (1 week old), and (b) a simultaneously measured lateral force image. The image size is $5 \times 5\ \mu m^2$ and the black-to-white colour scale in (a) (z-scale) is 0–50 nm. The friction image (b) reveals a homogenous surface (relative scale).

Here, we use atomic and friction force microscopy to characterize the ageing phenomena at the surface of TPS films. Some results of a tip-sample force–distance curve analysis are also presented. The molecular origin of ageing is discussed.

2. Materials and methods

2.1. Materials

Barley and oat starch were obtained from Primalco Ltd (Rajamäki, Finland), and glycerol was obtained from Akzo Chemicals (Riedel-de Haën, Seelze, Germany), (85%). Thermoplastic barley and oat starch films were prepared by the plasticization of a starch/glycerol/water mixture in a twin screw extruder (Clextral BC-21, Firming, France), and processing the plasticized mixture to films in a single screw extruder (Brabender Plasti-Corder, Duisburg, Germany). The processing was repeated three times to ensure homogeneity. In both extruders the barrel temperature was 170°C and the die temperature 120°C. Water content of the feed was about 12% by weight and glycerol content 30% by weight (dry basis). The fresh films were near transparent. The ageing occurred under controlled conditions by storing for 1–5 weeks at constant humidity and temperature (RH 50%, 20°C).

2.2. Methods

A Nanoscope III AFM (Digital Instruments, Inc., Santa Barbara, USA) with 200 μm sharpened Si_3N_4 tips, with a spring constant of $k = 0.12$ N/m was used to image the samples. Small pieces of TPS films ($4 \times 4\ mm^2$) were cut and placed on sample stubs. All images (512×512 pixels) were measured in air in the constant force mode (constant deflection). The roughness values were measured for images of the same size, $5 \times 5\ \mu m^2$. The friction mode measures the lateral forces, i.e. the torsion of the cantilever spring in the direction of scanning. The friction images were measured during retrace scanning, so that the dark colour indicates high friction and the light colour low friction, only images with relative friction scale, are presented. The microscope was placed on a vibration damping table to eliminate external noise.

3. Results and discussion

3.1. Ageing of thermoplastic starch films

Fig. 1(a) shows a $5 \times 5\ \mu m^2$ AFM image of the fresh barley film (1 week old), and Fig. 1(b) the corresponding friction force micrograph. The mean roughness of the porous surface was typically 4 ± 1 nm. The friction image indicates a homogeneous surface, i.e. the friction varies little within the studied surface. The fresh oat film (images not shown) is similar, although somewhat rougher, 10 ± 2 nm, and very sticky.

The 2-week-old barley film is rougher (12 ± 2 nm) than the fresh, but remains homogeneous regarding friction. Fig. 2 shows $10 \times 10\ \mu m^2$ micrographs of the 2-week-old oat film. The height profile is similar to that of a 1-week-old sample. The surface roughness has, however, decreased clearly, being 6 ± 1 nm. The main change is observed in

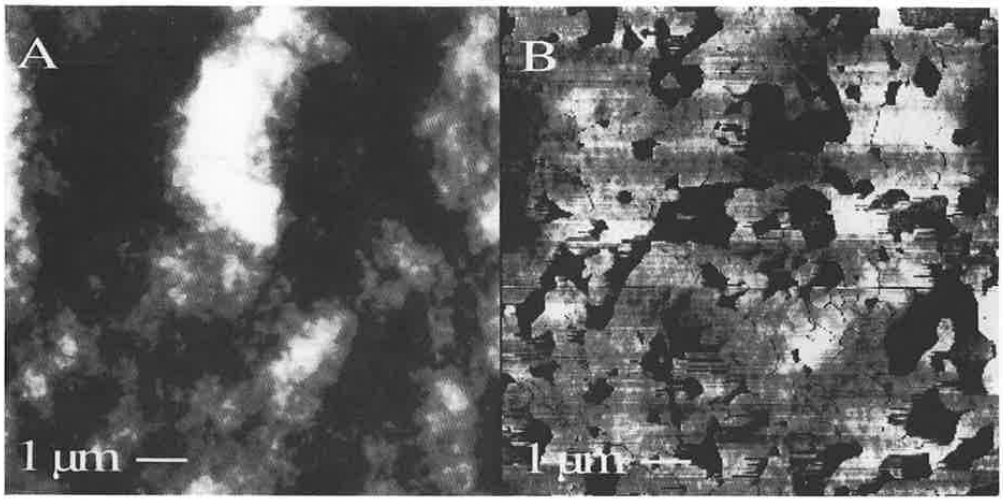

Fig. 2. (a) A 10 × 10 μm^2 top-view AFM image of the 2-week-old oat film, and (b) the respective FFM image. The black-to-white colour scale of (a) (z-scale) is 0–150 nm. The friction image (b) reveals a partly heterogenous surface stucture, i.e. there are dark and light areas of high and low friction.

the friction image, revealing a partly heterogeneous surface structure [Fig. 2(b)] featuring high (dark) and low (light) friction areas. The areas of low friction dominate the surface. The differences in friction are not due to changes in topography, as seen by comparing Fig. 2(a) and (b). The stickiness of the oat film has decreased considerably.

In the 3–4-week-old oat samples, the same two-phase structure was observed on the surface. The relative amount of the low friction areas has increased even further. The topographic image shows small, round, island-like structures. The friction images captured for barley still indicate a homogeneous surface at an age of 3–4 weeks.

At 5 weeks, the initial higher friction phase has disappeared almost completely from the surface of the oat film, even if local differences are significant. The mean roughness has increased to 15 ± 5 nm. At this age the surface structure of barley also begins to change, as indicated by the friction data. The total surface roughness has increased, but flat areas on the surface are observed from both image types [Fig. 3]. These flat areas are approximately 10 nm thick and often hundreds of nanometers in lateral size (Fig. 4), and appear to have a multilayer lamellar structure. These lamellae are not always straight, parallel, or of uniform thickness, but are typically slippery. Thus, the ageing

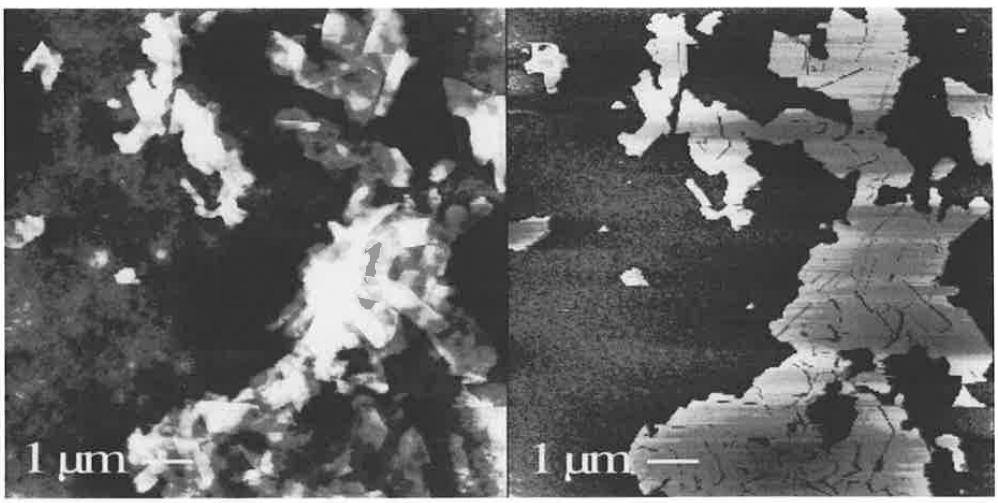

Fig. 3. The 5-week-old barley film, (a) a 10 × 10 μm^2 top-view AFM image, and (b) the respective FFM image. The black-to-white colour scale of (a) (z-scale) is 0–100 nm.

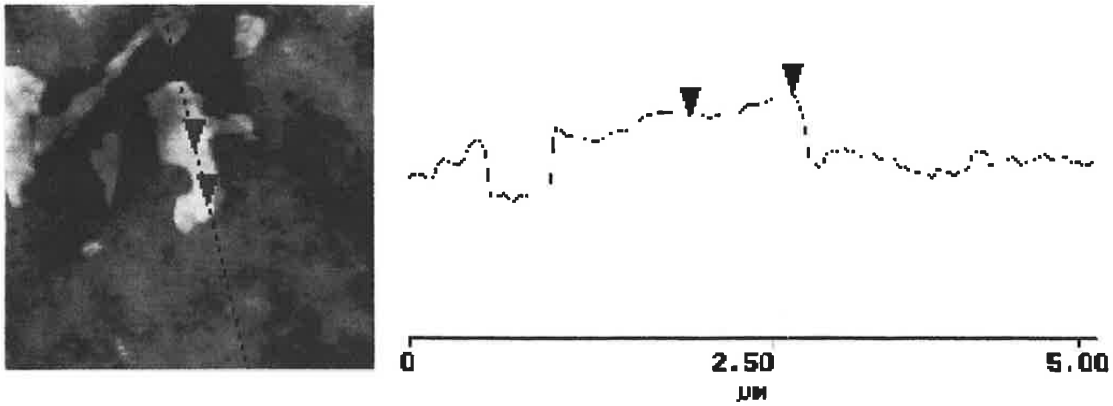

Fig. 4. The section analysis of one multilayer lamellar structure in the barley film. The vertical distance between the two arrows in the figure is 7.1 nm.

brings about a lower friction surface in both oat and barley based films.

An interesting detail ($4 \times 4\ \mu m^2$) of the suggested multilayer lamellar structure is shown in Fig. 5. The right-hand image was recorded immediately after the left-hand one. Part of the lamellar structure in Fig. 5(a) has been peeled off by the microscope tip, as seen in Fig. 5(b). The peeling occurs from the light areas but not from other topological features, which indicates that the flat, slippery areas are softer.

3.2. Force curve analysis

Measurement of the tip-sample, force–distance curves gave additional information about the ageing phenomenon, regarding the changes in the maximum attractive van der Waals force F_{attr} at the point of contact and the adhesion force F_{adh} at the pull-off point (Fig. 6). F_{attr} is directly proportional to the Hamaker constant A, according to the equation $F_{attr} = (AR)/(6d^2)$, where d is the tip-sample distance, normally in the range of 2–4 Å (Israelachvili, 1992), and R is the radius of the microscope tip, assumed to be 40 nm. In the studied system (tip–air–sample), only the sample properties change with time and thus affect the value of A. The adhesion force, F_{adh}, is proportional to the surface energy (Johnson et al., 1971) as $\gamma = F_{adh}/3\pi R$.

Both the Hamaker constant and the surface energy increased with age, although faster for the oat samples.

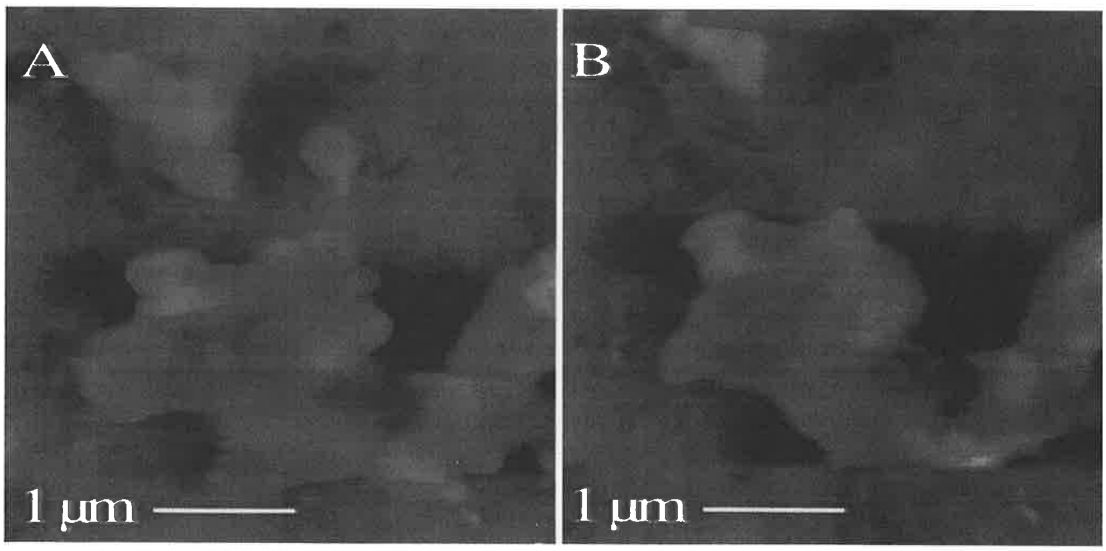

Fig. 5. An interesting detail of the suggested multilayer lamellar structure shown in Fig. 4. These $4 \times 4\ \mu m^2$ FFM images have been measured immediately after each other. Certain parts of the lamellar structure in (a) have been peeled off by the tip, as seen in (b).

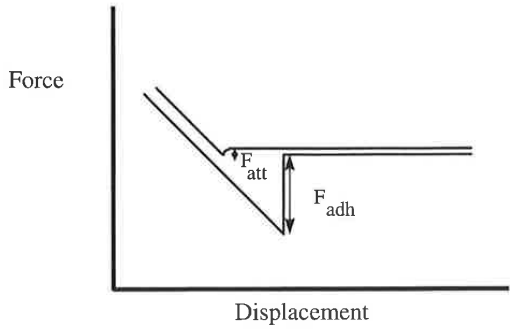

Fig. 6. The tip-sample force–distance curve. F_{attr} is the maximum attractive van der Waals force at the point of contact, and F_{adh} is the adhesion force at the pull-off point.

This is consistent with the observed FFM data which showed heterogeneous friction image already for the 2-week-old sample. The final surface energy of the oat sample is close to the literature value of glycerol, 64 mJ/m^2 (Israelachvili, 1992). However, these results should be considered as preliminary, due to the inaccuracy of the known tip radius and the geometry. The obtained value represents an average for the entire sample; statistics were not collected in a phase separated way. Further, the applied formula neglect any other interactions other than van der Waals.

3.3. Crystallinity changes

In a separate study we have determined the change in crystallinity in extruded starch films (Forssell et al., 1998). Oat and barley films were found to contain the same amount of B-type crystallinity. When fresh, the barley film contained a fair amount of Eh-type crystallinity, which slowly converted into Vh. The oat film contained only Vh-type crystallinity when fresh.

In connection with our results on surface changes, it appears that the Eh-type crystallinity may hinder glycerol diffusion, whereas the Vh-type does not, i.e. it allows the formation of pure glycerol patches on the film surface sooner for the oat film than for barley.

4. Conclusions

The aim was to study the surface of TPS films with FFM and to produce data, which could explain the obtained mechanical behaviour of TPS during ageing (Forssell et al., 1998). The frictional imaging enabled the observation of a contrast in a phase-separated substrate surface, even without topographical differences between the components.

Material-specific friction on the nanometer scale depends on the chemical and physical nature of the molecule. In particular, the stiffness of the molecule, the intra- and intermolecular forces, and the morphological state of the molecule are important. The starch–glycerol–water phase separation on the surface of oat and barley thermoplastic starch films differs from each other. On the surface of oat films, the reason seems to be the diffusion of glycerol. Glycerol, as a small and flexible molecule, seems to diffuse from the starch–glycerol–water matrix to the surface, making those low friction areas. The appearance of glycerol seems to be consistent with the increasing surface energy. In turn, the increasing surface energy coincides with increasing friction, which is in agreement with earlier reports (Green et al., 1995). Also, the decrease in the stickiness of the oat films point to glycerol diffusion.

In the case of barley starch films, the reason seems to be, at first, short-range reorientation of polymers, and finally, the crystallization of starch. The polymer chains form helical crystal structures, which seem to be rather soft material. Earlier results (Kassenbeck, 1975; Kassenbeck, 1978; Jenkins et al., 1993) concerning the thickness of the crystalline lamellae from different botanical sources support our result of approximately 10 nm. The crystalline lamellae in barley starch films are not so-called blockets (Gallant et al., 1997), which are spherical and range in diameter from 20–500 nm depending on starch type and location in the granule (Baldwin, 1995).

Acknowledgements

We thank Dr. A. P. Heiner for useful critical discussions and Prof. J. B. Rosenholm for providing the use of the microscope. Pirkko Forssell gratefully acknowledges financial support through the EC project AIR-2-CT94-1187.

References

Baldwin, P. (1995). Studies on the surface chemistry, minor component composition and structure of granular starches. PhD Thesis, The University of Nottingham, UK.

Bhushan, B., Israelachvili, J. N., & Landman, U. (1995). Nanotribology: friction, wear and lubrication at the atomic scale. *Nature*, *374*, 607–616.

Binnig, G., Quate, C. F., & Gerber, C. (1986). Atomic force microscope. *Phys. Rev. Lett.*, *56*, 930–933.

Bustamante, C., Erie, D., & Keller, D. (1994). Biochemical and structural applications of scanning force microscopy. *Curr. Opin. Struct. Biol.*, *4*, 750–760.

Bustamante, C., & Keller, D. (1995). Scanning force microscopy in biology. *Physics Today*, *Dec*, 32–38.

Butt, H.-J., Guckenberger, R., & Rabe, J. P. (1992). Quantitative scanning tunneling microscopy and scanning force microscopy of organic materials. *Ultramicroscopy*, *46*, 375–393.

Drake, B., Prater, C. B., Weisenhorn, A. L., Gould, S. A. C., Albrecht, T. R., Quate, C. F., Cannell, D. S., Hansma, H. G., & Hansma, P. K. (1989). Imaging crystals, polymers, and processes in water with the atomic force microscope. *Science*, *243*, 1586–1589.

Forssell, P. M., Hulleman, S. H. D., Myllärinen, P., Moates, G. K. M., & Parker, R. (1998). Ageing of rubbery thermoplastic starches prepared from barley and oat starches. *Carbohydrate Polymers*, submitted.

Gallant, D. J., Bouchet, B., & Baldwin, P. M. (1997). Microscopy of starch: evidence of a new level of granule organisation. *Carbohydrate Polymers, 32*, 177–191.

Gauldie, R. W., Raina, G., Sharma, S. K., & Jane, J.-L. (1994). Atomic force microscopy images of starch polymer; crystalline and amorphous structures. In Cohen et al. (Eds.), *Atomic force microscopy/scanning tunneling microscopy* (pp. 85–90). New York: Plenum Press.

Green, J.-B. D., McDermott, M. T., Porter, M. D., & Siperko, L. M. (1995). Nanometer-scale mapping of chemically distinct domains at well-defined organic interfaces using frictional force microscopy. *J. Phys. Chem., 99*, 10960–10965.

Hanley, S. J., Giasson, J., Revol, J.-F., & Gray, D. G. (1992). Atomic force microscopy of cellulose microfibrils: comparison of transmission electron microscopy. *Polymer, 33*, 4639–4642.

Hanley, S. J., Gray, D. G. (1994). Atomic force microscope images of black spruce wood section and pulp fibres. *Holzforschung 48*, 29–34.

Hansma, P. K., Elings, V. B., Marti, O., & Bracker, C. E. (1988). Scanning tunneling microscopy and atomic force microscopy: application to biology and technology. *Science, 242*, 209–216.

Hansma, H. G., Weisenhorn, A. L., Edmundson, A. B., Gaub, H. E., & Hansma, P. K. (1991). Atomic force microscopy: seeing molecules of lipid and immunoglobulin. *Clin. Chem., 37*, 1497–1501.

Israelachvili, J. N. (1992). *Intermolecular and surface forces* (p.176). New York: Academic Press.

Johnson, K. L., Kendall, K., & Roberts, A. D. (1971). Surface energy and the contact of elastic solids. *Proc. R. Soc. Lond. Ser. A, 324*, 301–313.

Jenkins, P. J., Cameron, R. E., & Donald, A. M. (1993). A universal feature in the structure of starch granules from different botanical sources. *Starch/Stärke, 45*, 417–420.

Kassenbeck, P. (1975). Elektronenmikroskopischer Beitrag zur Kenntnis der Feinstruktur der Weizenstärke. *Starch/Stärke, 27*, 217–227.

Kassenbeck, P. (1978). Beitrag zur Kenntnis der Verteilung von Amylose and Amylopektin in Stärkenkörnern. *Starch/Stärke, 30*, 40–46.

Kuutti, L., Peltonen, J., Pere, J., & Teleman, O. (1995). Identification and surface structure of crystalline cellulose studied by atomic force microscopy. *J. Microscopy, 178*, 1–6.

Mate, C. M., McClelland, G. M., Erlandsson, R., & Chiang, S. (1987). Atomic-scale friction of a tungsten tip on a graphite surface. *Phys. Rev. Lett., 59*, 1942–1945.

Meyer, G., & Amer, N. M. (1990). Simultaneous measurement of lateral and normal forces with an optical-beam-deflection atomic force microscope. *Appl. Phys. Lett., 57*, 2089–2091.

Overney, R. M., Meyer, E., Frommer, J., Brodbeck, C., Lüthi, R., Howald, L., Güntherodt, H.-J., Fujihira, M., Takano, H., & Gotoh, Y. (1992). Friction measurements on phase separated thin films with a modified atomic force microscope. *Nature, 359*, 133–135.

Peltonen, J. P. K., Pingsheng, H., & Rosenholm, J. B. (1992). Order and defects of Langmuir–Blodgett films detected with the atomic force microscope. *J. Am. Chem. Soc., 114*, 7637–7642.

Shogren, R. L., Swanson, C. L., & Thomson, A. R. (1992). Extrudates of corn starch with urea and glycols: structure/mechanical property relations. *Starch/Stärke, 44*, 335–338.

Sala, R., & Tomka, I. (1993). Water uptake in partially frozen and plasticized starch. In J. M. V. Blanshard & P. J. Lillford (Eds.), *The glassy state in foods* (pp.483–489). Nottingham: Nottingham University Press.

Thomson, N. H., Miles, M. J., Ring, S. G., Shewry, P. R., & Tatham, A. S. (1994). Real-time imaging of enzymatic degradation of starch granules by atomic force microscopy. *J. Vac. Sci. Technol., B12*, 1565–1568.

Wada, M., Sugiyama, J., Okano, T. (1993). Native celluloses on the basis of two crystalline (Iα/Iβ) system. *J. Appl. Polym. Sci. 49*, 1491–1496.

Yang, J., & Shao, Z. (1995). Recent advances in biological atomic force microscopy. *Micron, 26*, 35–49.

Zasadzinski, J. A. (1996). Scanning force microscopy: new instrumentation and applications. *Curr. Opin. Colloid Interface Sci., 1*, 264–269.

Zobel, H. F. (1992). Starch granule structure. In *Developments in carbohydrate chemistry* (pp. 1–36). American Association of Cereal Chemists, St. Pauls, MN.

PUBLICATION III

Novel method for preparation of spherical starch ester pigment with excellent optical properties in paper coatings

In: Applied Material Research at VTT. Symposium on Applied Materials, Espoo, Finland, 2006. VTT Symposium 244. Pp. 235–243.

Novel method for preparation of spherical starch ester pigment with excellent optical properties in paper coatings

Hannu Mikkonen[1], Lauri Kuutti[1], Kirsi Kataja[2], Pia Qvintus-Leino[2], Soili Peltonen[1]

VTT Technical Research Centre of Finland
[1] Tykkimäentie 15, P.O. Box 21, FIN-05201 Rajamäki, Finland
[2] Biologinkuja 7, P.O. Box 1602, FIN-02044 VTT, Finland

Abstract

The preparation of highly porous starch acetate particles suitable for filler for paper was studied using solution precipitation techniques. Chemically cleaved starch acetate with DS value of 2 to 3 and glass transition temperature of + 158–160 °C was used as starting material for the preparation of ideally spherical particles in diameter ½ of the wave length of the visible light. Particle shape and size take form spontaneously when solvated (e.g. acetone-ethanol mixture) starch polymer is mixed with non-solvent (e.g. water). The refractive index of the starch pigment is 1.47 and ISO brightness value as high as 94 have been measured. The preparation of starch pigment dispersion of 20–30% solid contents has been carried out in semi industrial scale by using 0,25 m^3 DRAISS reactor in combination with 0,2 micron cut-off continuous filtering unit. Starch pigment has improved affinity to paper surface and it can be used as such or mixed with other pigments to enhance optical or printing properties of paper.

Introduction

In print paper industry one of the main basis to produce high quality printings on paper are brightness and opacity, which are achieved by good fillers and coating pigments. Brightness and opacity are based on effective light scattering of the wood fiber network deposit by fillers and pigments. The mineral pigments and fillers have been used mainly for papermaking to produce high quality printings and the plastic pigments (typically consist of 100 % modified polystyrene) have been used only for certain special printing applications. The reasons for the major used of minerals pigments are cost-effectiveness, availability, high brightness and opacity.

However the mineral pigments has notable environmental aspect in de-inking waste. In Europe 81.7 million tons of paper was consumed and 46.1 million tons were recycled, 23.8 million tons of paper ended up directly to final disposal (landfill, combustion) after primary use. If fillers and pigments were organic and they could be combusted, 8 million tons of fuel oil could be replaced by them in energy production [1]. Contrary to mineral pigment de-inking waste, organic starch-based pigment waste can be incinerated. Other possible advantages of renewable starch based pigments are lightweight, better paper

strength properties, less abrasive character to paper machine components (wires, cutters etc.) and environment friendliness.

Our ambitious target was to develop from scratch starch based non-mineral paper pigments to replace mineral pigments. The opacity goal has been approached from three different directions. The first approach has been to process rigid, water in-soluble pigment particles with particle size ideal to obtain maximum light scattering properties.
The second approach to obtain maximum light scattering was to develop relatively rigid and porous pigment particles. The assumption was that appropriate pore structure in rigid pigment may increase its light scattering properties [2]. The third approach abandons completely solid and rigid pigment particles and uses foam (micro capsules) to built light scattering interfaces. A rigid foam structure containing suitable sized micro capsule structure coated on paper may also perform good light scattering properties [3].
In the literature there are actually very little references on non-mineral coating pigments or fillers. Mälkki *et al.* [4] has produced a method for preparing an organic filler pigment from starch. Starch granules are swollen to increase their volume and plasticity. Their stability towards changes in volume and shape is improved by cross-linking and by derivatization or by making the surface hydrophobic. Bengts *et al.* [5] has produced a method for production of spherical microparticles consisting totally or partly of at least one water-insoluble polysaccharide. The polysaccharide is dissolved in a solvent or solvent mixture and the solution thus formed is introduced into a precipitating agent or precipitating agent mixture. The mixture obtained is optionally cooled and the micro particles are separated.

Giezen *et al.* [6] has a process for producing biopolymers nanoparticles, in which the biopolymer is plasticized using shear forces, a cross-linking agent being added during the process. After said processing, the biopolymer can be dissolved or dispersed in an aqueous medium to a concentration between 4 to 40 wt. %. This results in starch nanoparticles which are characterized by an average particle size of less than 400 nm.

Biopolymer nanoparticles (the biopolymer latex adhesive) can be obtained by extruding a plasticized biopolymer, especially starch, in the presence of a cross-linking agent, e.g. glyoxal. The preparation of the latex adhesive and its application in corrugating operation do not require a gelatinization step, nor the use of caustic soda or borax [7].

We report in this paper the development of spherical particles in diameter ½ of the wave length of the visible light. Particle shape and size take form spontaneously when solvated (e.g. acetone-ethanol mixture) starch polymer is mixed with non-solvent (e.g. water). The optimization of the processes, the scale-up from laboratory scale to pilot scale and how to control the particle size distribution will be discussed in this paper. Some preliminary results on the pilot trials will also report here.

Methods and materials

The potato starch used in acetylating was provided by Periva Oy (Kokemäki, Finland). The used starch acetate was manufactured according to our patents (FI 107386, FI

20020313) [8], [9]. Chemically cleaved starch acetate (Mw : 50 000–250 000 with DS value of 2 to 3, glass transition temperature of + 158–160 °C and ISO brightness value of 88) was used as starting material for preparation of highly porous precipitated starch acetate. Molecular weight was determined with size exclusion chromatography. Three μHydrogel colons and one corresponding pre-colon was supplied by Waters Co.

Aqueous sodium hydroxide (50mM) was used as an eluant and a set of pullulan samples from Shodex were used as molecular weight standards.

One way to do highly spherical pigment structure is to dissolve starch based material to homogenous mixture of organic solvents and water. The choice of solvent combination and solid content of the solution is dependent on the solubility, molecular weight and degree of substitution of the starch derivative. 60 g starch derivative is dissolved to the mixture of 200 ml alcohol (denaturated alcohol, technical grade, Altia Ltd, Finland), 300 ml acetone (technical grade, Absor Ltd, Finland) and 50 ml water at 40 °C and after the complete dissolution, 300 ml alcohol is added more to the homogenous solution. To the solvated starch acetate solution is added very fast non-solvent water (2000 ml, 60 °C) stirring the solution at the same time (150 rpm). In the water has added 5 g surface-active agent (Kemira A41, Kemira Ltd, Finland) to prevent the agglomeration of the primary particle. During the dilution step a milky like particle dispersion forms. The formed dispersion is evaporated from the organic solvents at 60 °C many hours to remove especially acetone, which is a good plastiziser of starch acetate derivates. After the evaporation of the acetone and ethyl alcohol, we add 3 % wt $NaNO_3$ to the dispersion to salt out the formed particles to the bottom of the bottle. The precipitation is washed twice with excess of water to remove the small particles and impurity agents. The product is collected by using centrifugal forces and the dry content is between 20–30 %.

The produced filler particles were analysed by SEM to get information of the morphology of the primary particles and by Coulter® N4 Plus Particle Size Analyzer to get the particle size distributions.

Results and discussion

Morphology properties and particle size distribution

On the basis of experimental data, the real part of refractive index of starch acetate was observed to be 1,470 calculated by University of Joensuu (Department of Physics) [10], which was verified by microscopic immersion method. The optimum particle size of used materials has been calculated by University of Helsinki (Department of Astronomy) using complex light scattering models [11]. These models take into account morphology, packing density, size distribution and refractive index of the used material. The optimum particle size to obtain maximum light scattering properties for starch acetate was calculated to be between 150–200 nm in diameter. The optimum particle size is dependent of the packing density.

Small spherical particles in range 100–500 nanometres can be produced by dispersion method (fig. 1). We got bimodal particle size distribution (peaks at 258 and 893 nm) at the beginning of the project (fig. 2), when the dispersion was done at room temperature and the evaporation of the solvents at low pressure and temperature (112 mbar/40 ^{o}C). The SEM images showed the indication of agglomeration of primary pigment particles.

Using the procedure of elevated temperatures produced a very narrow unimodal particle size distribution, where the peak is located at 475 nm (fig. 2). The reason for the better quality of the distribution is more effective removal of the organic solvents from the pigment product. Especially the removal of acetone is important, because acetone is very good plastiziser of starch acetate derivate and complicate the optimization of the process a lot. At it's worst the primary particles fuse and agglomerate together as can been in fig 3. Too heavy mixing during the evaporation of the solvents (over 500 rpm in minute) agglomerates also the primary particles.

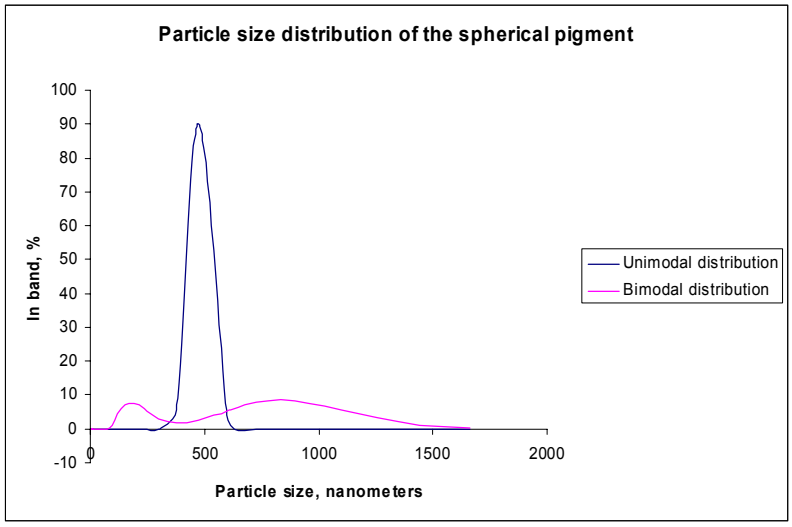

Figure 1. Particle size distribution of the spherical pigment before and after optimization of the process.

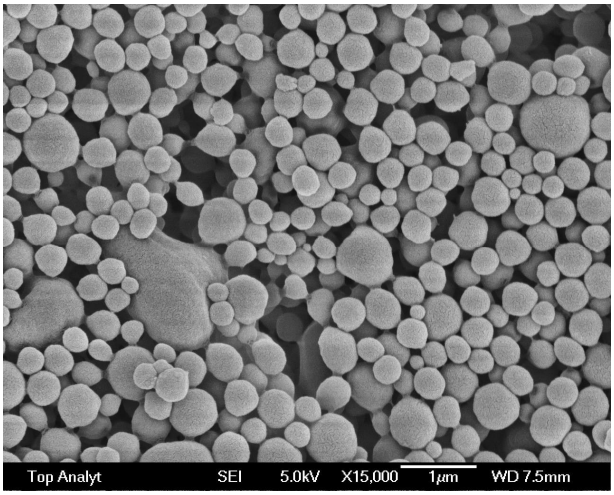

Figure 2. Spherical pigment particles.

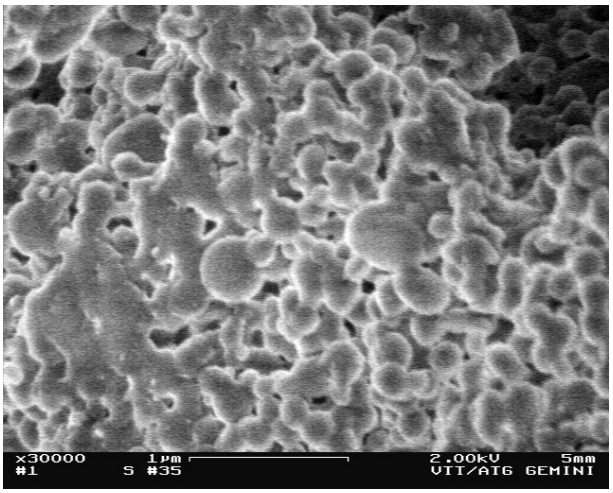

Figure 3. The fused and agglomerated primary particles.

Optical properties

Laboratory coating trials with K control coater were made to measure brightness and opacity of coated layer on paper. The opacity results of the different coating pigments are in figure 4 and the corresponding ISO-brightness results are in figure 5. PCC filler (FR-120, Huber) was used as a reference pigment and the used paper was uncoated book paper (62 % ISO-brightness and 96 % opacity). Commercial PCC is somewhat superior in both properties, but not drastically. The differences in the values of ISO-brightness and

opacity of the starch acetate pigments are mostly dependent of dry content and drying method. Some samples were in form of slurry dried by centrifugal forces (dry content between 20–30 %) and some samples were in form of powder dried by spray dryer. The final form of the pigment product has its influence to the particle size distribution and also to the degree of agglomerates of the primary pigment particle. As size distribution can be narrowed and brightness of starch product increased, these starch based pigments are good alternative to the PCC. The ISO-brightness results for the starch acetate pigment in standard compressed sample tablet form was as its best as good as 94,4 %.

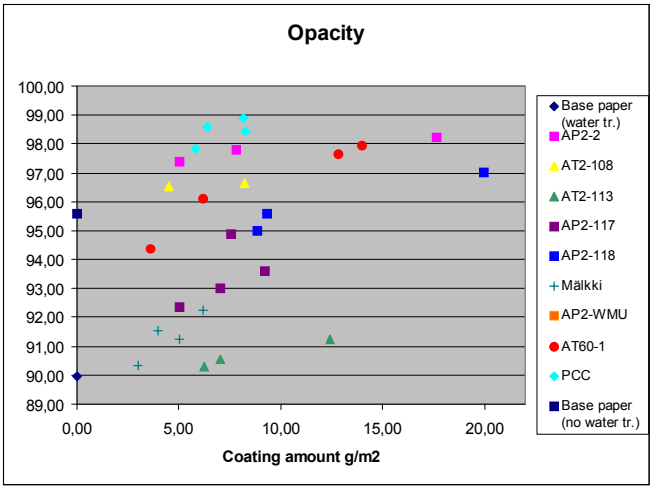

Figure 4. Opacity values of pigments and reference PCC coated on 52 g/m^2 book grade.

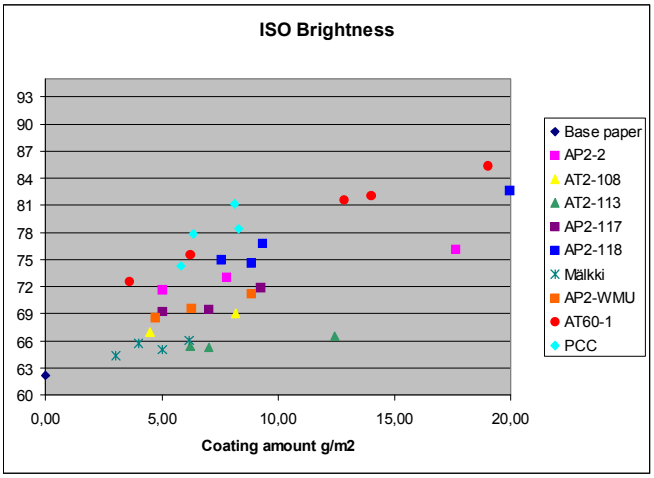

Figure 5. ISO-brightness values of experimental pigments and reference PCC coated on 52 g/m^2 book grade.

Up-scaling of the process

The preparation of the starting material starch acetate and starch pigment dispersion of 20–30% solid contents has been carried out in semi industrial scale by using 0,25 m^3 DRAISS TurbuDry T250 contact drier and reactor in combination with 0,2 micron cut-off continuous filtering unit. The reactor, which volume is 250 dm^3, is suitable for removal of water and organic solvents (ex-proof).

To get the starting material starch acetate with better ISO-brightness quality, the most important process parameter is the control of temperature during the non-pressurized acetate reaction. Also the use of nitrogen controlled atmosphere make the product whiter. The effective wash procedure is very important during the preparation of the filler particles. Vacuum is used for removal of the solvents, which has made the product of uniform quality. We have dried the coating pigment with spray dryer (NIRO Spray Dryer P-6.3) using surface-active agent to prevent the agglomeration of the filler particles.

Conclusion and future work

All the previous morphologies introduced have theoretical potential to replace mineral filler or coating pigments to obtain as good or even higher opacity and brightness to paper. Importantly it was shown that it is quite possible to produce water insoluble primary particles with optimum size to obtain light scattering that competes with commercial PCC products. Further work continues to narrow up the deviation in particle size. Also more concern is focused on increasing the brightness of the starting material and the final products.

As the project goes on, the approaches will be limited to develop one or two techniques and pigment morphologies to paper filler and coating applications. Also more emphasis has to be put on coating trials and to the retention issues in sheet and web forming (these tests have already started). Pilot scale coating and printing trials have been done at Western Michigan University. Preliminary results from pilot scale paper making trials indicate that usage of starch based coating pigment in fact increase the strength of paper. The result of the pilot scale trials reported elsewhere [12].

Reference list

1. European Fibre Flown Chart 2003, http://www.cepi.org, Confederation of European Paper Industries, 2003.

2. Mikkonen, H., Kuutti, L., Kataja, K., Qvintus-Leino, P. and Peltonen, S. Novel method for preparation of sub-micron scale highly porous starch acetate suitable for filler of paper with improved strength and optical properties*, in preparation.*

3. Miettinen, M., Mikkonen, H. and Luukkanen, S., *in preparation.*

4. Mälkki, H. and Lehtilä, R., US Patent 6, 582, 509, B2, 2003.

5. Bengts, H. and Grande, J., US Patent 6, 562, 459 B1, 2003.

6. Giezen, F., Jongboom, R., Feil, H., Gotlieb, K. and Boersma, A. PCT WO 00/69916, 2000.

7. Bloembergen, S., Kappen, F., and Van Leeuwen, M., EP 1254939, 2002.

8. Peltonen *et al.*, FI 107386, 1996.

9. Peltonen *et al.*, FI 20020313, 2002.

10. Karvinen, P., Oksman, A., Mikkonen, H. and Silvennoinen, R. Complex refractive index of starch acetate used as a biodegradable pigment and filler of paper, *in preparation.*

11. Penttilä, A., Lumme, K. and Kuutti L. Light scattering efficiency of starch acetate pigments as a function of size and packing density, *accepted to Applied Optics.*

12. J. Saari et al., *in preparation.*

Acknowledgement

This work is carried out in the projects of Nonfillpap-consortium (1.8.2003–31.7.2005), which is coordinated by the Technical Research Centre of Finland (VTT) and financially supported by National Technology Agency of Finland (Tekes), Metso Corporation, M-Real Corporation, Ciba Specialty Chemicals Corporation and Stora Enso Corporation. The authors wish to thank the project researchers of the University of Helsinki (University of Helsinki Observatory), the University of Joensuu (Department of Physics), the Geological Survey of Finland (GTK), the technician people of the laboratory and of the pilot plant at Rajamäki and the representatives of the above mentioned companies for fruitful cooperation and especially TEKES for financial support. In the management group the representatives from financing partners have contributed significantly to the project.

PUBLICATION IV

Starch-hybrid fillers for paper

In: Nordic Pulp and Paper Research Journal,
2010, 25(1), pp. 114–123.

Starch-hybrid fillers for paper

Lauri Kuutti, Kaisa Putkisto, Sari Hyvärinen, Soili Peltonen, VTT Technical Research Centre of Finland, Espoo, Finland, **Kimmo Koivunen, Hannu Paulapuro,** Aalto University, School of Science and Technology, Espoo, Finland, **Jere Tupala, Markku Leskelä, Tommi Virtanen, Sirkka Liisa Maunu,** University of Helsinki, Helsinki, Finland.

KEYWORDS: Starch-hybrid, Composite fillers, Complexation, Solution precipitation, Starch phosphate, Acetylated starch phosphate, Starch citrate, Carboxymethyl starch, Refractive index

SUMMARY: Starch-based pigmenting materials with improved optical performance have been prepared in the laboratory scale by the complexation approach. The water-based treatments using soluble, anionic starch derivatives target at insoluble hybrid materials between starch and ions of higher specific refractivity. Polymer derivatives selected from the group of starch phosphate, acetylated starch phosphate, starch citrate and carboxymethyl starch were combined with water-soluble inorganic salts to form insoluble pigmenting materials. The inorganic components were selected from the group of calcium-, barium-, zirconium-, zinc- and titanium-based compounds. The criteria for the selection included efficiency of polymer functionalization as well as the insolubility, yield and optical properties of the hybrid structures. Further evaluation has been made in respect of processability, suitability for cryogenic grinding and potential for paper manufacturing. The resulting precipitates exhibited composite structures and refractive indices depending on the inorganic constituent. In contrast to the inherent refractive index around 1.45 of starch-based materials, refractive indices between 1.50 and 1.55 (using Ca-, Zn- and Ba-components) and closer to 1.60 (using Zr- and Ti-components) have been observed for complexed materials. The prepared materials were characterized for complexation structure and stability and for suitability for filler applications in laboratory scale sheet formation.

ADDRESSES OF THE AUTHORS: **Lauri Kuutti** (lauri.kuutti@vtt.fi), **Kaisa Putkisto** (kaisa.putkisto@vtt.fi), **Sari Hyvärinen** (sari.hyvarinen@vtt.fi), **Soili Peltonen** (soili.peltonen@vtt.fi), VTT Technical Research Centre of Finland, P.O. Box 1000, FIN-02044 VTT, Finland. **Kimmo Koivunen** (kimmo.koivunen@tkk.fi), **Hannu Paulapuro** (hannu.paulapuro@tkk.fi), Aalto University School of Science and Technology, P.O. Box 6300, FIN-02015 TKK, Finland. **Jere Tupala** (jere.tupala@helsinki.fi), **Markku Leskelä** (markku.leskela@helsinki.fi), **Tommi Virtanen** (tommi.virtanen@helsinki.fi), **Sirkka Liisa Maunu** (sirkka.maunu@helsinki.fi), University of Helsinki, P.O. Box 55, FIN-00014 University of Helsinki, Finland.
Corresponding author: Lauri Kuutti

Inorganic pigment and filler materials are used to improve optical and printability properties as well as the cost performance of paper. Plastic coating pigments that typically consist of petroleum-derived, modified polystyrene have been used only for special printing applications. The reasons for utilization of mineral materials are cost-effectiveness, availability, high brightness and opacity effects. We have earlier developed starch-based non-mineral paper pigments and fillers targeting to replace mineral pigments. During the work, the opacity goal has been approached from three different directions. The first approach has been to process rigid, water insoluble pigment particles of modified starch with particle sizes optimized for maximum light scattering properties in paper coatings (Varjos et al. 2004; Peltonen et al. 2005; Mikkonen et al. 2006; Saari et al. 2005). The second approach to obtain maximum light scattering has been the formation of relatively rigid and porous pigment particles. The assumption was that appropriate pore structure in rigid pigment may increase its light scattering properties (Johansson et al. 2005). The third approach abandoned completely the solid and rigid pigment structures and was based on foam or microcapsules to create light scattering interfaces. A stabilized rigid foam structure coated on paper and containing suitable sized microcapsule structure may also contribute to improved light scattering properties (Penttilä et al. 2006). The used hydrophobic modification of starch was acetylation and the trial materials were prepared according to our patents (Lammers et al. 1998; Mikkonen et al. 2003).

Contribution of inorganic fillers on the light scattering of paper is partly based on their preventive effect on bonding between fibers. This is however also observed as decreased strength properties, limiting the possibilities to increase the filler content of paper from the current level. In addition, at high filler content, the paper bulk is usually reduced due to the relatively high specific gravity of inorganic fillers. The bulk is further reduced in calendering. Fillers contribute to the light scattering effect also by increasing the number of solid-air interfaces in the paper structure. However, the refractive indices (RI) of current fillers are usually close to that of cellulose, restricting the light scattering effect on the filler-fiber interfaces. Less work has been done to modify the refractive indices of papermaking materials. Due to these shortcomings, there is a need for new functional hybrid filler materials with increased RI capable of interacting both with the surrounding cellulosic fibers and light. Such fillers could enable simultaneous development of optical and mechanical performance of paper. A study made earlier within this project suggests that the RI of precipitated calcium carbonate (PCC) filler can be increased using zinc induced formation of nanostructures (Koivunen et al. 2009).

Here we take again another approach to produce pigmenting filler materials based on starch. The water-based treatments using soluble, anionic starch derivatives target at insoluble hybrid materials between starch and inorganics. Anionic groups in the polymer structure, such as COO^- and $(PO_3)^{2-}$ can provide sites for binding metal ions, e.g. Ca^{2+}, Ba^{2+} or Zr^{4+}. In addition to introducing anionic functionality, poly(carboxy acids) such as citric acid and poly(phosphoric acids) or phosphoric acid salts can act as crosslinking agents of starch, reducing the hydrophilic character of the material. Carboxymethyl starch is water-soluble and commercially available in

large quantities. It is widely used as an additive in the paper industry, and as a thickener in the formulation of textile printing pastes. In hybrid materials the aim is to incorporate elements of higher density in polymers to produce starch-based fillers with refractive index greater than that of starch raw materials, starch acetate, or cellulosic fibres. Hybrid starch-inorganic precipitates could also provide particle sizes more adapted to filler usage.

Organic-inorganic complex polymer is a generic name for a system where polymer bonds chemically or physically to inorganic element(s). The structure is controlled by the combination mechanisms between the inorganic and organic constituents and the constituents are organized in a molecular level. Mechanism of complexation of starch onto different minerals has been investigated and explained in many papers. In the cases of unmodified polysaccharides, hydrogen bonding naturally played a major role (compared to electrostatic interaction) in adsorption (Weissenborn et al. 1995; Liu et al. 2000). However, reactive chemisorption of starch onto hematite surface has also been suggested (Pavlovic, Brandao 2003). The acidity/basicity of the chemical system probably determines whether the adsorption is hydrogen bonding or chemical complexation in the case of adsorption of polysaccharides onto mineral surfaces. Modified, water soluble and insoluble charged starch derivatives have been used e.g. for binding of heavy metal ions in waste waters (Khalil, Farag 1998; Khalil, Abdel-Halim 2001; Guo et al. 2006). For example, the calcium-binding capacity of carboxymethyl starch was observed by the hardness changes of the remaining aqueous phase (Volkert, et al. 2004) but the resulting hybrid products were not analyzed.

Materials

Polymer components

The synthesis of starch phosphate (SPHOS), starch citrate (SCIT) and carboxymethyl starch (CMS) were carried out. A native potato starch or starch with reduced molecular weight was used as the starting material.

Preparation of starch phosphate

Starch was phosphorylated by a reaction with mono- and disodium hydrogen phosphate under dry conditions at elevated temperature. Mono- and disodium hydrogen phosphate were dissolved in water and the pH of the solution was adjusted to 7. Native potato starch was slurried in the solution and the mixture was stirred and conditioned overnight at room temperature. The mixture was placed in the oven in an open dish to dehydrate at 50ºC for 24 h and the dry mixture was ground in a mortar mill. The oven temperature was adjusted to 130ºC and the dried and ground mixture was allowed to react for additional 3 h. The reaction product was washed with excess of water, the precipitate was dried and the water-soluble part was ultrafiltrated (cut-off 10 000) and freeze-dried. The soluble fraction was used in the further experiments.

Preparation of starch citrate

Reaction of hydrolysed starch and citric acid was carried out. Citric acid was dissolved in water under constant stirring and adjusted to pH 3.5 with aqueous sodium hydroxide. Starch was added into the solution and the mixture was conditioned overnight at room temperature. The mixture was placed in the oven in an open dish to dehydrate at 50ºC for 24 h. Reaction products were washed with excess of water. Precipitate was dried and the water-soluble part was ultrafiltrated (cut-off 10 000) and freeze-dried. The soluble fraction was used in the trials.

Preparation of carboxymethyl starch

The synthesis of carboxymethyl starch was carried out in two steps. In the first step, alkalization was performed by mixing hydrolysed starch, ethanol and aqueous sodium hydroxide at room temperature. The reaction mixture was stirred for 20 minutes, then monochloroacetic acid was added and the reaction mixture was heated up to around 58ºC and stirred at that temperature for 4 h. The sample was purified by dissolving in water, neutralized and precipitated with ethanol. Precipitated sample was filtered and dried under vacuum at 40ºC.

Commercial reference

As reference polymeric materials we have used commercial di-starch phosphate (dSPHOS) (C_StabiTex-Instant 12631) and acetylated di-starch phosphate (adSPHOS) (C_StabiTex-Instant 12632), both samples kindly donated by Cargill Nordic Oy, Finland. The starting material in both products was pregelatinized, crosslinked waxy maize starch and these products are intended for food applications.

Inorganic salts

The criteria for selection of the inorganic salts were the solubility in water and, if available, the refractive index values obtained from literature. Low solubility was taken as an indication of a low capability to form complex with starch and thereby contribute to the refractive index of the resulting water insoluble hybrid. The criterion was therefore that the inorganic salt should dissolve without great effort to water. *Table 1* summarizes the solubility values (in grams per 100 ml cold water) of the used inorganic salts: calcium chloride ($CaCl_2$), barium chloride ($BaCl_2$), zinc acetate [$Zn(O_2CCH_3)$], zinc acetylacetonate [$Zn(OCCH_3CHCOCH_3)_2xH_2O$], zirconium nitrate [$Zr(NO_3)_4xH_2O$], zirconyl nitrate hydrate [$ZrO(NO_3)_2xH_2O$], zirconium oxochloride ($ZrOCl_2xH_2O$) and titanium potassium oxalate [$TiO(OCOCOOK)_2$]. The appearance of the water solutions is also included in the table. All the chemicals were used as received without further purification. If not otherwise mentioned, the chemicals were of industrial grade.

Preparation of water insoluble hybrids

The precipitation experiments were done by mixing water solutions of the anionic starch derivative and the inorganic component. The polymer components were carboxymethyl starch (CMS), starch citrate (SCIT),

Table 1. Solubility values and appearance of water solutions of the used inorganic salts.

Inorganic salt	Solubility in grams per 100 ml cold water	Solubility, 1 gram in 20 ml cold water
calcium chloride	74.5	soluble, clear
barium chloride	37.5	soluble, clear
zinc acetate	30	soluble, clear
zinc acetylacetonate	very soluble	soluble, milky
zirconium nitrate	very soluble	soluble, milky
zirconyl nitrate hydrate	na	soluble, milky
zirconium oxy chloride	na	soluble, clear
titanium potassium oxalate	na	soluble, clear

Table 2. Particle size of the reference fillers.

ID	Type	Particle size, µm	
		Mean	Median
R-PCC	Rhombohedral precipitated calcium carbonate	3.353	1.873
A-PCC	Aragonitic precipitated calcium carbonate	3.498	3.092
GCC	Ground calcium carbonate	1.959	1.586

starch phosphate (SPHOS) and commercial di-starch phosphates (dSPHOS) and (adSPHOS). The prepared water solutions typically contained 1 g polymer in 20 ml distilled water. Similarly with the inorganic salts, water solutions containing 1 g salt in 20 ml water were used. Precipitation was obtained by mixing the clear or mildly turbid solutions together and the formed product was recovered by filtration. The precipitate was washed with ethanol (about 20 ml) and dried in oven at 50ºC.

For filler studies, two hybrid materials were selected to be prepared using a larger batch size. The polymer component was carboxymethylated starch (CMS) (DS 1.06), 100 g dissolved in 2000 ml water. Similar weights and concentrations of water solutions using $BaCl_2$ and $ZrO(NO_3)_2xH_2O$ were made. The clear or mildly turbid solutions were mixed together and the pH of the aqueous precipitates were adjusted. The pH of the Ba-containing mixture was kept at 9.1 and the pH of the Zr-containing mixture was adjusted from the original 1.8 to 6. The formed precipitates were recovered by filtration, washed with ethanol (over 600 ml) and oven-dried at 50ºC.

Reference filler materials and furnish

Dried pine and birch chemical pulp samples delivered by Finnish pulp mills were used in stock and handsheet preparation. A stock starch (Raisamyl 50021 by Ciba Specialty Chemicals, Inc., Finland) and a retention agent (Fennopol K 3400R by Kemira Oyj, Finland) were used as additives. Two precipitated (R-PCC and A-PCC) and one ground calcium carbonate (GCC) grades (by Omya Oy, Finland) were used as reference fillers. For the particle size measurements, dry calcium carbonate samples were dispersed in sodium hexametaphosphate and the particle sizes were measured with Beckman Coulter LS 13 320 Particle Size Analyzer. Average particle sizes are listed in *Table 2*.

Methods

Characterization of components, component mixtures and formed hybrids

The degree of substitution (DS) of CMS was determined by potentiometric titration. The degree of phosphorylation was determined by total phosphorous content. The thermal characteristics of the derivatives were determined by Differential Scanning Calorimetry (DSC) and Thermogravimetry (TGA). By DSC, the glass transition temperature was recorded on the second heating at a heating rate of 10ºC/min.

The chemical structure of modified polymers and formed insoluble hybrids were evaluated using Fourier Transform Infrared (FTIR) spectroscopy. The spectra were determined using a Perkin-Elmer Spectrum BX FT-IR System with data collection parameters of 50 scans at 4 cm^{-1} resolution. Transmission spectra were detected in tablet form (mixing about 1-2 mg of the dried sample and 250 mg of potassium bromide).

The refraction index (RI) of solid particles was evaluated according to Becke line test in immersion liquids. An optical transmission microscope (Leitz Diaplan type 020-437.035, equipped with a quartz halogen lamp at 2700 K, Ernst Leitz Wetzlar GMBH, Germany) and a set of immersion liquids in the RI range of 1.40-1.70 (Cargille Laboratories, New Jersey, USA) were used. The fine-ground sample, immersed in a drop of a test liquid is placed on the glass slide and covered with a cover glass. A bright halo (Becke lines) is observed around the sample particles when viewed through a microscope with the aperture closed down. The lines are observed to move as the distance between the sample and the objective is changed; the halo moves toward a material of higher RI when the distance is increased from that at the focus and towards a material of lower RI when the distance is reduced from that at the focus. The RI of a sample can be estimated by comparing the movement in several immersion liquids at known RI. When the RI of the sample and the liquid level, the crystals appear transparent and their edges fade.

X-ray diffractograms (XRD) were measured with PANalytical X'Pert Pro MPD diffractometer using CuK(x) radiation detected with PIXcel detector. Measurements were made in theta-2theta geometry using angular range of 5-50° and programmable divergence and antiscatter slits that were set to 6 mm constant irradiation length. Peaks were fitted with HighScore Plus software (PANalytical) and the crystallite sizes were evaluated using the Scherrer's equation.

With solid state cross-polarization magic angle spinning (CPMAS) ^{13}C NMR spectroscopy it is practical to detect any conformational changes in a material, induced for instance by various sample pre-treatments or derivatizations. These changes may include alterations and defects in crystalline packing, or conversions from a crystalline state to amorphous or vice versa. This is because the chemical shift for a given site in a molecule is strongly dependent on the local magnetic environment experienced by the site, and it is therefore susceptible to conformational changes. All solid state NMR spectra were measured with Varian Unity INOVA 300 spectrometer with a magnetic flux density of 7.05 T. A 7 mm silicon nitride rotor was used for sample rotation with rotation frequency being 5 kHz. Cross-polarization

contact time for the measurements was set to 2 ms, spectral width was 18 kHz with acquisition time of 20 ms. Recycle delay was 3 s and 2000 scans were accumulated for each spectrum. Spectra were referenced externally to TMS via hexamethylbenzene (HMB) by assigning the methyl signal in HMB to 17.3 ppm.

Air jet milling and characterization of powdery products

The grinding of formed hybrid precipitates was done using Hosokawa Micron Multi-processing System equipped with Alpine Fluidised Bed Opposed Jet Mill 100 AFG, classifier and a feed cooling system. Cooling of the sample container and the feeding screw was done by liquid nitrogen and the classifier speed was 7000 rpm.

A combustion analysis was done using a standard method to obtain the dry contents and mass fraction of inorganic components. The samples were first dried at 105°C overnight to assess the dry content. After drying the samples were annealed at 550°C to determine the ash content.

The element composition of the ground samples was determined by using Philips PW2404 X-ray fluorescence spectrometer (XRF) and semi-qualitative SemiQ-software. Fluorine and heavier elements were analyzed. The detection limit is approx. 0.01 wt-%.

The particle size distributions of the ground products were measured in water using laser light scattering analyzer (Lecotrac LT-100, LECO Corporation, Tampa, USA). The Scanning Electron Microscopy (SEM) analysis was used for particle morphology examination after a thin gold coating. Dispersibility of the filler particles into distilled water and the effects of pH changes on the dispersions were evaluated visually.

Preparation and characterization of filled sheets

Handsheets were prepared with a Moving Belt Former (MBF) apparatus which applies pulsating dewatering and yields more anisotropic sheet structure than a traditional sheet mold. A more detailed description of the MBF can be found in the literature (Räisänen 1998). Dried pine and birch pulp samples were soaked in water and combined to have a typical fine paper fibre blend furnish with birch and pine contents of 70 wt-% and 30 wt-%, respectively. The blend was first disintegrated with a hollander for 30 minutes and further beaten to reach Schopper Riegler value 18, and finally diluted to stock consistency of 3.0 g/l for handsheet preparation. Targeted basis weight of the sheets was 80 g/m^2. Target filler contents were 15%, 25%, and 35% relative to the weight of the base paper. The pH of the stock was checked and adjusted to 7 when needed. The stock starch was cooked prior to handsheet preparation. The addition sequence of the chemicals was to mimic the wet end operations of a typical paper machine. First a portion of stock was added in the mixing container of the MBF. After this the starch (5 g/kg) was added, and after a 20 s delay the filler was added. 10 seconds after the filler addition the retention agent (0.2 g/kg) was dosed, and an additional period of 15 seconds was waited prior to dewatering. The whole sequence was carried out under continuous mixing. The resulting filler content was estimated by comparing the dry weight of the filled handsheet to that of an unfilled reference sheet. The handsheets were pressed for four minutes in 490 kPa between blotting boards and drum-dried for two hours in 60°C. A set of the sheets were calendered through a single nip with EP-210 laboratory calender using 70 kN/m line load, 70°C hot roll surface temperature, and 35 m/min speed. The handsheets were stored in constant temperature and humidity before measuring the standard optical and mechanical properties. The strength properties were measured in machine direction.

Results and discussion

Characteristics of polymer components

Several derivatization syntheses were carried out and of the most promising ones the water-soluble derivatives were selected for further evaluation. The degree of substitution DSCM of the used carboxymethylated starch was 1.06. The glass transition temperature of CMS was at around 63°C. On average, the total phosphorus content of SPHOS was 2.6 wt-%.

The structures of the modified starches were confirmed by FTIR spectroscopy, by comparing the characteristics absorption wavenumbers of the esterified derivatives to those of native potato starch. In the FTIR spectrum of starch citrate (SCIT) the formed ester bonds can be observed as absorptions at 1725 cm^{-1}, that of starch phosphate (SPHOS) appears at 1650-1620 cm^{-1} and characteristic bands for P=O bond at 1350-1250 cm^{-1}. For CMS, the representative absorptions can be observed at 1600, 1426 and 1324 cm^{-1}.

Formation and characterization of the hybrid materials

The water solubility of the polymer had to be high and the chemical structure of the polymer also had to be appropriate to contribute to the refractive index of the resulting insoluble hybrid. For example, CMS bound very effectively the inorganic components and the yields of the hybrid materials were typically over 70% (based on the feed solids). By DSC, there were no significant differences in the thermal properties between the polymer components and their corresponding hybrid materials.

FTIR-analysis

The FTIR-absorption spectra of the polymer derivatives, inorganic components and the hybrid precipitates were compared to observe the possible differences in the intensity and wavenumber of the main absorptions, especially in those related to the characteristic absorptions of the anionic groups of the polymers (-COO$^-$, -PO$_2^{2-}$). Thus, due to the expected dissociation of an inorganic salt in its solution, the absorptions observed for the solid salt may not contribute to the hybrid spectrum at equivalent wavenumbers. However, possible salt residues may cause overlapping absorptions in the spectra of the hybrid materials.

The mere CMS exhibited strong absorption bands at 1700-400 cm^{-1} and also the absorptions typical for the derivative were observed (around 1600, 1426 and 1324 cm^{-1}). The carbonyl peak for CMS was detected at 1617 cm-1, whereas less intensive absorptions at 1735 cm^{-1} and 1602 cm^{-1} were obtained for the hybrid precipitate. More narrow absorption bands at similar wavenumber regions were found for $Zr(NO_3)_4xH_2O$. The most notable spectral differences between CMS and the hybrid were at 800-400 cm^{-1}, where the absorption intensities observed for the hybrid were lower.

Medium-intensity absorptions around 1650-1620 cm^{-1} were observed for both the commercial dSPHOS and the related hybrid precipitate of dSPHOS + $[ZrOCl_2xH_2O]$. The wavenumber range 1350-1250 cm^{-1} assigned to P=O was unspecified. The hybrid product possessed lower intensity absorption bands in the regions of 1200-900 cm^{-1} and 850-400 cm^{-1}. Also the mere inorganic salt exhibited strong absorptions at around 1623 cm^{-1} and in the range of 600-400 cm^{-1}.

The carbonyl-derived absorption band for SCIT was determined at around 1725 cm^{-1} and for the corresponding hybrid with somewhat lower intensity at around 1730 cm^{-1}. Otherwise the spectrum of the hybrid of SCIT + $BaCl_2$ incorporated the main absorptions of the both starting components; the region 1410-1000 cm^{-1} resembled that of the polymer derivative, and specific absorptions of $BaCl_2$ at 1637-1600 cm^{-1} and at 700-400 cm^{-1} were also found.

XRD-analysis

By XRD-analysis, starch phosphate SPHOS showed clear crystalline properties and the inorganic components, when solid, were crystalline. The hybrid precipitate formed of solutes of zinc acetate and SPHOS appeared amorphous. The precipitation of SPHOS and $Ba(OH)_2$ formed a hybrid that exhibited both amorphous and crystalline nature and was evidently different from the result obtained for a simple mechanical mixture of the two starting components. Substantially amorphous structure of the products made it uncertain to model the crystal sizes.

Carboxymethylated starch CMS was identified as an amorphous component, supported by the DSC analysis and corresponding to previous reports (Lawal 2008). Hybrid formed by CMS + $BaCl_2$ was amorphous and the crystalline contribution of the inorganic component was not evident. Similar amorphous indication was obtained for a hybrid formed in CMS + $[ZrO(NO_3)_2xH_2O]$ precipitation. Precipitated CMS + $Ba(OH)_2$ hybrid possessed amorphous structure with some apparent crystallinity derived from the barium-containing component. For the mere $Ba(OH)_2$ powder, the crystallite size was around 60-80 nm, whereas in the hybrid product similar crystals ranging from 5 to 8 nm in size were recorded in the modelling stage.

NMR-analysis

Here CPMAS 13C NMR spectroscopy was utilized to study the complex formation between CMS and Zr^{4+} originating from a solution of $Zr(NO_3)_4xH_2O$). Since the primary interaction of the Zr^{4+} ion and the CMS is considered to involve the ether and hydroxyl oxygens in the carboxymethyl group, it is expected that the formation of the complex would be seen in the signal originating from the carbonyl carbon. The measured spectra for CMS and the precipitate of CMS + $[Zr(NO_3)_4$ x $H_2O]$ are presented in *Fig 1*. Dominating signals at 55 - 110 ppm originate from the carbons in glucopyranose units and from CH_2-groups present, and the signal at 178 ppm comes from carboxylic carbon in the carboxymethyl group. The most notable difference between the two spectra is seen here in the signal at 178 ppm as a change in the line width, while in other regions of the spectra there are no significant changes. As a sign of a complex formation the carboxylic signal is clearly broadened for the hybrid sample, the line width being 522.4 Hz (FWHM), while the non-treated sample gives a line width of 269.2 Hz. This can be taken as a verification of the assumption that complexation is closely related to the carboxymethyl group.

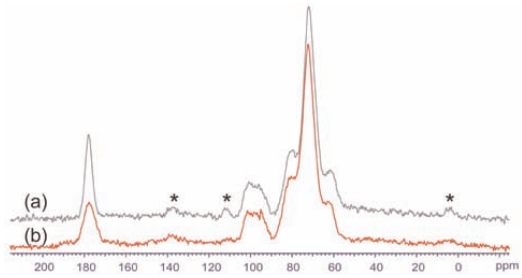

Fig 1. Characterization of the complex formation using solid state 13C CPMAS NMR. (a) Carboxymethyl starch (CMS), (b) Hybrid of CMS + $[Zr(NO_3)_4xH_2O]$. Signals marked with (*) are spinning sidebands.

Refractive properties of the hybrid materials

Refractive index studies were carried out in immersion liquids for several starting polymers, inorganic salts as such, as well as for the hybrid precipitates formed. Here, only a few cases are presented as pictures. The set for each sample contains four pictures taken in two adjacent immersion liquids where the halo effect differ; the upper row pictures were taken in focus and the lower row pictures with increased distance from the focus. The product RI estimation is given as an interval determined by the liquids' RI (given on the top of each picture column). For pure CMS the RI estimate was 1.50-1.55 (*Fig 2*, above) and similar values were observed for SPHOS, SCIT and commercial di-starch phosphates dSPHOS and adSPHOS. Calcium-containing inorganic salts gave similar RI levels, whereas for Ba-, Zn-, Zr- and Ti-containing salts, the estimates fell between 1.55-1.65 (*Fig 2*, middle and below).

Hybrid precipitates of CMS with Ca-containing salts exhibited somewhat lower RI compared to hybrids prepared with Ba- and Zr-containing salts (*Fig 3*). The highest RI estimates for CMS-based hybrids were in the range of 1.55-1.60.

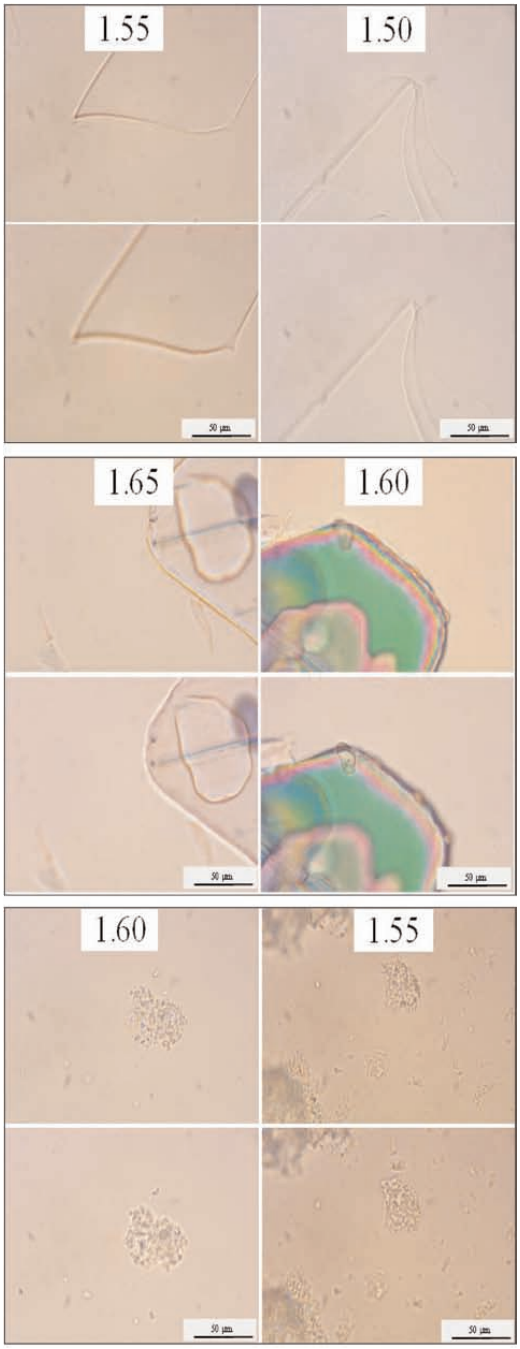

Fig 2. RI-estimation by immersion liquid method: CMS (above, in a scale of 50 µm), $BaCl_2$ (middle) and $ZrO(NO_3)2xH_2O$ (below).

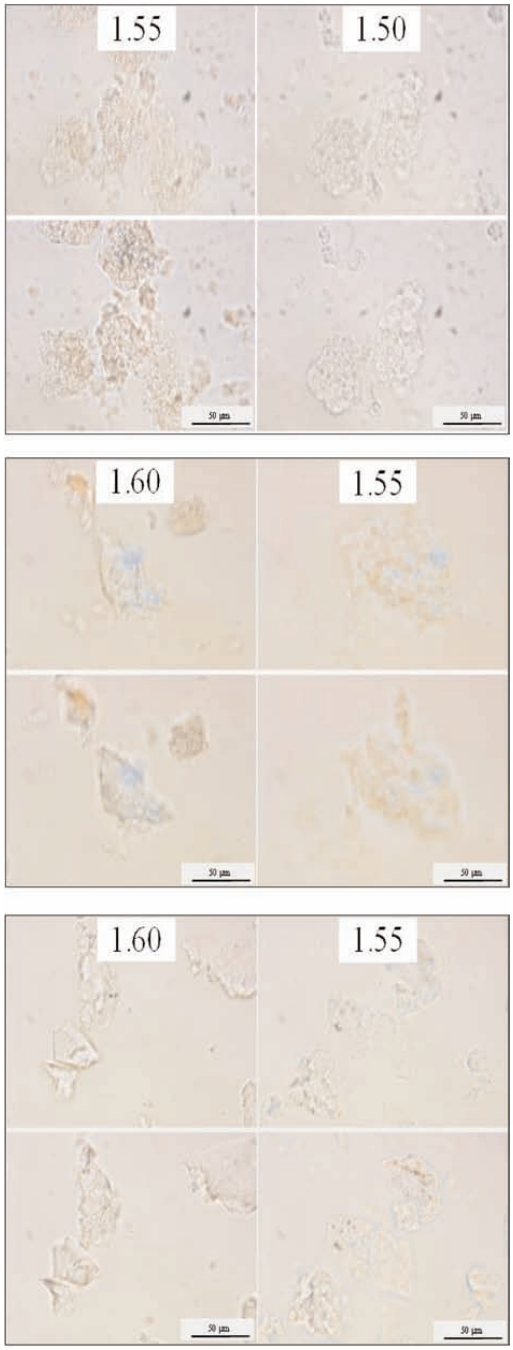

Fig 3. RI-estimation by immersion liquid method: hybrids of CMS + $CaCl_2$ (above, in a scale of 50 µm), CMS + $BaCl_2$ (middle) and CMS + $[ZrO(NO_3)2xH_2O]$ (below).

Some examples of hybrids based on other starch derivatives are given in *Fig 4*. Improved RIs were observed for SPHOS-, dSPHOS- and SCIT-based hybrids with Zr- and Ti-containing salts.

Particle composition, morphology and dispersability of the hybrid materials

The larger batches of the prepared two hybrid materials were dry ground in order to produce particle sizes adaptable to use as fillers. The ground samples were both characterized to contain 10 wt-% of water. By combustion analysis, the organic/inorganic ratio was 41/59 wt-% for hybrid CMS + $BaCl_2$ and 64/36 wt-% for hybrid CMS + $[ZrO(NO_3)_2xH_2O]$.

The semi-qualitative XRF analysis revealed, that in the

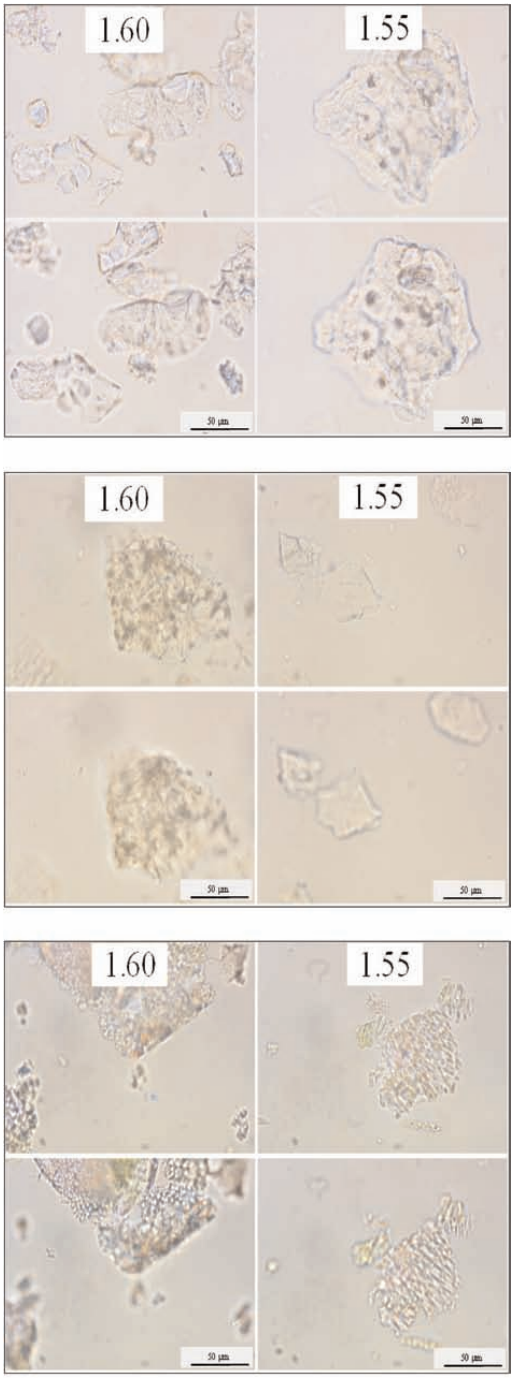

Figure 4. RI-estimation by immersion liquid method: hybrids of SPHOS + [$Zr(NO_3)_4$ x H_2O] (above, in a scale of 50 µm l), dSPHOS + [$ZrOCl_2$ x H_2O] (middle) and SCIT + [$TiO(OCOCOOK)_2$] (below).

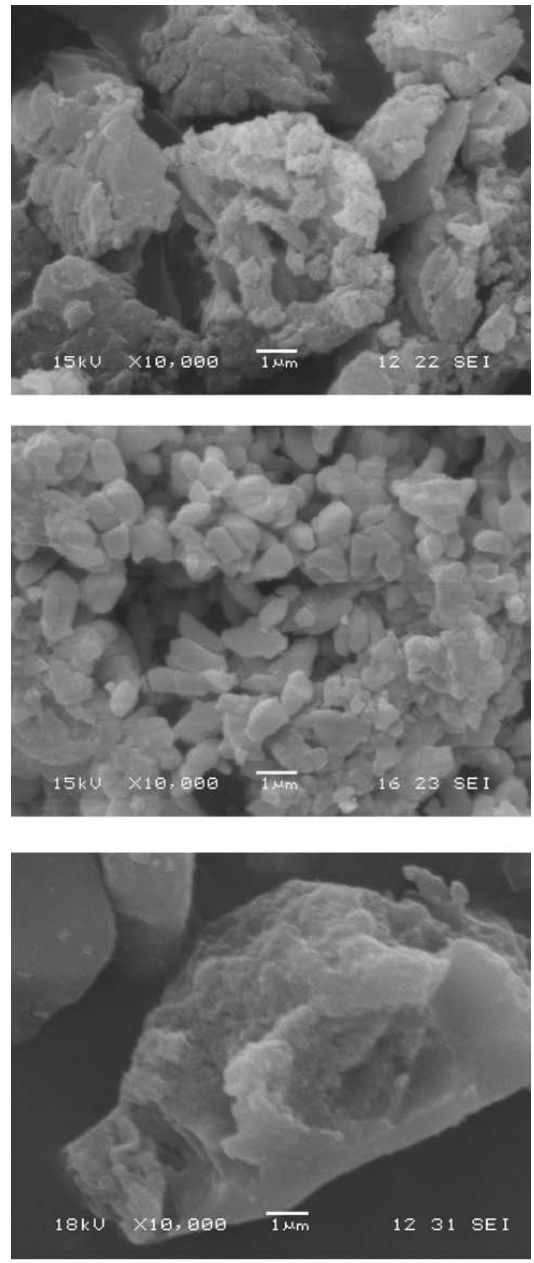

Fig 5. SEM: pure CMS (above), $ZrO(NO_3)_2$ x H_2O (middle) and milled hybrid product of CMS + [$ZrO(NO_3)_2$ x H_2O] (below). Scale bars of 1 µm.

hybrid of CMS + $BaCl_2$ the heavy element content was Ba 34 at.%, Cl 1.9% and Na 0.7%. Similarly for hybrid material CMS + [$ZrO(NO_3)_2xH2O$] contents of Zr and were 24% and 2.1% and less than one percent were detected for other elements.

The obtained mean particle size was larger and the size distribution wider than considered optimal for paper fillers. Especially in the case of milled hybrid product of CMS + $BaCl_2$, a large particle size distribution was detected (from peak value of 20 µm to 60 µm) . For the hybrid of CMS + [$ZrO(NO_3)_2xH_2O$], the size distribution centered at around 10 µm. Considering improvements in the preparation procedure, a higher milling impact, i.e. a higher classifier speed in the air jet mill would have been favourable. The relatively large particle size can be expected to affect also the filled sheet properties, both from the optical and mechanical properties point of view.

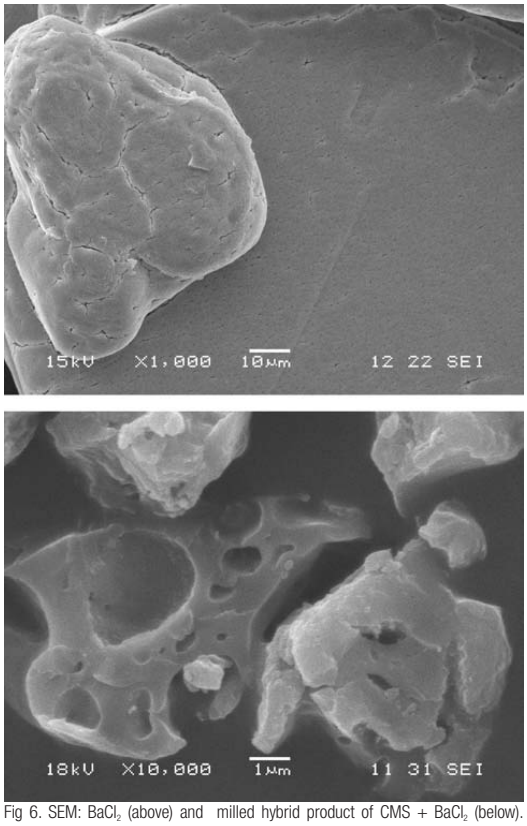

Fig 6. SEM: $BaCl_2$ (above) and milled hybrid product of CMS + $BaCl_2$ (below). Scale bars of 1 µm.

The SEM analysis revealed that the milled hybrid fillers were coarse and contained some degree of porosity (*Fig 5* below and *6* below). A high degree of porosity is considered beneficial for the particle size reduction by grinding but also for increasing the light scattering of the fillers. The formed particle structures (*Fig 5* below and *6* below) resembled more of the starting CMS (*Fig 5* above than those of the pure inorganics (*Figs 5* middle and 6 above).

Dispersability of the particles into distilled water appeared satisfactory and without softening or swelling even after weeks of storage. However, sedimentation of the filler powders of formed particle size was fast without any dispersing additives. In the case of CMS + $BaCl_2$ hybrid dispersion, a lowered pH below 5 turned the turbid mixture clear, however the viscosity did not change markedly. At high pH (above 9), no transparency or swelling effects were noted. In the CMS + [$ZrO(NO_3)_2$x H_2O] hybrid dispersion, a pH increase above 9 caused increase in viscosity of the turbid mixture, indicating increased solubility. In any of these cases, pH-change induced (re)precipitation of the inorganics was not observed indicating a stabile bonding between the polymer and inorganic constituents.

Optical and mechanical properties of the filled sheets

Observations made during the handsheet preparation suggested that both of the hybrid fillers, CMS + $BaCl_2$ and CMS + [$ZrO(NO_3)_2xH_2O$], can be well introduced in the paper as fillers using the conventional forming procedure. Visual examination suggested adequate formation and comparable appearance with the reference sheets, especially in the case of CMS + [$ZrO(NO_3)_2xH_2O$] hybrid. According to the measurements, the CMS + [$ZrO(NO_3)_2xH_2O$] hybrid filler had some contribution on opacity at high filler content although generally the light scattering properties of the handsheets were not significantly affected (*Figs 7-8*). The sheets filled with

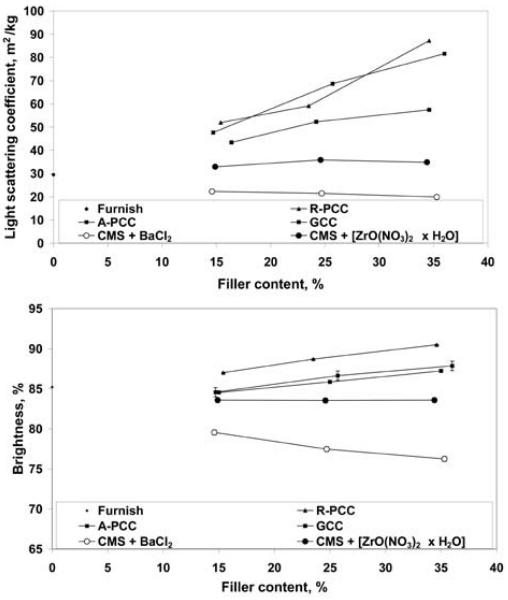

Fig 7. The light scattering coefficient of unfilled and filled sheets at varying filler contents (above) and brightness of unfilled and filled sheets at varying filler contents, prior to calendaring (below).

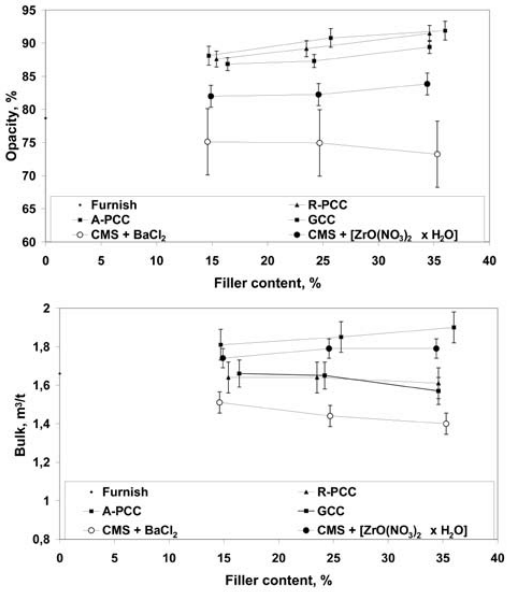

Fig 8. Opacity of unfilled and filled sheets at varying filler contents (above) and the bulk of unfilled and filled sheets at varying filler contents, prior to calendaring (below).

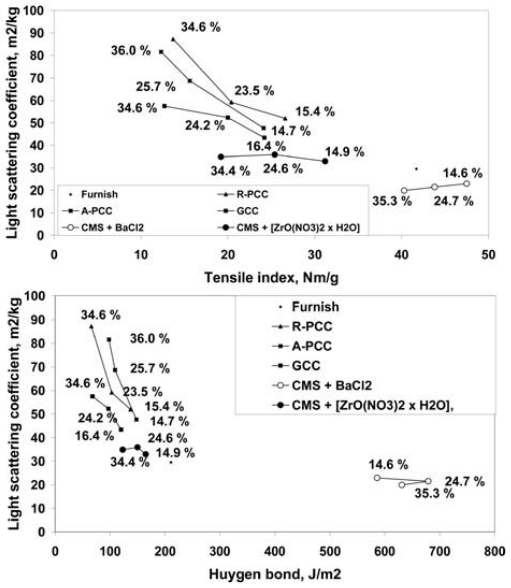

Fig 9. The property combination light scattering coefficient – tensile strength index of unfilled and filled sheets at varying filler contents, prior to calendering (above) and the property combination light scattering coefficient – Huygen bond of unfilled and filled sheets at varying filler contents, prior to calendaring (below)

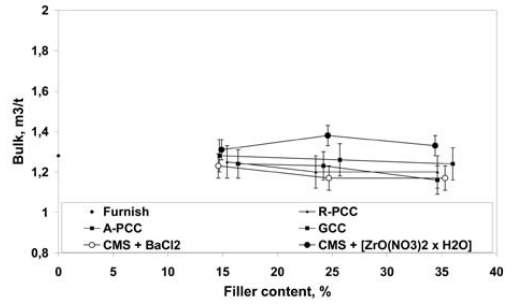

Fig 10. Bulk of calendered unfilled and filled sheets at varying filler contents.

the CMS + $BaCl_2$ hybrid attached strongly to the blotting boards. Impaired scattering properties are expected to be due to strong tendency to increase the internal bonding of the sheets, observed also by the low bulk (*Fig 8* below). Only A-PCC and CMS + [$ZrO(NO_3)_2xH_2O$] hybrid provided higher bulk than the sheets without fillers (*Fig 8* below).

Both CMS + $BaCl_2$ and CMS + [$ZrO(NO_3)_2xH_2O$] hybrid fillers yielded higher tensile strength indices and Huygen bond energies than the sheets prepared with the reference fillers (*Figs 9* above and *9* below). CMS + [$ZrO(NO_3)_2$ x H_2O] hybrid yielded better property combinations than CMS + $BaCl_2$.

After calendering the CMS + [$ZrO(NO_3)_2$ x H_2O] hybrid gave the highest bulk (*Fig 10*). The benefit was most significant at the 25 % filler content where a 10-20 % improvement compared to the other fillers was observed.

Conclusions

Starch-based hybrid pigmenting materials with reduced water sensitivity and improved optical performance were prepared in the laboratory scale by the complexation approach. Different procedures in the combination of inorganic components and the polymer derivatives were used. The criteria for selection of the inorganic salts and the modified starch derivatives were the water solubility and the refractive index values obtained from literature. The solubility of the starting materials had to be high enough and the chemical structure of the polymer also appropriate to contribute to the refractive index of the resulting water insoluble hybrid. The resulting precipitates exhibited composite structures and improved refractive indices depending on the inorganic constituent. In contrast to the inherent refractive index around 1.45 of starch-based materials, refractive indices between 1.50 and 1.55 (using Ca-, Zn- and Ba-components) and closer to 1.60 (using Zr- and Ti-components) were observed for complexed materials.

The results of this first laboratory scale papermaking potential study of the starch-based hybrid pigmenting materials suggest that they can be readily introduced in paper as fillers using the conventional forming procedure and similar wet end operations that are used in the current papermaking processes. Both the experiences obtained during the sheet forming experiments and visual examination of the starch-hybrid filled sheets suggested feasible behavior in the examined application especially with the CMS + [$ZrO(NO_3)_2$ x H_2O] hybrid. The hybrid performed high bulking ability both before and after calendering. The CMS + $BaCl_2$ hybrid gave strong bonding and significant densification of the sheets in spite of its particle-like structure. The scattering properties of the hybrids will be optimized using existing knowledge in the field of starch based pigments; for instance, an improved milling response is required. The findings of this study help to develop functional hybrid fillers enabling adjusted optical properties of paper while maintaining the bulk and strength.

Acknowledgements

This work was carried out in the Nanopap project (Improvement of Optical Properties of Paper by Increasing Refractive Indices of Materials) during 2006-2008, financially supported by the Finnish Funding Agency for Technology and Innovation (TEKES), Omya Oyj, J.M. Huber Finland Oy, UPM-Kymmene Oyj and M-real Oyj.

Literature

Guo, L., Zhang, S.F., Ju, B.Z., Yang, J.Z., and Quan, X. (2006): Removal of Pb(II) from aqueous solution by cross-linked starch phosphate carbamate, J. Pol. Res. 13(3), 213.

Johansson, A., Qvintus-Leino, P., Varjos, P., Peltonen, S., Mikkonen, H., Miettinen, and M., Luukkainen, S. (2005): Porous filler or coating pigment of paper and cardboard and a method of manufacturing it, WO2005030847 to VTT Technical Research Centre of Finland, Publ. April 7.

Khalil, M.I., and Farag, S. (1998): Utilization of some starch derivatives in heavy metal ions removal, J. Appl. Pol. Sci. 69(1), 45.

Khalil, M.I., and Abdel-Halim, M.G. (2001): Preparation of anionic starch containing carboxyl groups and its utilization as chelating agent, Starch/Stärke 53(1), 35.

Koivunen, K., Niskanen, I., Peiponen, K.-E., and Paulapuro, H. (2009): Novel nanostructured PCC fillers, J. Mat.Sci. 44(2), 477.

Lammers, G., Tiitola, P., and Vuorenpää, J. (1998): Process for the preparation

of a starch ester, WO9829455 to VTT Technical Research Centre of Finland, Publ. July 9.

Lawal, O. S., Lechner, M. D., and Kulicke, W. M. (2008): Single and multi-step carboxymethylation of water yam (Dioscorea alata) starch: Synthesis and characterization, Int. J. Biological Macromolecules, 42, 429.

Liu, Q., Zhang, Y., and Laskowski, J.S. (2000): The adsorption polysaccharides onto mineral surfaces: an acid/base interaction, International Journal of Mineral Processing, 60(3-4), 229.

Mikkonen, H., Peltonen, S., and Gädda, T. (2003): Novel starch derivatives and a method for their preparation, WO03068823 to VTT Technical Research Centre of Finland, Publ. Aug. 21.

Mikkonen, H., Kuutti, L., Kataja, K., Qvintus-Leino, P., and Peltonen, S. (2006): Novel method for preparation of spherical starch ester pigment with excellent optical properties in paper coatings, Applied Material Research at VTT Proceedings, VTT Symposium 244, Ritschkoff, A. C., Koskinen, J. and Paajanen, M. (Eds.), VTT Technical Research Centre of Finland, Espoo, pp. 235-243.

Pavlovic, S., and Brandao, P.R.G. (2003): Adsorption of starch, amylose, amylopectin and glucose monomer and their effect on the flotation of hematite and quartz, Minerals Engineering, 16(11), 1117.

Peltonen, S., Mikkonen, H., Qvintus-Leino, P., Varjos, P., and Kataja, K. (2005): Pigment and filler and a method of manufacturing it, WO2005030844 to VTT Technical Research Centre of Finland, Publ. April 7.

Penttilä, A., Lumme, K., and Kuutti, L. (2006): Light-scattering efficiency of starch acetate pigments as a function of size and packing density, Applied Optics, 45(15), 3501.

Räisänen, K. (1998); Water removal by flat boxes and a couch roll on a paper machine wire section. Ph.D. Thesis, Helsinki University of Technology, Espoo, Finland.

Saari, J., Kataja, K., Qvintus-Leino, P., Kuutti, L., Peltonen, S., Mikkonen, H., and Joyce, M. (2205): Coating trial results with non-mineral starch based pigments, TAPPI 2005 Coating Conference and Exhibit Proceedings, TAPPI Press, Toronto, pp. 271-276.

Varjos, P., Mikkonen, H., Kataja, K., Kuutti, L., Luukkainen, S., Peltonen, S., and Qvintus-Leino, P. (2004): Non-mineral starch based pigments, Pulpaper 2004 Conferences Coating Proceedings, The Finnish Paper Engineers Association, Helsinki, pp. 131-134.

Volkert, B., Loth, F., Lazik, W., and Engelhardt, J. (2004): Highly substituted carboxymethyl starch, Starch/Stärke, 56(7), 307.

Weissenborn, P.K., Warren, L.J., and Dunn, J.D. (1995): Selective flocculation of ultrafine iron ore. 1. Mechanism of adsorption of starch onto hematite, Colloids Surfaces A: Physicochem. Eng. Aspects, 99(1), 11.

Manuscript received October 5, 2009
Accepted November 24, 2009

PUBLICATION V

Properties and flocculation efficiency of cationized biopolymers and their applicability in papermaking and in conditioning of pulp and paper sludge

In: BioResources, 2011, 6(3),
pp. 2836–2850.

PROPERTIES AND FLOCCULATION EFFICIENCY OF CATIONIZED BIOPOLYMERS AND THEIR APPLICABILITY IN PAPERMAKING AND IN CONDITIONING OF PULP AND PAPER SLUDGE

Lauri Kuutti,* Sanna Haavisto, Sari Hyvärinen, Hannu Mikkonen, Riikka Koski, Soili Peltonen, Tapani Suortti, and Hanna Kyllönen

Safe biodegradable "green" alternatives with minimal environmental and health risks have received widespread research interest. Thirty different kinds of bio-based flocculants (modified starches, modified celluloses, native chitosan, and lignin-based flocculant) were pre-tested using a simple jar test for the examination of the applicability of new organic flocculants in papermaking and in conditioning of waste activated sludge from the pulp and paper industry. Three starch-based and two cellulose-based polymers were chosen for further flocculation and filtrations tests. Key optimization parameters for the polymer were identified as the increasing of molecular weight and nitrogen content. The starch-based polymer had the best performance in both applications, but in neither of the cases did it function as well as the commercial polyacrylamide-based polymers. The importance of the molecular weight came up in the experiments. The developed starch-based polymer was cationic and had the charge density used in industry. On the other hand, although cationic flocculants are the most used in sludge conditioning, also anionic and non-ionic polymers are needed, depending on the characteristics of the sludge to be flocculated. Overall action of the tailored polymers was also studied in order to predict their potential as papermaking retention and dewatering aids.

Keywords: Biodegradable flocculants; Starch; Cellulose; Papermaking retention; Dewatering

Contact information: VTT Technical Research Centre of Finland, Espoo, Finland, P.O. Box 1000, FIN-02044 VTT, Finland. ***** *Corresponding author: lauri.kuutti@vtt.fi*

INTRODUCTION

Large amounts of wet sludge are produced annually in municipal and industrial wastewater treatment. Already the pulp and paper industry produces more than ten million tons of primary sludge, waste activated sludge (WAS), and de-inking sludge. Due to legislation and increased taxes, landfills are quickly being eliminated as a final destination for wastes in Europe (Monte et al. 2009), and other disposal methods, such as incineration and fertilizer use, are becoming more important. For proper disposal, mechanical dewatering plays a key role in the treatment chain of sludge. WAS is a difficult type of sludge to dewater. The dry solids content after traditional dewatering process can still be less than 15%. Flocculation is an important stage of mechanical dewatering, especially when using cationic flocculants, but also anionic and non-ionic flocculants are needed, depending on the sludge to be flocculated. Proverbial synthetic

flocculants are highly efficient, but they have poor biodegradability with respect to fertilizer use, and the environmental aspects are more and more the focus of critical discussions. In Germany sludges treated with polyacrylamides will be excluded from application on areas under cultivation by the end of 2013. Safe biodegradable "green" alternatives with minimal environmental and health risks, based on biopolymers such as starch or cellulose, have thus a strong research interest.

Flocculating agent systems are extensively used to improve the retention of fibre fines and fillers in papermaking. The flocculating agents are often polyelectrolytes whose mechanisms of operation depend on the molecular weight and charge density. The efficiency of the flocculating agents in papermaking is generally evaluated by measuring the state of flocculation or retention efficiency under the desired flow/process conditions.

The cationizing agent most commonly used today is 2,3-epoxypropyltrimethyl-ammonium chloride or, alternatively, a corresponding cationizing agent with a chloro-hydrin functional nature. These compounds have the characteristic that they can establish an ether bond with the OH groups of starch. Thus, they react with starch so as to form a compound that is stable over a very wide pH range. They are particularly stable over the basic pH range. This characteristic is advantageous during long-term storage, since high pH gives an increased resistance to microbiological attack.

The flocculation efficiency of the various cationic starches depends on (a) the amino group type and follows the order: quaternary > tertiary > secondary > primary, and (b) the chemical structure of the flocculants, i.e. the flocculants prepared by grafting have higher flocculation efficiency than those prepared via etherification. Structural aspects of starch have been found that with a decrease of molar mass and radius of gyration, and hence the flocculation efficiency decreases (Shirzad-Semsar et al. 2007).

Bio-based flocculants can be produced from starch (amylose and amylopectin based) (Pavlovic and Brandao 2003; Khalil and Abdel-Halin 2001), cellulose (Ott et al.1989), chitosan (Ashmore and Hearn 2000; Roussy et al. 2004), phosphate-modified glucomannan (Xie et al. 2007), or by grafting acrylamide onto natural polysaccharides such as guar gum (Nayak and Singh 2001), and carboxymethyl cellulose (Biswal and Singh 2004). Starch derivatives have potential to replace petroleum-based flocculants and chelating agents (Oelmeyer et al. 2002; Bratskaya et al. 2005) for applications where the sludges are used on cultivated areas by reason of tighter environmental laws. A high degree of substitution (DS) in cationization of up to 1.1 in a one-step synthesis of the samples can be controlled by adjusting the molar ratio of cationization agent to anhydroglucose unit. A two-step reaction yields products of a DS of up to 1.5 (Heinze et al. 2004). Adsorption of polysaccharides onto mineral surfaces has been investigated and explained in many papers (Weissenborn et al. 1995; Liu et al. 2000). The recent patents (Karppi et al. 2007; Likitalo and Käki 2005) have been shown, that the molecular weight of the flocculant, at least for sludge applications, should get much higher concerning applications of papermaking retention and dewatering.

The flocculation performance of 30 different kinds of the bio-based polymers was first examined using a simple jar test, where a suspension of 0.05 % kaolin and 0.1 % thermo-mechanical pulp (TMP) fines was used for the flocculation studies. The best modified ones were further tested using more realistic filtration tests and compared with some commercial polyacrylamide-based flocculants.

EXPERIMENTAL

Materials

Various starch-based materials, such as enzymatically hydrolysed potato starch (N%: 0.4-2.8%), hydroxypropylated starches or acetylated potato starch (DS = 0.9-2.5), maize starch (amylose rich, N% = 1.3-1.57%), or enzymatically hydrolysed barley starch (N% = 0.66%)) have been chemically or enzymatically modified before the cationization. The starting material for the cationized modification of carboxymethyl cellulose, lignin, and chitosan were commercial samples. The acetylated samples were prepared using VTT´s own technology. The flocculants had not been optimized for further studies with respect to molecular weight, molecular weight distribution, chemical structure of the polymers, or the nature or ratio of functional groups on the polymeric backbone.

For the flocculation and filtration tests, the starting material was hydroxypropyl starch (MS=0.4, M_w=2.3 MDaltons) made in a pilot plant (Peltonen et al. 1998). As a hydroxyethyl cellulose sample, Aqualon's Natrosal 250 MBR (M_w=220000) was used. To increase the molar mass of selected samples, epiclorohydrin (Fluka) was used as a crosslinking agent. The mostly used cationization reagent, Raisacat 151 (2,3-epoxy-propyl-trimethylammonium chloride, industrial grade, Ciba Speciality Chemicals OY, Mietoinen, Finland) was used. All of the above-mentioned chemicals were used as received without further purification. If not otherwise mentioned, all other chemicals were of industrial grade.

The used furnish in the papermaking drainage and in flocculation measurements was a thermomechanical pulp (TMP)-based news-type recipe with a filler content of 30%. The fines content of the furnish was 25%. The flocculants in sludge application were tested using waste activated sludge (WAS) from a pulp mill. The samples were fresh and taken daily when needed. The total solids content of the WAS was 0.9±0.2%, the average particle size was 70±5 µm, the capillary suction time (CST) was 16±2 s, and the pH was 7.9±0.3.

Methods

Acetylation

The potato starch used in acetylating was provided by Periva Oy (Kokemäki, Finland). The used starch acetate was manufactured according to VTT´s patents (FI 107386). Reaction was carried out in the mixture of acetic acid anhydride and acetic acid in the presence of sodium hydroxide at reflux temperature, typically for 6 hours. Crude product was typically washed with an excess of water and dried.

Cationization of starch

Starch granules were suspended in water (e.g. 20% w/v), typically at 30°C, and were adjusted to pH 11.0 with NaOH. A commercial etherifying agent containing 2,3-epoxypropyltrimethylammonium chloride (RAISACAT, Raisio Chemicals Oy) was added to the slurry. The reaction temperature was raised to 80°C, and the reaction was stopped after 7-20 hr by adjusting to pH 6.5 with HCl (34% v/v). The slurry was filtered and washed with water and then with ethanol. The sample was freeze-dried.

Crosslinking

The crosslinking of the hydroxypropyl starch sample was carried out typically as follows: an aqueous suspension of 70 g hydroxypropyl starch and 0.5 mL epiclorohydrin in 1000 mL of water (pH over 11) was stirred at low speed at room temperature and then stirred for 1 hour at 60°C. On the next day, 35 g 50% NaOH (catalyst for the cationic reaction) and 85 g Raisacat 151 were added to the solution at room temperature and stirred for 10 hours at 80°C. The pH of suspension was adjusted to 7, and the product was purified with ultrafiltration (Microza UF Module, PALL Corporation) and freeze dried.

Analysis

The quantitative determinations of nitrogen in chemical substances were done by the Kjeldahl method. Gel permeation chromatography (GPC) was used to analyze molar mass distributions and mass average molar masses. A refractive index detector was used to determine the absolute molar masses in 1 M NaOH. The molar masses of the cross-linked samples were also evaluated by the viscosity measurement with a Brookfield DV-II+Pro viscometer at 25 °C.

A simple jar test was conducted as a pre-test for the examination of the applicability of new organic flocculants. 4 beakers of suspension of 0.05 % kaolin or 0.1 % TMP fines were used for flocculation studies at pH 4 and pH 7. Immediately after the addition of flocculants, all the suspensions were stirred at a constant speed of 100 rpm for 10 min, followed by slow agitation at 40 rpm for 10 min. The suspensions were then allowed to settle for 15 min. The turbidity of the suspension was measured with a Hach Model 2100P Portable Turbidimeter. The dose of flocculants was varied within the range of 0 to 4 ppm.

Flocculants

Starch- and cellulose-based polymers with different charge densities and molecular weights were screened in pre-tests, and the best ones were chosen for flocculation and filtration tests (Table 1, A-E). The pre-tested flocculants were further modified and compared to commercial polyacrylamide-based flocculants (C-PAM) used in industry (Table 1, F-I). The molar masses of the crosslinked samples A, C, and D measured by the viscocity measurements indicated increasing molar masses respectively.

The aim was to examine the applicability of new organic flocculants in conditioning of WAS from a paper mill. The sludge was coagulated with ferric sulphate and/or flocculated using flocculants having different charge densities and molecular weights (Table 1). The success of flocculation was determined by using a visual estimation of floc appearance and the dewatering methods discussed below.

Also the capillary suction time (CST) measurements using a Triton Electronics CST meter were conducted, indicating the ability of the liquid phase to propagate in the filter paper. Particle size measurements were carried out using a Malvern 2600c analyser. However, the CST values were too low to obtain reliable differences between different flocculants. The particle size measurement proved to be unsuitable for floc size determination.

Table 1. Flocculants Used in Flocculation and Filtration Tests and the Information for Modified Polymers. *

Polymer	Charge density [meqv/g]	M_w (g/mol)	M_n (g/mol)	PDI	Material	Special information
A=	+0.78	2.3 M	330000	7	HPS	
B=	+0.95	0.22 M	67000	3.3	HEC	
C=	+1.1	2.22 M	300000	7.5	HPS	Crosslinking product of A
D=	+3.74	2.08 M	430000	4.9	HPS	Crosslinking product of A
E=	+0.33	0.17	32000	5.2	HEC	
F=	~+1	~5-7 M	-	-	C-PAM	Comm. flocculant
G=	~+1	~1.5 M	-	-	C-PAM	Comm. flocculant
H=	~+1.2	~9.5 M	-	-	C-PAM	Comm. flocculant
I=	~+1.2	~4.5 M	-	-	C-PAM	Comm. flocculant

HPS = Hydroxypropyl Starch, HEC = Hydroxyethyl Cellulose and C-PAM= Commercial Cationic Polyacrylamide

Sludge Treatments

Two different types of laboratory-scale dewatering methods were tested for WAS, a batch type gravity filtration procedure and continuous belt filter pressing (Fig. 1). Gravity filtration tests were carried out using a filter cloth (Tamfelt DP313, permeability 2500 m^3/m^2h) in a funnel, when the sludge was coagulated and/or flocculated in a separate mug and decanted to the funnel in an identical manner. Success of the filtration was determined by measuring the amount of filtrate, the DS-content of the gathered cake and the filtrate, and the turbidity of the filtrate.

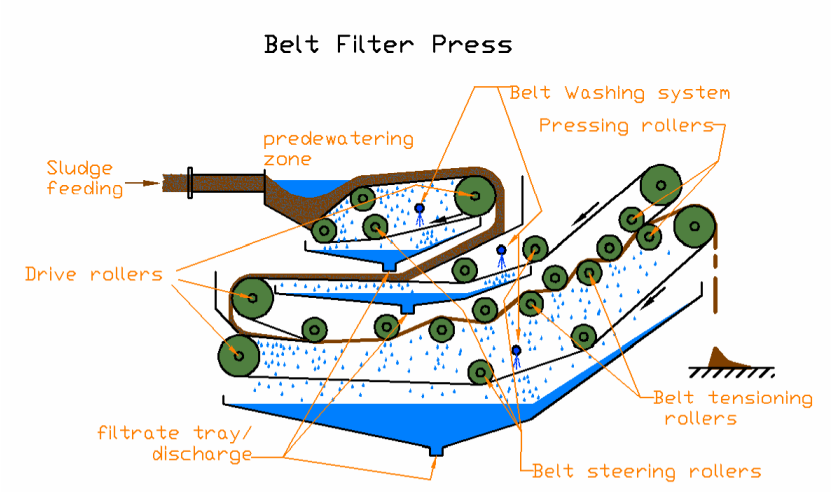

Fig. 1. Schematic illustration of the belt filter press

Laboratory-Scale Drainage and Flocculation Measurement Equipment

Drainage and retention efficiency of each polymer were studied with a laboratory-scale drainage device, as shown in Fig. 2. The device consists of a sample chamber, a filtrate flask, a scale, a vacuum pump, and a manometer. The wire in the bottom of the sample chamber was a 200 mesh metallic screen. The cumulative filtrate mass was measured with a scale and recorded by a computer. The experiments were carried out with a typical news furnish containing 30% of filler with an initial total consistency of 8 g/L. Each sample was prepared by mixing the polymer manually in the sample chamber for 30 seconds at a temperature of 50°C. The pressure in the filtrate flask was initially set to -10 kPa. After the measurement, the filtrate in the flask was collected and analysed for turbidity. The efficiency of the polymers was evaluated as the change in the dewatering rate and the change in turbidity of the filtrate.

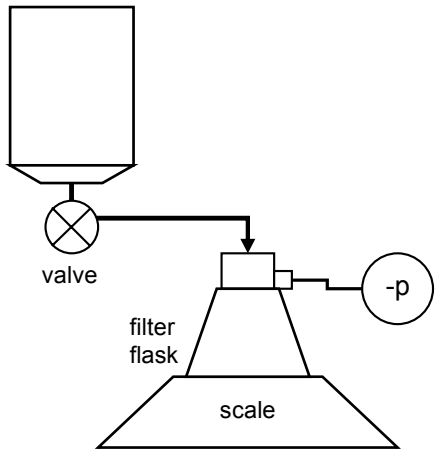

Fig. 2. Schematic illustration of the laboratory drainage device

The state of flocculation in the furnish following the addition of the polymers was studied in a laboratory flow loop system with a contraction channel simulating the conditions in a headbox of paper machine. The flow geometry and measurement set-up are presented in Fig. 3.

The flocculation and retention capabilities of the polymers were evaluated using an image analysis technique. The average size of flocs was determined downstream after the abrupt contraction in the slit channel using a pulsed light emitting diode (LED) light source and a fast CCD camera. After correcting the images for uneven illumination, the floc size was determined in the flow direction and the transverse direction as a run-length average of the median thresholded image (Kellomäki and Karema 1999; Karema and Salmela 2001; Salmela and Kataja 2005). The retention efficiency was evaluated by calculating the mean intensity and deviation of the intensity of the light transmitted through the channel. The light scattering efficiency of pulp decreases as the filler particles attach onto fibres. As a result, the mean intensity and deviation of intensity are increased when more light is able to pass the pulp layer flowing in the channel.

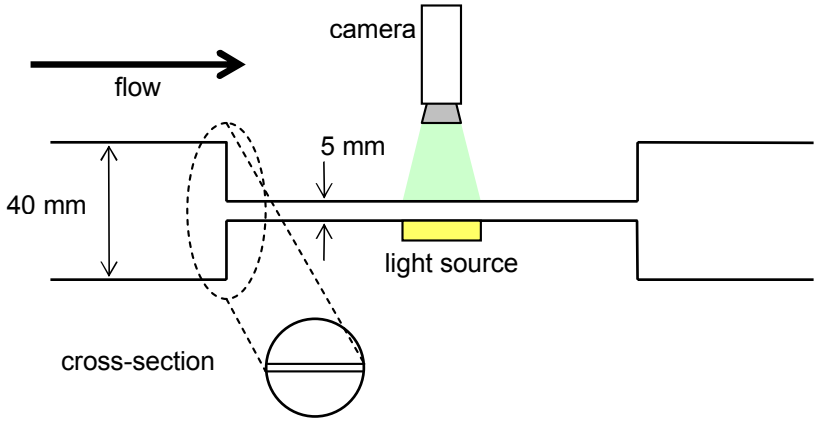

Fig. 3. Schematic illustration of the flow loop system with circular tube of 40 mm in diameter and a rectangular slit channel with height of 5 mm

RESULTS AND DISCUSSION

Pre-Test Result and the Further Developed Polymers

Thirty flocculants for the jar test were selected randomly from other projects. As source material either hydrolysed potato (N%: 0.4-2.8 %) or acetylated potato starch (DS = 0.9-2.9), maize starch (amylose rich, N% = 1.3-1.57 %), or enzymatically hydrolysed barley starch (N% = 0.66%) were used.

Table 2. Turbidity Results of Jar Test Study

	TMP fines		Kaolin	
	1 ppm	2 ppm	1 ppm	2 ppm
5 x cationized potato starch	++	++	++	+
2 x cationized maize starch	++	+++	+	- -
2 x enzymatic + cationized barley	+	-	++	- -
9 x cationized + modified starch	-	-	++	++
3 x cationized CMC	--	-	- -	- -
3 x acetylated starch	+	+++	+	- -
cationized starch acetate	-	++	+	-
cationized chitosan	+	+++	-	- - -
commercial cationic starch	++	+++	+	- -
3 x commercial cationized PAM	+++	+++	+	+
2 x cationized hydroxyethyl cellulose	++	++	+	- - -
cationized lignin	-	-	-	- - -

Symbol values : +++ = under 5, ++ = 6 to 20, + = 20 to 49, - = 50 to 100, - - = 101 to 199 and - - - = over 200 NTU. NTU = nephelometric turbidity units.

Also one sample was made of chitosan and cationized lignin. Total nitrogen content of the flocculants was typically very low, below 1%, i.e. medium cationization DS values of 0.14. As a general observation from the studies (Table 2) it can be said that products that had been subjected to anionic modifications, such as crosslinked and cationized CMC-flocculants, acted as dispersing agents, whereas an increasing degree of acetylation or increased nitrogen content improved the efficiency of the flocculant. Also, lowering of the pH in the suspension improved the efficiency of the flocculants.

Figure 4 presents the influence of the side chain of modified starch (HPS) on the effectiveness of TMP fines flocculation. The bigger the side chain was, from methyl to stearyl, the more ineffective was the flocculation. The comparison of the best flocculants to commercial flocculants revealed that at small dosage the commercial flocculants were more effective than the modified starches.

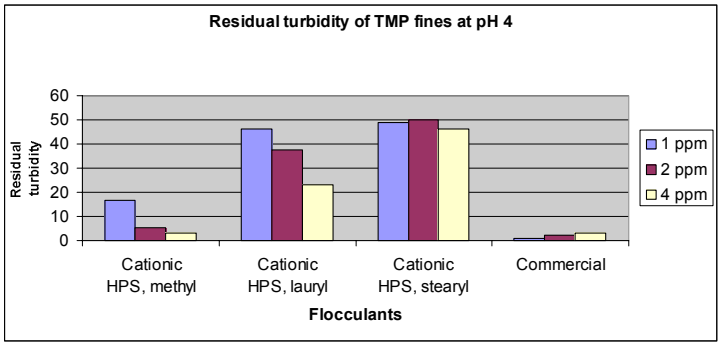

Fig. 4. Effect of side chain of the modified starch to the flocculation of TMP fines at pH 4

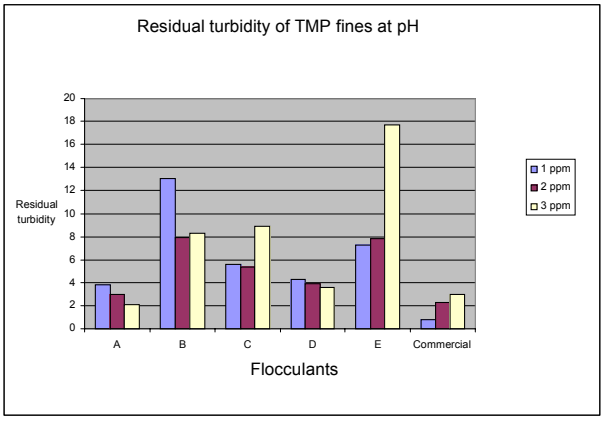

Fig. 5. Comparison of modified flocculants compared to a commercial flocculant in relation to the flocculation efficiency

Based on the jar test results it was concluded that the molecular weight or nitrogen content of bio-based polymer should increase. The best candidates for the application studies were further developed to optimize the flocculation properties. The optimization parameters for the polymer were chosen as increasing the molecular weight and the nitrogen content. Table 1 lists information pertaining to the modified polymers considered during the project. The jar test data of the modified polymers revealed that the best flocculants achieved almost at same efficiency level than the commercial products (Fig 5.).

Sludge Treatment

In an ideal situation, a flocculating polymer intended for sludge dewatering produces flocs that are large and stable enough for filtration, gives a clear filtrate (turbidity and dry solids are low), yields a high dry solids content of the cake, and the amount of clear filtrate is also high.

The cellulose-based polymers did not produce flocs in sludge application, based on estimating floc appearance visually. The starch-based polymers functioned clearly better. The tested polymer D, which was a cross-linked starch based polymer, functioned the best of all the developed polymers in this application (Table 3). It also had the highest molecular weight of the developed polymers. However, the best flocs were obtained using commercial flocculants with smaller dosages. The most satisfactory flocs for further dewatering tests were obtained using the commercial flocculant H with the molecular weight of 9.5 MMW. The use of ferric sulphate produced better flocs only with flocculants C and I.

Table 3. Visual Estimation of Floc Appearance. *

No flocs	Slightly flocky	Good flocs	Excellent flocs
Reference (0)	C (15) + Ferric	I (4) + Ferric	H (8)
Reference (0) + ferric	D (8)	I (8) + Ferric	H (8)
A (4)	D (15)	I (15) + Ferric	
A (8)	D (15) + Ferric	H (4) + Ferric	
A (15)	I (4)	H (4) + Ferric	
C (4) + Ferric	I (8)		
C (4)	I (15)		
C (15)			
D (4)			
D (4) + Ferric			
D (8) + Ferric			

* Polymer dose (kg/t DS) in parenthesis

The filtration tests gave similar results to the visual estimation of floc appearance. There was no cake on the filter when filtering sludge flocculated using cellulose-based polymers. Correspondingly, the filtrates had similar total solids content (TS) to the reference with no flocculant addition. Starch-based polymers produced better filtration results. When the sludge was flocculated using the polymer D (polymer dose 15 g/t TS), the DS of the cake obtained was fairly good, 4.3%. However, the filtrate was turbid and

the TS of the filtrate was high (>0.6%). The TS values of the cakes when using either of the commercial polymers were >5.0%. The filtrates were clearer (TS < 0.4%) than when using the starch-based polymers. The commercial polymer I produced more turbid filtrate (380 FTU) than the polymer H (260 FTU). Also the filtration rate with the polymer H was higher and the polymer needed for flocculation lower than with the polymer I.

The continuous belt filtering was carried out with the starch-based polymer D and the commercial polymer H. The TS 10 % obtained using the polymer D was fairly good. The TS with the polymer H was, however, a bit higher (12 %), and the filtrate was clearer. The polymer needed for flocculation was 1.5-fold higher for the polymer D than for the polymer H.

Drainage and Flocculation Efficiency in Papermaking

The effect of polymer additions on free water removal rate from the furnish was analysed by measuring cumulative mass of the filtrate as a function of time during the dewatering process (Fig. 6). The total filtration times when the maximum amount of filtrate was achieved are presented in Table 4. All flocculants increased the dewatering rate of the furnish. This is not surprising, since all the polymers evaluated were cationic and therefore flocculation is expected at least due to electrostatic attraction. A decrease in specific surface area of the pulp through flocculation of fines and fillers onto fibres leads to an increase in porosity of the consolidating pulp layer during the dewatering process.

Despite the similar charge density and molecular weight of polymers C and G, the commercial CPAM-based polymer G outperformed the starch-based polymer C in dewatering efficiency. Furthermore, the starch-based polymers C and D achieved almost identical dewatering behaviour, albeit the noticeable difference in both charge density and molecular weight. The highest dewatering rate was achieved with C-PAM having relatively low charge density but very high molecular weight. The performance of the cellulose-based polymer as a flocculating agent proved very weak.

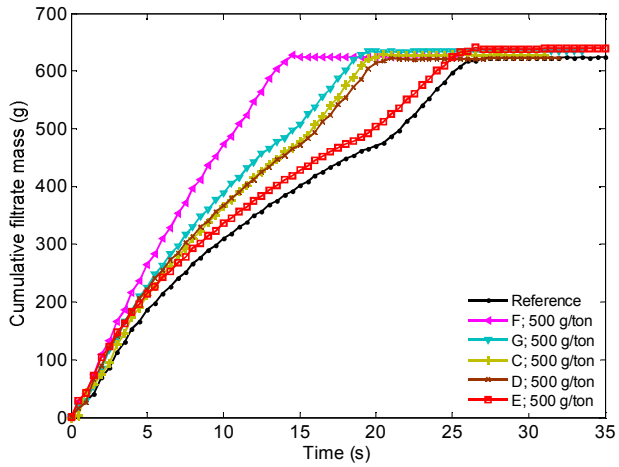

Fig. 6. Cumulative filtrate mass as a function of time for polymer dosage of 0.5 kg/ton

Table 4. Total Filtration Times of the Pulp Samples *

	500 g/ton	1000 g/ton
Reference	26.5 s	26.5 s
F (CPAM)	15 s	14 s
G (CPAM)	20 s	16.5 s
C (Starch)	20.5 s	20 s
D (Starch)	21 s	20.5 s
E (Cellulose)	27 s	28.5 s

* (time when maximum filtrate amount is achieved)

The effect of different polymers on retention was characterized in terms of turbidity. Filtrate turbidity values are presented relative to the value of reference pulp in Fig. 7. The commercial CPAMs F and G were able to reduce the turbidity to 20% of the reference. The tailored starch-based polymers C and D decreased turbidity to 30% of the reference, whereas the cellulose-based polymer E only yielded turbidity that was approximately 65% of the reference. The reason for the poorer performance of the cellulose-based polymer in dewatering and retention might be the significantly lower charge density and somewhat lower molecular weight.

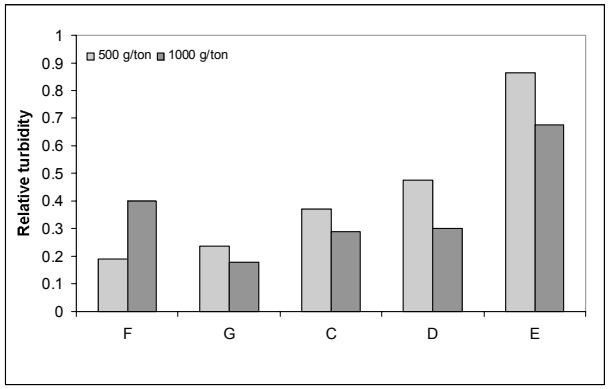

Fig. 7. Filtrate turbidities relative to the reference pulp filtrate

The starch-based flocculant C and the commercial flocculant F were selected for studies in a laboratory flow loop system. The cross-sectional area of the flocs produced by the different polymers relative to the reference without additives is shown in Fig. 8. Similarly, the relative mean intensity and deviation of intensity are presented in Fig. 9. As seen from the results, the commercial polymer F produced 1.9 to 2.3 times larger flocs, depending on the flow conditions and polymer dosage, when compared to the reference. The increase in intensity and deviation of intensity indicate that filler particles were attached onto fibres.

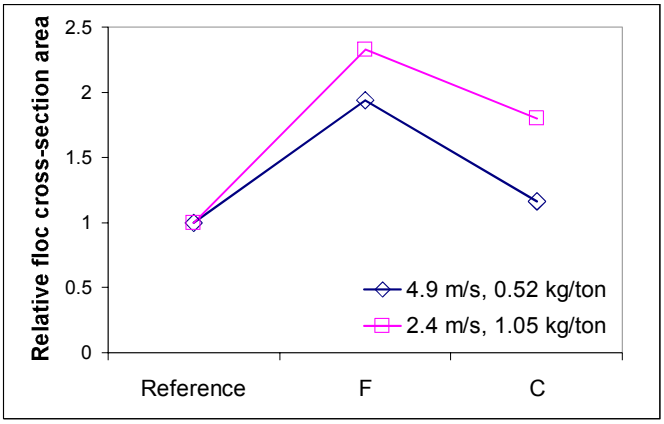

Fig. 8. Cross-sectional area of the flocs relative to the reference pulp. Similar flow conditions and polymer dosage are connected with a line.

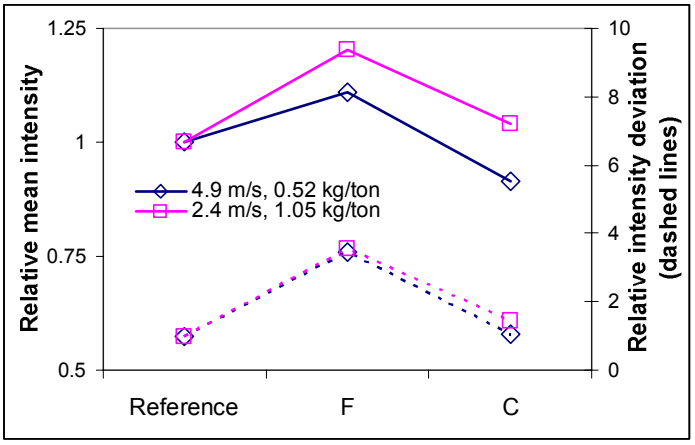

Fig. 9. Mean intensity (solid lines) and deviation of intensity (dashed lines) relative to the reference pulp. Similar flow conditions and polymer dosage are connected with a line.

The polymer C was able to increase the flocculation level with high dosage and slow flow velocity, but as the velocity was doubled and the dosage halved the floc size remained almost unchanged. Furthermore, the intensity quantities indicate that a major part of the fillers remained in the water phase.

Figure 10 shows an example of the acquired images for each studied case. Clear flocculation into localized mass concentrations (variations in gray levels) was observed for pulp treated with polymer F, whereas the flocculation pattern produced by polymer C was quite close to that of the reference pulp without additives.

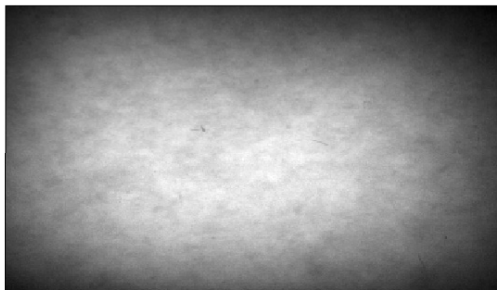

reference, 2.4 m/s

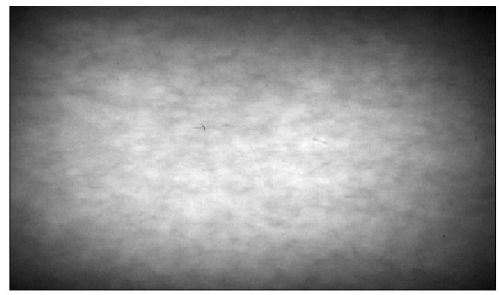

reference, 4.9 m/s

polymer C, 2.4 m/s, 1.05 kg/ton

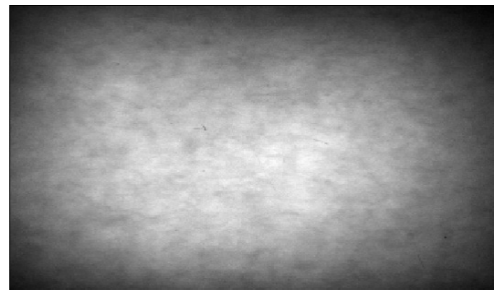

polymer C, 4.9 m/s, 0.52 kg/ton

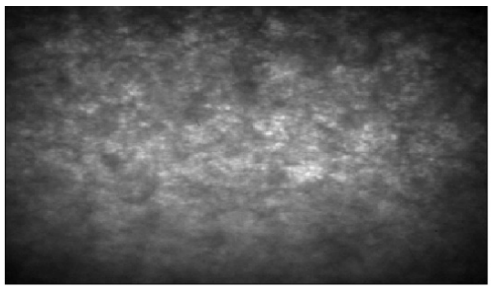

polymer F, 2.4 m/s, 1.05 kg/ton

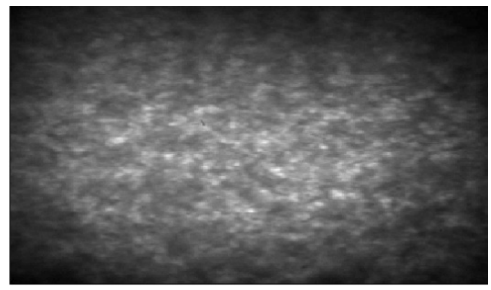

polymer F, 4.9 m/s, 0.52 kg/ton

Fig. 10. Examples of transilluminated pictures of the flow in the channel with different flow conditions and polymer dosages. These images were corrected for uneven illumination for further analysis.

CONCLUSIONS

1. Promising modified bio-based flocculants from jar tests were evaluated further. A starch-based polymer functioned best in both sets of experiments, but in neither of the cases did it function as well as the commercial polyacrylamide-based polymers. The importance of the molecular weight was highlighted by the experimental results.

2. The flocculation and retention efficiency of the starch-based polymers were generally lower than those of commercial C-PAM. In shearless dewatering conditions with auxiliary filtrating fibre network, the retention and dewatering properties were quite good compared to the studied C-PAMs. However, the flow studies at higher shear conditions showed that the starch-based polymers could not produce a significant flocculation level as would be needed to maintain sufficient retention properties with studied dosages. The performance of the cellulose-based polymer as flocculating agent was very weak.
3. The molecular weight of the prepared flocculant should be much higher in order to perform well in applications of papermaking retention and dewatering. Also, the effective dosage of the flocculant should be lower, which might be feasible when the molecular weight is higher. The different charge densities, the molecular structure, and rigidity should also be tested more closely in further studies.

ACKNOWLEDGMENTS

This work is carried out in the projects in the Fiber-based Innovation Chain – Consortium, which is coordinated and financially supported by the Technical Research Centre of Finland (VTT).

REFERENCES CITED

Ashmore, M., and Hearn, J. (2000). "Flocculation of model latex particles by chitosan of varying degrees of acetylation," *Langmuir* 16(11), 4906-4911.

Biswal, D. R., and Singh, R. P. (2004). "Characterization of carboxymethyl cellulose and polyacrylamide graft copolymer," *Carbohydrate Polymers* 57, 379-387.

Bratby, J. (1980). *Coagulation and Flocculation*, Uplands Press Ltd, Croydon.

Bratskaya, S., Schwartz, S., Liebert, T., and Heinze, Th. (2005). "Starch derivates of high degree of functionalization 10. Flocculation of kaolin dispersions," *Colloids and Surfaces A: Physicochemical and Engineering. Aspects* 254, 75-80.

Heinze, T., Haack, V., and Rensing, S. (2004). "Starch derivatives of high degree of functionation,7. Preparation of cationic 2-hydroxypropyltrimethylammonium chloride starches," *Starch/Stärke* 56, 286-296.

Karema, H., and Salmela, J. (2001) "Predication of paper formation by fluidization and reflocculation experiments," 12th, *Fundamental Research Symposium*, UK, 559-589.

Karppi, A. Knubb, B.-E., and Reinicke, H. (2007). "Cationic polysaccharide, its preparation and use," W02007121981.

Kellomäki, M., and Karema, H. (1999). "Fiber flocculation measurement in pipe flow by digital image analysis," *Proc. TAPPI Intl. Paper Physics Conf.* 461-463.

Lammers, G., Tiitola, P., and Vuorenpaeae, J. (1996). Patent, FI 107386, 1996.

Likitalo, A., and Käki, J. (2005). "Method for manufacturing high-cationic starch solutions," US 6855819.

Liu, Q., Zhang, Y., and Laskowski, J. S. (2000). "The adsorption polysaccharides onto mineral surfaces: An acid/base interaction," *International Journal of Mineral Engineering* 9, 1227-1234.

Monte, M. C., Fuente, E., Blanco, A., and Negro, C. (2009). "Waste management from pulp and paper production in the European Union," *Waste Management* 29(1), 293-308.

Nayak, B. K., and Singh, R. P. (2001). "Comparative studies on the flocculation characteristics of polyacrylamide grafted guar gum and hydroxypropyl guar gum," *Polymer International* 50, 875-884.

Oelmeyer, G., Krentz, O., and Kuliche, W.-M. (2002). "Combined flocculant systems with cationic starches in the soils/liquid separation of harbor sediments," *Chemical Engineering & Technology* 25, 47-50.

Ott, G., Schempp, W., and Krause, T. (1989). "Preparation of cationic cellulose with high degree of substitution in lithium chloride/dimethylacetamide," *Papier* 43(12), 694-699.

Pavlovic, S., and Brandao, P. R. G. (2003). "Adsorption of starch, amylose, amylopectin and glucose monomer and their effect on the flotation of hematite and quartz," *Minerals Engineering* 16, 1117-1122.

Peltonen, S., Tiitola, P., Vuorenpää, J., Happonen, H., and Törmälä, P. (1998). "Hydroxyalkylated starch ester and preparation and use thereof," WO9829456.

Roussy, J., Van Vooren, M., and Guibal, E. (2004). "Chitosan for the coagulation and flocculation of mineral colloids," *Journal of Dispersion Science and Technology* 25(5), 663-677.

Salmela, J., and Kataja, M. (2005). "Floc rupture and re-flocculation in turbulent shear flow," 13th, *Fundamental Research Symposium*, Cambridge, UK, 35-50.

Shirzad-Semsar, M., Scholz, S., and Kuliche, W.-M. (2007). "Cationic starch as substitute for synthetic cationic flocculants in solid-liquid separation of harbor sludge," *Journal of Physical Chemistry B* 111, 8641-8648.

Weissenborn, P. K., Warren, L. J., and Dunn, J. D. (1995). "Selective flocculation of ultrafine iron ore. 1. Mechanism of adsorption of starch onto hematite," *Colloids and Surfaces A: Physicochemical and Engineering. Aspects* 99, 11-27.

Xie, C., Feng, Y., Cao, W., Xia, Y., and Lu, Z. (2007). "Novel biodegradable flocculating agents prepared by phosphate modification of Konjac," *Carbohydrate Polymers* 67, 566-571.

Article submitted: August 3, 2010; Peer review completed: November 20, 2010; Revised version received and accepted: June 7, 2011; Published: June 8, 2011.

Series title and number
VTT Science 31

Title	**Cellulose, starch and their derivatives for industrial applications** **Structure-property studies**
Author(s)	Lauri Kuutti
Abstract	Despite the similarity of their structural basic units, cellulose- and starch-based materials behave differently in many industrial applications. In this thesis, the structure and properties of these polysaccharides and their selected derivatives were studied by means of five comprehensive examples. In the first investigation, highly crystalline cellulose was identified from *Valonia macrophysa* vesicles by atomic force microscopy. The role of water as a possible modifier on the surface of cellulose was found to be very important. The monoclinic phases were found on the cellulose surfaces with a lateral resolution of about 4 Å, indicating that water molecules cannot penetrate and thus disturb the surface structure of monoclinic cellulose. On the other hand, the absence of triclinic phases was explained by the used measuring geometry without liquid cell. The ageing of metastable oat and barley thermoplastic starch films was followed by frictional imaging. As a consequence of the ageing, the films lose some of their mechanical properties. In the oat films, glycerol used as a plasticiser diffused from the starch-glycerol-water matrix to the surface of thermoplastic starch, resulting in areas with low friction. In the case of barley starch films, the ageing first resulted in short range reorientation of polymers and finally slow crystallization of amylopectin branches. Solution precipitation techniques were applied to produce ideally spherical starch ester particles (with a diameter about half the wavelength of visible light), suitable for fillers in paper coatings in the third study. Particles assume their shape and size spontaneously when solvated starch polymer is mixed with non-solvent, due to the free mobility of the modified starch chains. Starch pigment has improved affinity to paper surface and it can be used as such or mixed with other pigments to enhance the optical or printing properties of paper. Starch-based pigmenting materials with improved optical performance were prepared in the laboratory by the complexation approach. Analytical results indicated that the complexation of carboxymethyl starch and inorganics strongly depends on the carboxymethyl group in the starch-based hybrid pigmented materials. The formed insoluble hybrids were mostly amorphous and the crystalline contribution of the inorganic component was not evident. The resulting precipitates exhibited composite structures. Finally, three starch-based and two cellulose-based polymers were selected for flocculation and filtration tests. In shearless dewatering conditions, the retention and dewatering properties of the starch-based polymers were similar to those of commercial polyacrylamide-based polymers. The flow studies in higher shear conditions showed that with the studied dosages the starch-based polymers could not reach the flocculation levels needed to maintain sufficient retention properties. The performance of the cellulose-based polymers as flocculating agents was less efficient. The reasons for the more limited performance of the polysaccharide-based flocculants were too low molecular weight and the charge density distribution. Better understanding of how to improve the hydrodynamic properties of bio-based polymers will be essential when planning new bio-based flocculants. The deeper understanding of the relationships between the desired structures and properties of polysaccharides helps to utilize them more effectively. In this way it is possible to obtain better bio-based and environmentally sustainable products in the competition with the current products based on conventional petrochemistry.
ISBN, ISSN	ISBN 978-951-38-7997-6 (Soft back ed.) ISBN 978-951-38-7998-3 (URL: http://www.vtt.fi/publications/index.jsp) ISSN-L 2242-119X ISSN 2242-119X (Print) ISSN 2242-1203 (Online)
Date	May 2013
Language	English, Finnish abstract
Pages	72 p. + app. 55 p.
Keywords	Cellulose, starch, derivative, industrial, application, structure, property
Publisher	VTT Technical Research Centre of Finland P.O. Box 1000, FI-02044 VTT, Finland, Tel. 020 722 111

Julkaisun sarja ja numero
VTT Science 31

Nimeke	**Selluloosan, tärkkelyksen ja niiden johdosten teollisia sovelluksia** **Rakenteen ja ominaisuuksien tutkimuksia**
Tekijä(t)	Lauri Kuutti
Tiivistelmä	Selluloosa- ja tärkkelyspohjaisten materiaalien ominaisuudet eroavat toisistaan huomattavasti monissa teollisissa sovelluksissa perusyksiköiden rakenteellisista yhtäläisyyksistä huolimatta. Tässä työssä tutkittiin näiden polysakkaridien ja niiden valikoitujen johdosten rakenteen vaikutusta ominaisuuksiin viiden kattavan esimerkin avulla. Ensimmäisessä työssä tutkittiin atomivoimamikroskoopilla hyvin kiteisen selluloosanäytteen Valonia macrophysa -rakkuloiden pintaa. Vesi todettiin merkittäväksi selluloosapinnan mahdollisena muokkaajana. Selluloosan pinnasta löydettiin monokliinisiä kidepintoja. Löytö tarkoittaa, että vesimolekyylit eivät pääse tunkeutumaan monokliinisiin selluloosapintoihin ja siten häiritsemään niitä. Toisaalta trikliinisten kidepintojen puuttuminen selitettiin johtuvan ilman nestekennoa toteutetusta mittausgeometriasta. Kitkakuvaamisella seurattiin puolipysyvien kaura- ja ohralämpömuovautuvien tärkkelyskalvojen vanhenemista. Kalvot menettivät vanhenemisen seurauksena osan mekaanisista ominaisuuksistaan. Kaurakalvoissa pehmittimenä käytetty glyseroli tunkeutui tärkkelys-glyserolivesi-matriisista lämpömuovattavan tärkke-lyksen pinnalle aiheuttaen alhaisen kitkan alueita. Ohratärkkelyskalvojen tapauksessa ikääntyminen aiheutti ensiksi polymeerien uudelleensuuntautumista ja lopulta amylopektiinihaarojen hitaan kiteytymisen. Kolmannessa työssä liuoksista tuotettiin saostustekniikalla ideaalisen pyöreitä tärkkelysesteri-pigmenttejä (halkaisija on noin puolet näkyvän valon aallonpituudesta) mahdollisiksi täyteaineiksi paperin päällystyksiin. Partikkeleiden oletetaan saavuttavan muotonsa ja kokonsa spontaanisti muunnettujen tärkkelysketjujen vapaan liikkuvuuden takia, kun tärkkelysliuos sekoitetaan ei-liuottimeen. Tärkkelyspigmentillä on parantunut affiniteetti paperin pintaan, ja sitä voidaan käyttää joko sellaisenaan tai sekoitettuna muun pigmentin kanssa parantamaan paperin optisia tai painatusominaisuuksia. Optisilta ominaisuuksiltaan parannettuja tärkkelyspohjaisia pigmenttimateriaaleja valmistettiin laboratoriossa kompleksoimalla. Analyyttiset tulokset osoittivat, että karboksimetyylitärkkelyksen ja epäorgaanisten komponenttien kompleksointi riippuu voimakkaasti tärkkelyspohjaisten hybridipigmenttimateriaalien karboksimetyyliryhmästä. Liukenemattomat hybridit olivat useimmiten amorfisia. Viimeiseksi kolme tärkkelys- ja kaksi selluloosapohjaista polymeeriä valittiin flokkulaatio- ja suodatuskokeisiin. Leikkautumattomissa vedenpoisto-olosuhteissa tärkkelyspohjaisten polymeerien retentio- ja vedenpoisto-ominaisuudet ovat samanlaiset kuin kaupallisilla polyakryyliamidipohjaisilla polymeereillä, joita käytettiin vertailuaineina. Virtaustutkimus suuremmissa leikkausvoimissa osoitti, että tutkituilla annostuksilla tärkkelyspohjaiset polymeerit eivät kykene saavuttamaan tarvittavia flokkulaatioita ylläpitämään riittäviä retentio-ominaisuuksia. Selluloosapohjaisten polymeerien teho flokkulantteina oli tärkkelyspohjaisia heikompi. Syy polysakkaridipohjaisten flokkulanttien rajoittuneeseen tehokkuuteen oli liian pieni molekyylipaino ja varaustiheysjakauma. Parempi tietämys siitä, kuinka biopohjaisten polymeerien hydrodynaamisia ominaisuuksia voidaan parantaa, on oleellista suunniteltaessa uusia biopohjaisia flokkulantteja. Molekyylirakenteiden ja ominaisuuksien välisen yhteyden syvällisempi ymmärrys helpottaa polysakkaridien tehokkaampaa hyödyntämistä. Tällä tavalla on mahdollista saavuttaa parempia biopohjaisia ja ympäristöä säästäviä tuotteita kilpailtaessa nykyisten konventionaalisten petrokemian tuotteiden kanssa.
ISBN, ISSN	ISBN 978-951-38-7997-6 (nid.) ISBN 978-951-38-7998-3 (URL: http://www.vtt.fi/publications/index.jsp) ISSN-L 2242-119X ISSN 2242-119X (painettu) ISSN 2242-1203 (verkkojulkaisu)
Julkaisuaika	Toukokuu 2013
Kieli	Englanti, suomenkielinen tiivistelmä
Sivumäärä	72 s. + liitt. 55 s.
Avainsanat	Cellulose, starch, derivative, industrial, application, structure, property
Julkaisija	VTT PL 1000, 02044 VTT, Puh. 020 722 111

Cellulose, starch and their derivatives for industrial applications

Structure-property studies

Despite the similarity of their structural basic units, cellulose- and starch-based materials behave differently in many industrial applications. In this thesis, the structure and properties of these polysaccharides and their selected derivatives were studied by means of five comprehensive examples.

Highly crystalline cellulose was identified from Valonia macrophysa vesicles by atomic force microscopy. The role of water as a possible modifier on the surface of cellulose was found to be very important. The monoclinic phases were found on the cellulose surfaces with a lateral resolution of about 4 Å, indicating that water molecules cannot penetrate and thus disturb the surface structure of monoclinic cellulose. On the other hand, the absence of triclinic phases was explained by the used measuring geometry without liquid cell.

The ageing of metastable oat and barley thermoplastic starch films was followed by frictional imaging. In the oat films, glycerol used as a plasticiser diffused from the starch-glycerol-water matrix to the surface of thermoplastic starch, resulting in areas with low friction. In the case of barley starch films, the ageing first resulted in short range reorientation of polymers and finally slow crystallization of amylopectin branches.

Solution precipitation techniques were applied to produce ideally spherical starch ester particles (with a diameter about half the wavelength of visible light), suitable for fillers in paper coatings in the third study. In the fourth study, starch-based pigmenting materials with improved optical performance were prepared in the laboratory by the complexation approach.

Finally, three starch-based and two cellulose-based polymers were selected for flocculation and filtration tests. The reasons for the more limited performance of the polysaccharide-based flocculants were too low molecular weight and the charge density distribution. Better understanding of how to improve the hydrodynamic properties of bio-based polymers will be essential when planning new bio-based flocculants.

The deeper understanding of the relationships between the desired structures and properties of polysaccharides helps to utilize them more effectively. In this way it is possible to obtain better bio-based and environmentally sustainable products in the competition with the current products based on conventional petrochemistry.

ISBN 978-951-38-7997-6 (Soft back ed.)
ISBN 978-951-38-7998-3 (URL: http://www.vtt.fi/publications/index.jsp)
ISSN-L 2242-119X
ISSN 2242-119X (Print)
ISSN 2242-1203 (Online)